Chapter 3: Magnetic Chitosan stabilized Palladium and Magnetic Chitosan stabilized Nickel - Palladium Nanostructures: Synthesis, Characterization and Applications

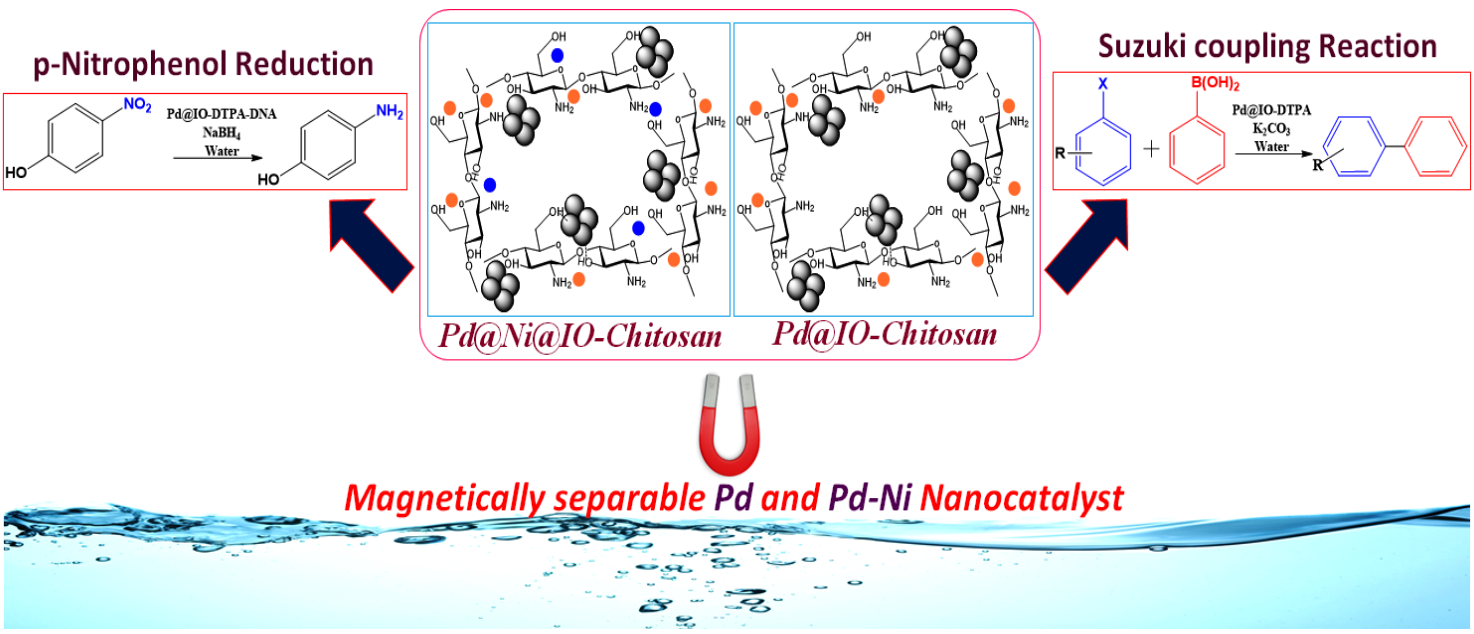

3.1. Introduction

There are several metal ions capable of catalyzing Suzuki coupling reaction, but the palladium catalysts remains the first choice due to its high catalytic activity for a wide range of substrates (Dong et al., 2021; Rai et al., 2015). For the fabrication of Pd catalysts reducing agents like $NaBH_4$ or hydrazine are required which are toxic. Further, presence of PdO is reported to enhance the catalytic efficiency of Pd in Suzuki coupling reaction as reported by Yang et al (Yang et al., 2015). They fabricated Pd/PdO nanoparticles decorated on carbon nanotubes containing varying percentages of PdO (59%, 63% and 73%). Suzuki coupling reaction with bromoanisole and phenylboronic acid using 73% gave maximum conversion.

The use of Pd and PdO clusters could greatly improve the catalytic efficiency for Suzuki coupling reactions because of large surface area and increased proportion of surface atoms. However, the small particle size can also lead to aggregation of particles due to which catalytic potential of Pd catalyst decreased(Rai et al., 2015).

Apart from Pd, there are reports on the use of nano NiO for Suzuki coupling reaction (Park et al., 2005) though with decreased efficiency. Increased attention is also being directed towards bimetallic catalysts because of synergistic influence coming from different transition metals (Nan et al., 2020).

Several Pd based bimetallic systems such as Pd-Au, Pd-Ag, Pd-Rh, Pd-Ru, Pd-Cu, Pd-Co or Pd-Ni (Rai et al., 2016) are reported for Suzuki coupling reactions, out of which Pd–Ni nanoparticles are notably efficient due to the excellent synergistic effect(Bao et al., 2019). Ni and Pd are easily miscible because of their similar crystal structure and electronic configuration (Jang et al., 2017) with $4d^{10}5s^0$ and $3d^84s^2$ outer electronic configuration respectively. Bimetallic nanosystem (Pd-Ni) will be a more effective catalyst than the individual monometallic (Pd or Ni) nanoparticles (Seth et al., 2014). Bao et. al., synthesized bimetallic Pd–Ni without ligands loaded on carbon nanofibers and used it for Suzuki coupling reaction (Bao et al., 2019). Jang et al. synthesized nickel doped palladium-iron oxide hybrid nanoparticles with crumpled ball-like morphology and used it for Suzuki coupling reaction(Jang et al., 2017). Further, Ghanbari et. al. fabricated palladium-nickel/iron oxide core-shell nano alloys via ultrasonic assisted method and applied it for Suzuki coupling and p-Nitrophenol reduction reaction (Ghanbari et al., 2017).

Furthermore, recently surface electronic state of metal nanoparticles was modified with a layer of metal oxides. The energy difference between the highest occupied molecular orbital (HOMO) of the metal oxides and the Fermi level of the metal induced spontaneous electron tunneling

through the thin dielectric barrier resulting in a change in electron density on the metal surface(Jiao et al., 2020)

Thus, the introduction of magnetic support materials with Ni –NiO could effectively stabilize the Pd clusters, Pd and PdO as well as augment the catalytic properties.

Biopolymers like Chitosan, cyclodextrin agarose, cellulose etc. have gained great research attention for their use as a support for Pd catalyst due to environmental impact concerns and eco-sustainable pathway for the demand of green chemistry (Dong et al., 2021). This low-cost biopolymer possesses unique affinity towards most transition metals ions, making it a desirable solid support for the stabilization of nanocatalyst (Dong et al., 2021).

Veisi et al. prepared magnetic nanoparticles comprising palladium immobilized on chitosan-biguanidine by insitu reduction and applied for Suzuki Miyaura coupling reactions(Veisi et al., 2018). Sedghi et al developed multi walled functionalized magnetic chitosan on N-heterocyclic carbene-palladium (M-f-MWCNTs@chitosan-NHC-Pd) (Sedghi et al., 2019).

In the present chapter, we report an eco-friendly synthesis process for preparation of Pd nano particles on the surface of chitosan supported magnetic iron oxide nanoparticles (IO-Chitosan) and nickel immobilsed chitosan supported magnetic iron oxide nanoparticles (Ni@IO-Chitosan) as a reusable heterogeneous catalyst. Initially, magnetic nanoparticles were prepared under ambient conditions (IO-Chitosan & Ni@IO-Chitosan). This was followed by in situ reduction of palladium ions to form magnetically separable palladium nanosystem (Pd@IO-Chitosan & Pd@Ni@IO-Chitosan). The catalytic efficiency of the synthesized nanocatalyst in Suzuki coupling reaction of aryl halides with arylboronic acid in water and p-Nitrophenol reduction has been demonstrated.

3.2. Materials and methods

3.2.1. Materials

All chemicals and solvents were purchased as analytical grade from commercial suppliers and were used without further purification. Chitosan and palladium chloride were purchased from Sigma Aldrich.

3.2.2. Procedure for the preparation of Chitosan capped Iron oxide nanoparticles (IO-Chitosan)

Iron oxide nanoparticles capped with chitosan were prepared by chemical co-precipitation method in alkaline condition. $FeSO_4 \cdot 7H_2O$ (0.96 g) was dissolved in 5% 10

mL HCl solution followed by the addition of 1.12 g $FeCl_3.2H_2O$ and stirred for 10 minutes. To this solution, 10 mL of 1% chitosan solution prepared in acetic acid was added dropwise and stirred for 30 min. This was followed by the dropwise addition of 25 mL of 50% ammonia solution to adjust the pH to 10 and stirred for 3 h resulting in the formation of black particles (IO-Chitosan) which were collected using an external magnet and washed with 100 mL water followed by 10 mL acetone and then dried at 100°C in oven for 9-10 h.

3.2.3. Procedure for the immobilization of Palladium on Chitosan capped Ironoxide nanoparticles (Pd@IO-Chitosan)

For the preparation of Pd@IO-Chitosan, 100 mg IO-Chitosan was sonicated in 20 mL ethanol for 20 min followed by the addition of 2 mg $PdCl_2$ to the suspension with gentle stirring at RT (30-35 °C) for 12h. The resultant Pd@IO-Chitosan nanoparticles were separated with a handheld magnet, washed with ethanol and finally dried at 100 °C for 5 h.

3.2.4. Preparation of Chitosan capped Nickel doped Iron oxide nanoparticles (Ni@IO-Chitosan)

The synthesis of Ni@IO-Chitosan was performed using chemical precipitation method. Firstly, 0.96g $FeSO_4 \cdot 7H_2O$ was taken in round bottom flask and dissolved in a mixture of 10 mL 5% HCl solution in water and stirred for 10 min followed by the addition of 1.12 g $FeCl_3$. $2H_2O$ and stirring for 10 min. After 10 minutes, 10 mL of 1% Chitosan solution prepared in acetic acid was added drop wise and stirred for 30 min followed by addition of 25mL of 50% ammonia solution to adjust the pH of the medium to 10 and stirring for 3 h resulting in precipitation of black particles. After 3 h of stirring, 3 mL of 0.3M $NiCl_2.6H_2O$ solution was added drop wise and stirred for an additional 3 h(Ahmad et al., 2015). The black particles of Ni@IO-Chitosan were collected using an external magnet and washed with 100 mL water followed by 10 mL acetone and then dried in an oven at 100 °C for 7-8 h.

3.2.5. Procedure for the immobilization of Palladium on Chitosan capped Nickel doped Iron oxide nanoparticles (Pd@Ni@IO-Chitosan)

Pd@Ni@IO-Chitosan nanoparticles were prepared by sonicating a suspension containing 100 mg Ni@IO-Chitosan in 20 mL ethanol for 10 min. Subsequently, 2 mg $PdCl_2$ was added to Ni@IO-Chitosan suspension with gentle stirring for 12 h at room temperature. The resultant

Pd@Ni@IO-Chitosan nanoparticles were collected with a magnet, washed with 10 mL EtOH followed by 5 mL water and was finally oven dried at 100 °C for 5 h.

3.2.6. General method for p-Nitrophenol reduction catalysed by Pd@IO-Chitosan and Pd@Ni@IO-Chitosan

The effectiveness of Pd@IO-Chitosan and Pd@Ni@IO-Chitosan as catalysts for reduction of p-NP was evaluated by taking 50 mL of a solution of p-NP (50 ppm) and 5-10 mg $NaBH_4$ and stirred for 1 min. To the resulting mixture, 1 mg of nanocatalyst was added to initiate the reaction and the concentration of the products was measured by an UV–Vis spectrophotometer at definite time intervals at λmax 400 nm.

The reusability of the catalyst was tested by a scale-up experiment with 10 mg of catalyst maintaining the same ratio of catalyst/p-NP. After completion of the experiment, the catalyst was collected by magnetic separation and washed twice with 20 mL conductivity water and then placed in a drying oven to dry at 100 °C for 12 h before proceeding to the next cycle of nitrophenol reduction.

3.2.7. General procedure for the Suzuki coupling reaction catalysed by Pd@IO-Chitosan and Pd@Ni@IO-Chitosan

The coupling reaction was carried out by taking 1.59 mmol each of aryl halide, arylboronic acid, K_2CO_3, 1 mg of catalyst and 10 mL H_2O in a 25 mL round-bottomed flask and heated on an oil bath at 90-100 °C with stirring for 4 to 15 h depending on the aryl halides used. The reaction was monitored by thin layer chromatography (TLC). After completion of the reaction the mixture was cooled to room temperature and the catalyst was collected by an external magnet. Subsequently, the mixture was extracted with ethyl acetate three times (3*5 mL). The ethyl acetate phase was then collected, dried with Na_2SO_4 and coupled products were obtained by evaporation which were further analysed by GC-MS. The crude product was purified using column chromatography packed by silica gel to afford the desired product. NMR spectra of the purified products are given in the Appendix.

To test the recyclability of catalyst, after each cycle, catalyst was separated by using an external magnet and washed twice with 10 mL water followed by 10 mL of ethyl acetate. The catalyst was further dried in an oven at 100°C for 5 h. The recovered catalyst was further used for the next cycle of reaction.

3.2.8. Characterization of IO-Chitosan, Pd@IO-Chitosan, Ni@IO-Chitosan and Pd@Ni@IO-Chitosan)

The structural and morphological properties of Pd@IO-Chitosan and Pd@Ni@IO-Chitosan were analyzed by using UV-Vis, IR, XRD, SEM, EDX, VSM, HRTEM, XPS, HRTEM, TG-DTA and XANES techniques.

The X-ray diffraction patterns of the samples were identified using Bruker D8 Advance X-ray diffractometer, Scanning Electron Microscopy measurement was performed on a HITACHI SU1510 instrument. Energy dispersive X-ray spectroscopy (EDS) analysis was done using a JEOL (JSM 7600F model) FEG-SEM spectrometer, X-ray photoelectron spectroscopic (XPS) analysis was performed using PHI 5000 Versa Probe II spectrometer, FEI Inc, and XPS analysis of recycled catalyst was recorded using PHI 5000 Versa Probe III. Thermo Gravimetric (TG) and Differential Thermal Analysis (DTA) in Nitrogen atmosphere from 30°C to 750°C using TG-DTA-6300, INCARP EXSTAR 6000 instrument. UV-visible spectroscopy studies were carried out on a JASCO dual-beam spectrophotometer (model V-630) and UV-visible spectroscopy studies of p-NP reduction were performed out on a Perkin Elemer Lamda 35 spectrophotometer. High Resolution Transmission Electron Microscopy (HRTEM) was performed on a JEOL (JEM 2100F Model) instrument, operated at an accelerating voltage 200kV Fourier transforms infrared (FTIR) spectroscopy measurements were performed on a BRUKER ALPHA, IR spectrometer, using procedure described in chapter 2 section 2.2.6.

Pd and Fe k-Edge XANES analysis

Pd K-edge and Fe K-edge XANES spectra were recorded at the beamline BL12, INDUS-2 of the RRCAT Facility, Indore. Pellets of samples were prepared by grinding in a mortar and pestle and pressing under high pressure under vacuum Pd K-edge XANES spectra were recorded in the transmission mode

VSM analysis

Dried magnetic nanomaterials were used to obtain the VSM spectra using Lakeshore VSM 7410 magnetometers.

ESR analysis

ESR analysis was performed on a JES-FA200 ESR Spectrometer with X band at room temperature using dried powder samples.

Palladium leaching study by ICP-MS

The palladium leaching study was performed by using PerkinElmer ICP-MS, NexION 2000 spectrometer. After completion of Suzuki coupling reaction at 100℃, products were isolated by solvent extraction using ethyl acetate and aqueous phase was preserved for leaching study. These aqueous samples were digested using 5 mL HNO_3 in microwave digester and the digested samples were made up to 20 mL using Milli Q water and further used for ICP-MS analysis.

GC-MS and NMR analysis

GC-MS spectra of all the biaryl derivatives obtained from coupling reaction were recorded on Thermo Fisher Trace GC Ultra Gas Chromatograph using TR-5MS column. Helium was used as a carrier gas and chloroform as a solvent. Column chromatography of biphenyl derivatives was done using silica column and Hexane:Ethayl acetate as a mobile phase.

NMR spectra were recorded on Bruker avance III spectrometer operating at 600 MHz after dissolving compounds in $CDCl_3$ in NMR sample tube.

3.3. Result and Discussion

3.3.1. Characterization of IO-Chitosan, Pd@IO-Chitosan Ni@IO-Chitosan and Pd@Ni@IO-Chitosan

3.3.1.1. FTIR spectroscopy

The FTIR spectra for pristine chitosan, IO-Chitosan and Pd@IO-Chitosan, Ni@IO-Chitosan and Pd@Ni@IO-Chitosan nanoparticles under study are shown in Figure 3.1. Characteristic peaks of chitosan as well as iron oxide were present in the spectra of all the 4 nanosystems.

The bands observed at 632,557 cm^{-1} in IO-Chitosan; 632, 561 cm^{-1} in Pd@IO-Chitosan; 629, 581 cm^{-1} in Ni@IO-Chitosan and at 629, 583 cm^{-1} in Pd@Ni@IO-chitosan corresponded to the Fe-O stretching vibration (MTh-O-MOh of the tetrahedral and octahedral sites). Further the band at ~441 cm^{-1} in IO-Chitosan and Pd@IO-Chitosan; at ~446 cm^{-1} in Ni@IO-Chitosan and Pd@Ni@IO-Chitosan may be attributed to the Fe-O stretching mode of octahedral sites of maghemite and a shoulder at ~480 cm^{-1} was attributed to Fe_3O_4 indicating the possible presence of both magnetite and maghemite (Arumugam et al., 2020).

The stretching vibrations of –CH, -CH_2OH; C-O stretching; C-O-C antisymmetric /C-N stretching and OH bending vibration of chitosan were observed at 2921 cm^{-1}, 1427 cm^{-1}, 1373 cm^{-1}, 1152 cm^{-1} and 1060 cm^{-1} respectively in IO-Chitosan. The broad peak of hydrogen-bonded

hydroxyl groups and N-H groups was observed at 3440 cm^{-1}. Further the peaks of NH_2 group scissoring (amide I band) mode and glycoside linkage of saccharide structure were observed at ~1633 cm^{-1} and 804 cm^{-1} respectively. The N-H and O-H bands at ~3400 cm^{-1} observed in chitosan became weak confirming the stabilization of nanosystems with NH_2 and OH groups of chitosan(Zhou et al., 2013).

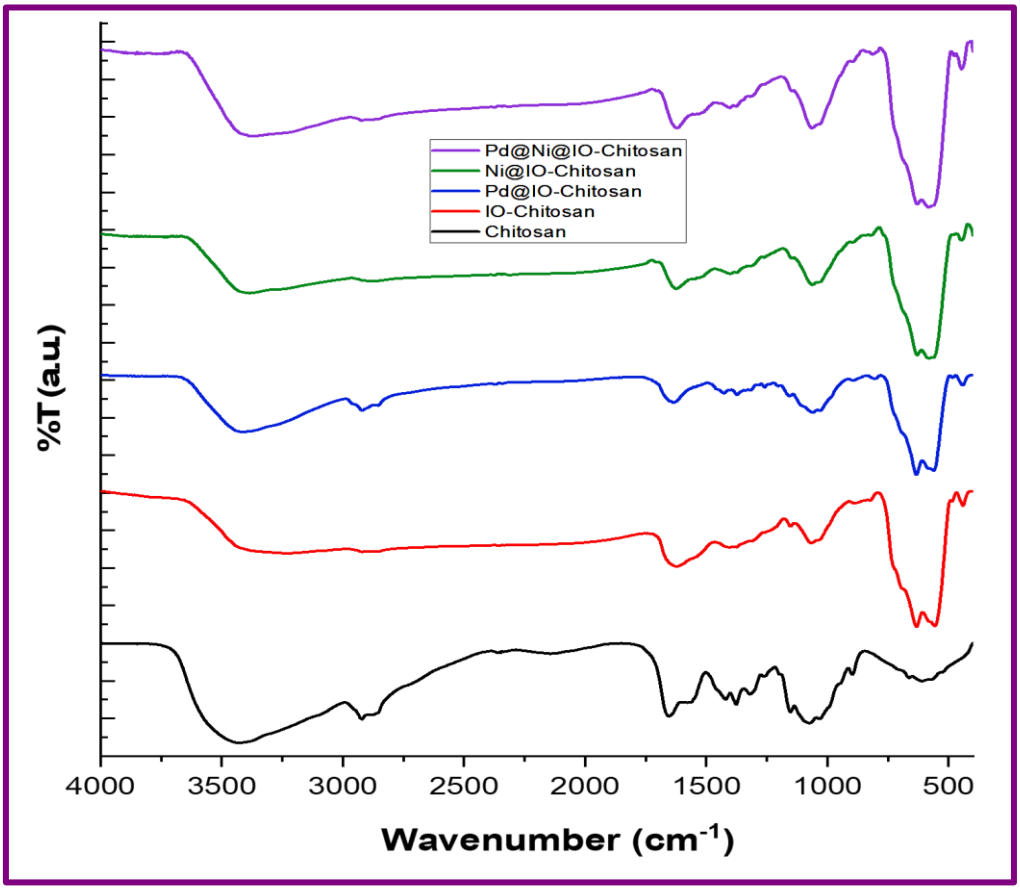

Figure 3.1 *Overlay IR spectra of Chitosan, IO-Chitosan, Pd@IO-Chitosan, Ni@IO-Chitosan, Pd@Ni@IO-Chitosan*

The IR band at 1310 cm^{-1} in chitosan attributed to amide III band was observed at 1314, 1318, 1325, 1312 cm^{-1} in IO-Chitosan and Pd@IO-Chitosan, Ni@IO-Chitosan and Pd@Ni@IO-Chitosan respectively. The peak at 1067 cm^{-1} in IO-Chitosan corresponding to OH bend was shifted to 1060 cm^{-1} in Pd@IO-Chitosan confirming the conjugation of iron oxide and Pd nanoparticle with chitosan. Similarly, the peak at 1062 cm^{-1} in Ni@IO-Chitosan was shifted to 1065 cm^{-1} in Pd@Ni@IO-Chitosan.

3.3.1.2. ICP-MS, SEM-EDS and TEM

The Pd and Fe content of Pd@IO-Chitosan estimated by Inductively Coupled Plasma-Mass Spectrometry (ICP-MS) were observed to be 1.065 wt% and 44.54 wt% respectively. ICP-MS analysis revealed the presence of 1.79wt% Pd, 0.55 wt% Ni and 43.33 wt% Fe in Pd@Ni@IO-Chitosan. The elemental composition and morphology of synthesized nanosystems were investigated by SEM and EDX mapping. (Figure 3.2)

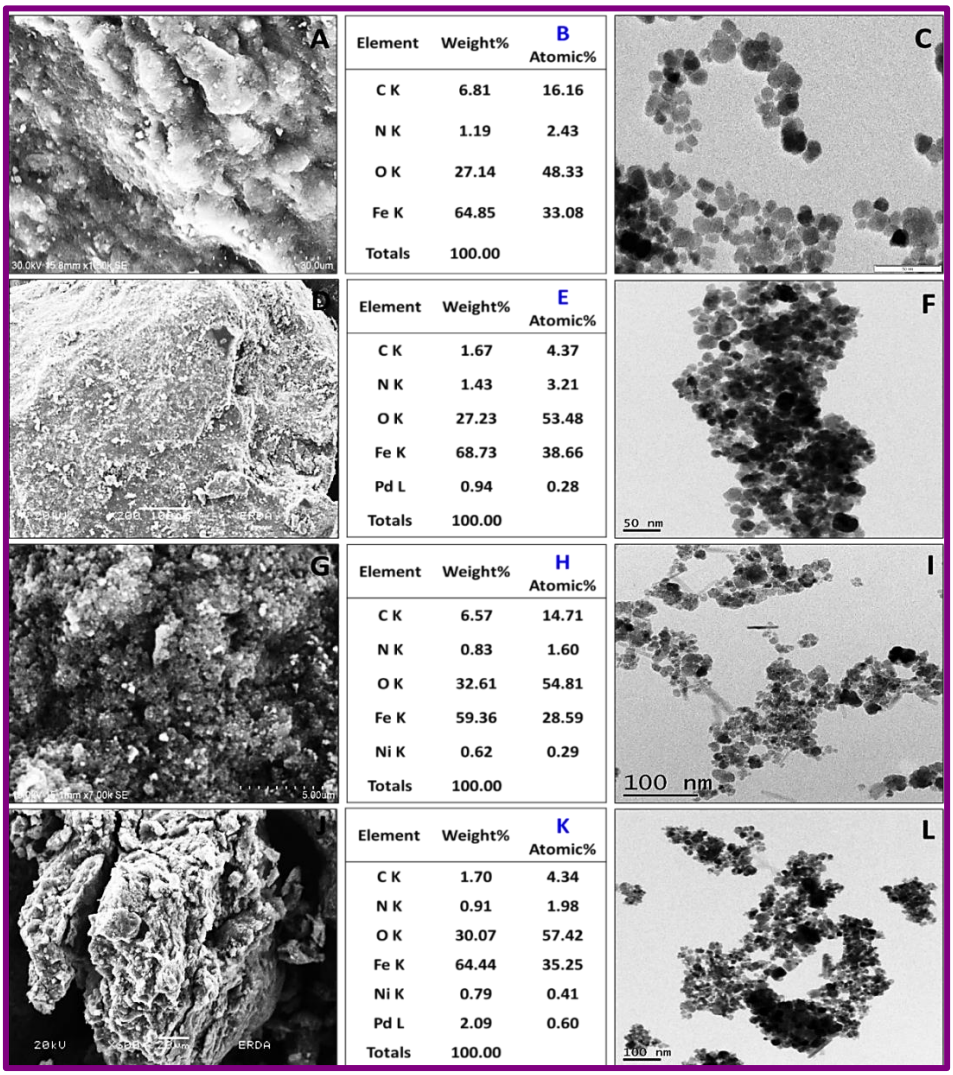

Figure 3.2: *(A) SEM image of IO-Chitosan, (B) EDX of IO-Chitosan, (C) TEM image of Io-Chitosan, (D) SEM image of Pd@IO-Chitosan, (E) EDX of Pd@IO-Chitosan, (F) TEM image of Pd@IO-Chitosan, (G) SEM image of Ni@IO-Chitosan, (H) EDX of Ni@IO-Chitosan, (I) TEM image of Ni@IO-Chitosan, (J) SEM image of Pd@Ni@IO-Chitosan, (K) EDX of Pd@Ni@IO-Chitosan, (L) TEM image of Pd@Ni@IO-Chitosan*

The EDX spectrum confirmed presence of C (6.81 wt%), N (1.19 wt%), O (27.14 wt%), Fe (64.85 wt%) in IO-Chitosan (Figure 3.2B); C (1.67 wt%), N (1.43 wt%), O (27.23 wt%), Fe

(68.73 wt%) and Pd (0.94 wt%) in Pd@IO-Chitosan (Figure 3.2E); C (6.57 wt%), N (0.83 wt%), O (32.61 wt%), Fe (59.36 wt%) and Ni (0.62 wt%) in Ni@IO-Chitosan (Figure 3.2H); C (1.7 wt%), N (0.91 wt%), O (30.07 wt%), Fe (64.44 wt%), Ni (0.79 wt%) and Pd (2.09 wt%) in Pd@Ni@IO-Chitosan (Figure 3.2K).

The TEM images (Figure 3.2(C, F, I, L)) of synthesized nanocatalysts showed that Pd NPs were dispersed on IO-Chitosan and Ni@IO-Chitosan. The supported Pd NPs were spherical in shape with size in the range of 5-20 nm. (IO-Chitosan: 5-20 nm, Pd@ IO-Chitosan: 5-15 nm, Ni@IO-Chitosan: 5-10 nm, Pd@Ni@IO-Chitosan: 5-18 nm). Aggregation of spheres to form nanorods were observed in Ni@IO-Chitosan and Pd@Ni@IO-Chitosan to a small extent.

3.3.1.3. HRTEM and SAED

High resolution transmission electron microscopy (HRTEM) images exhibited clear lattice fringes for maghemite/magnetite nanoclusters indicating crystallinity of the sample. It is difficult to distinguish magnetite and maghemite when mixed phases are present. Characteristic lattice fringes (Figure 3.3) of magnetite/ maghemite (Iron oxide) were observed at ~0.23, ~0.25, ~0.29 and ~0.50 nm assigned to 222, 311 and 220 planes(Amendola et al., 2011).

Well dispersed Pd and PdO (at the edges in the grey region) nanoparticles on IO-Chitosan support were observed in HRTEM images of Pd@IO-Chitosan (Figure 3.3B). Lattice fringes at 0.20 nm and ~0.24 nm observed in the black areas correlated with (200) and (111) planes of fcc Pd nanoparticles. Further the lattice fringes at ~0.29, ~0.26, ~0.218 nm were attributed to 100, 002 and 110 planes of tetragonal PdO (Su et al., 2015).

Ni@IO-Chitosan showed lattice fringes (Figure 3.3D) characteristic of magnetite/ maghemite were observed at 0.272, 0.251 and 0.498 nm attributed to 222, 311 and 111 planes. Further, lattice fringe spacings of Pd@Ni@IO-Chitosan (Figure 3.3F) at 0.203 nm and 0.241 nm that correlated with (200) and (111) planes of fcc Pd, and lattice spacing of ~0.26, ~0.218 nm, attributed to 002 and 110 planes of tetragonal PdO wherein the PdO (110) plane (spacing ~0.218 nm) was used to differentiate from Pd (200) and (111) planes. Moreover, lattice spacing of ~0.177 nm was attributed to Ni (200) plane while 0.203 nm was attributed to NiO (200), Ni (111) and Pd (200).

The SAED concentric ring pattern indicated polycrystalline nature of the sample. A weak diffuse pattern from the chitosan layer was also observed. SAED pattern of IO-Chitosan in (Figure 3.3A) was indexed to Fe_3O_4 (*JCPDS* 88-0315) and γ-Fe_2O_3 (*JCPDS* No. 39-1346), the diffraction rings are assigned to the (220), (311), (222), (400), (422), (511) and (440) planes respectively. The

SAED pattern of Pd@IO-Chitosan (Figure 3.3C) corresponded to the (111) and (220) planes of fcc Pd nanocrystallites as well as the maghemite and magnetite diffraction planes.

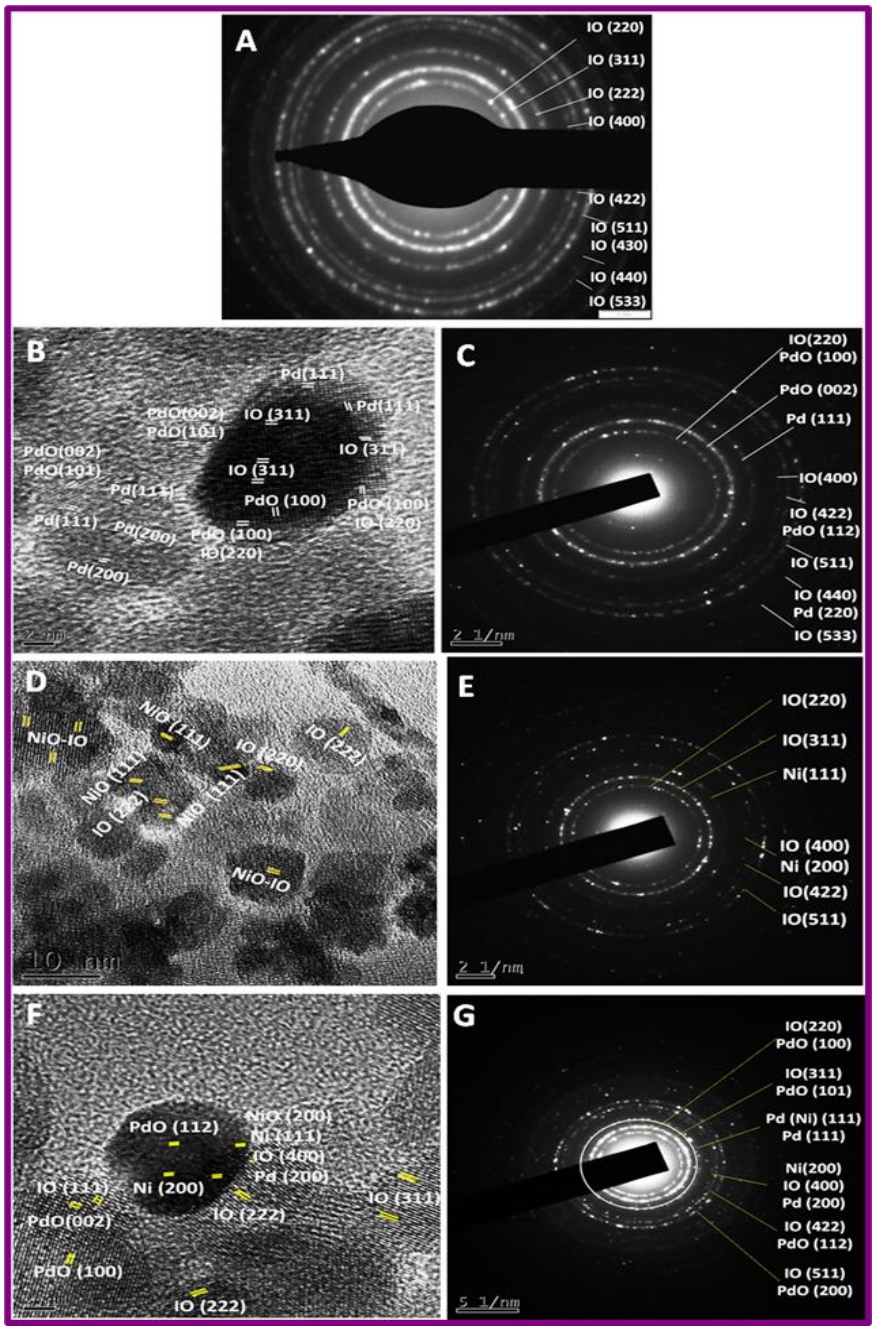

Figure 3.3: (*A) SAED image of IO-chitosan, (B) HRTEM image of Pd@IO-chitosan, (C)SAED image of Pd@IO-chitosan, (D) HRTEM image of Ni@IO-chitosan, (E)SAED image of Ni@IO-chitosan, (F) HRTEM image of Pd@Ni@IO-chitosan, (G) SAED image of Pd@Ni@IO-chitosan*

The diffraction rings in SAED pattern of Ni@IO-Chitosan (Figue 3.3E) were attributed to IO (220), IO (311), Ni (111), IO (400) & Ni (200), IO (422) and IO (511) planes. The SAED diffraction pattern of Pd@Ni@IO-Chitosan (Figure 3.3G) exhibited rings corresponding to (111)

and (220) planes of fcc Pd in addition to Fe_3O_4 and γ-Fe_2O_3 diffraction planes. The ring pattern also exhibited (100), (101) and (112) diffraction planes of PdO and (200) diffraction plane of Ni. The ring at 9.43 nm attributed to PdNi (111).

3.3.1.4. HAADF-STEM and EDX

The morphology of Pd@Ni@IO-Chitosan was further investigated by High Angle Annular Dark Field Scanning Transmission Electron Microscope (HAADF-STEM) and Energy dispersive X-ray (EDX) spectrometry. As shown in Figure 3.4, it is evident that the metal atoms are homogeneously distributed except for aggregation of few palladium nanoclusters (Figure 3.4 (E and F)) uniformly over the Ni@IO-Chitosan.

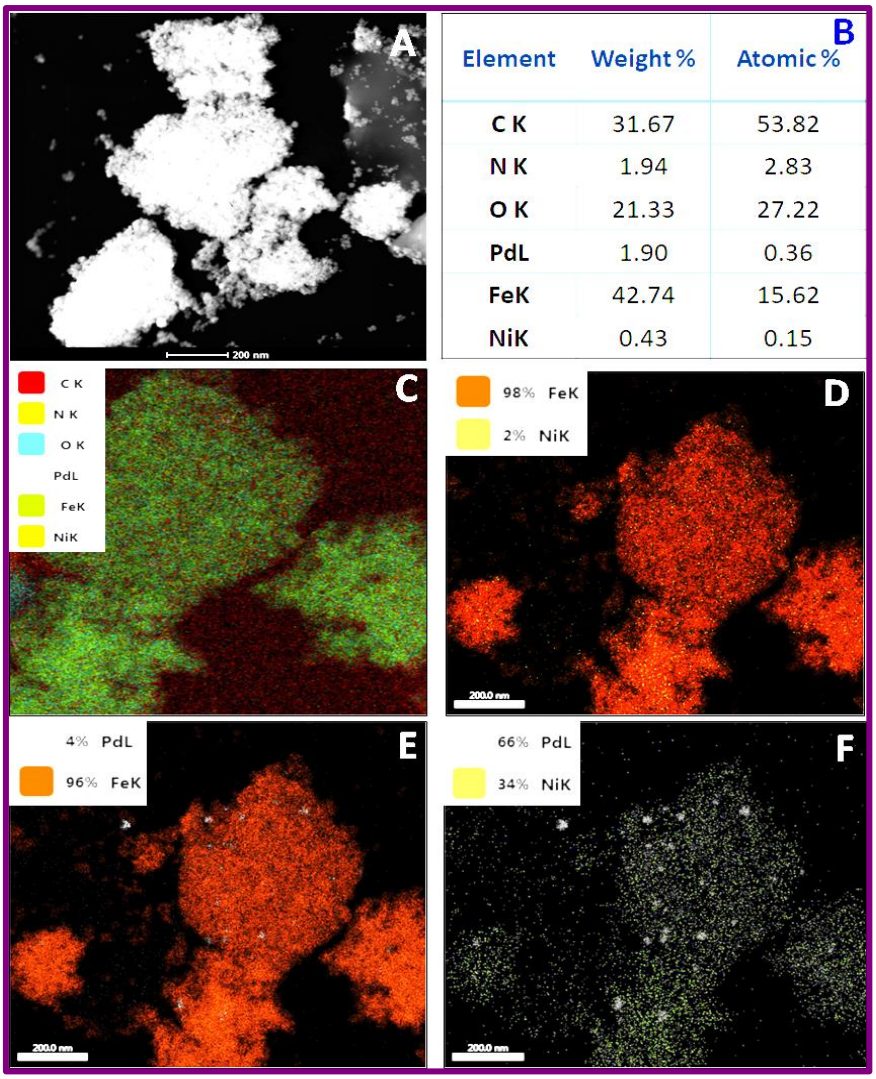

Figure 3.4.: *HAADF-STEM images of Pd@Ni@IO-Chitosan*

3.3.1.5. PXRD analysis

X-ray powder diffraction (XRD) analysis was used to further examine the crystallinity and phase purity. As shown in Figure 3.5A, the XRD pattern of the IO-Chitosan catalyst displayed typical maghemite and magnetite peaks, primarily at 2θ 30.2°, 35.6°, 43.3°, 53.8°, 62.8°, and 74.5°, which correspond to the diffraction planes of (220), (311), (400), (422), (511), (440) and (533) crystal faces of maghemite or magnetite spinel structures respectively. A broad peak at $2\theta = 21.4^{\circ}$ indicated the presence of weakly crystalline chitosan in IO-chitosan.

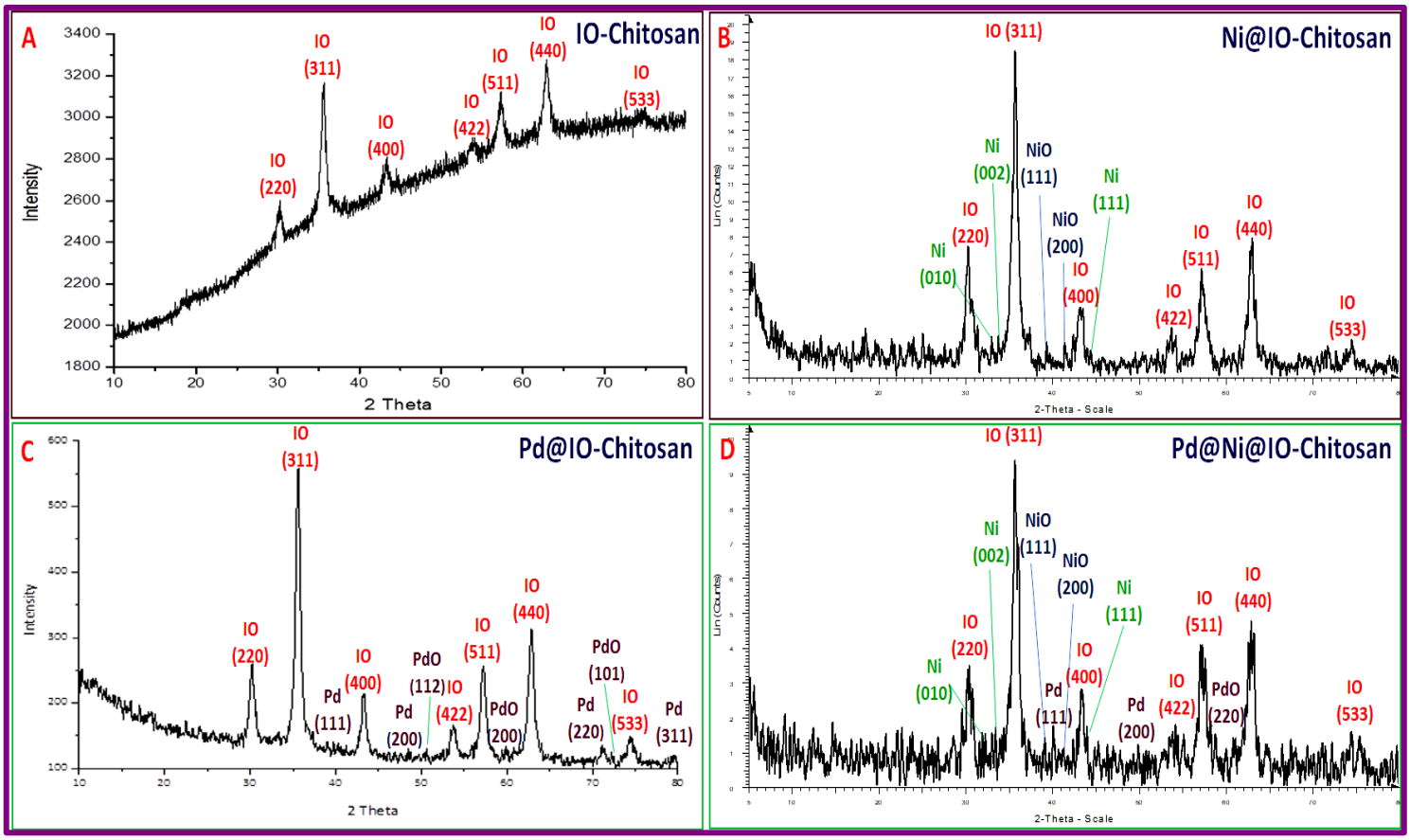

Figure 3.5: *(A) XRD pattern of IO-Chitosan, (B) XRD pattern of Pd@IO-Chitosan, (C) (B) XRD pattern of Ni@IO-Chitosan, (D) (B) XRD pattern of Pd@Ni@IO-Chitosan*

The XRD spectra of Pd@IO-chitosan in Figure 3.5B, showed XRD peaks at 2θ 30.1°, 35.6°, 43.3°, 53.7°, 57.3°, 62.9° and 74.4° attributed to (220), (311), (400), (422), (511), (440) and (533) diffraction planes of maghemite or magnetite spinel structure respectively. Due to very weak diffraction and a very disordered iron oxide structure, the powder diffraction pattern did not exhibit a (110) diffraction peak. The presence of maghemite was confirmed by the low intensity diffractions at 2θ 23.9° (210) and 26.5° (211), which suggested the presence of both magnetite and maghemite. (Jie et al., 2008; Kim et al., 2012). Furthermore, due to the high

dispersion, small crystallite size and low loading of Pd, modest distinctive diffraction peaks at 2θ = 48.7° and 71.06° revealed (200) and (220) diffraction planes of palladium (0). In addition, PdO diffraction peaks corresponding to the (112), (200), and (101) planes were seen, which supports our findings from HRTEM and SAED experiments.

As shown in Figure 3.5B, the XRD pattern of the Ni@IO-Chitosan showed the characteristic peaks of magnetite and maghemite at 30.2°, 35.6°, 43.3°, 53.8°, 57.3°, 62.8° and 74.5° which correlated to the diffractions of (220), (311), (400), (422), (511), (440) and (533) crystal faces of maghemite or magnetite spinel structure. XRD peaks can be observed at 44.9° corresponding to (110) plane of Ni(0), peaks at 2θ 38.5° and 41.9° corresponded to (111), (200) planes of NiO (Neelabh & Srivastava, 2010)(Richardson et al., 2003).

The XRD pattern of Pd@Ni@IO-chitosan in Figure 3.5D catalyst showed the characteristic peaks of IO NPs. In addition to characteristic peaks of IO, Ni and NiO, additional weak peaks could be observed at 2θ 40.1° and 49.5° which were well-indexed to the (111) and (112) crystalline plane of face cantered Pd(0) and a peak at 2θ ~61° corresponded to (200) plane of PdO (200), which were also observed in SAED studies.

3.3.1.6. XPS analysis

The C1s, N1s, O1s and Fe 2p XPS spectra of IO-Chitosan are shown in Figure 3.6(A-C). In the deconvoluted Fe2p XPS spectrum (Figure 3.6D), the peaks at 710.9, 713.29, 723.9 eV and 726.29 were ascribed to Fe2p3/2 and Fe2p1/2 of Fe^{3+} ions along with satellite peaks(Han et al., 2007; Kolen et al., 2014). The de-convoluted O 1s XPS spectra (Figure 3.6C) showed a peak at binding energy 528.14 eV assigned to iron oxide's lattice oxygen, while the peaks at 531.497 eV and 533.7 eV were attributed to chitosan's N-C=O bond and C-O-H respectively. Furthermore, the N1s (Figure 3.6B) de-convoluted peaks with binding energies of 399.47 eV were assigned to chitosan's -NH_2 or -NH, 401 eV to C-N, and 402.75 eV to NH_2-Fe(Unsoy et al., 2012). The the C 1s XPS spectra of chitosan showed a peak (Figure 3.6A) with a binding energy of 284.6 eV for C-C, 286.2 eV for C-OH and C-NH_2 and 288.299 eV for O-C-O. (Kong et al., 2010).

The XPS spectra of Pd@IO-Chitosan are shown in Figure 3.6 (E-I). In Fe2p XPS spectrum (Figure 3.6H), characteristic peaks of Fe2p3/2 and 2p ½ of Fe^{3+} are seen with the satellites. The presence of multiplet peaks may be due to the interaction with IO with chitosan and palladium(Verma et al., 2018).-The Pd 3d XPS spectra (Figure 3.6I)) exhibited peaks at binding energies 336.73 eV and 341.73 eV assigned to charged metallic Pd particles (Tsyrul et al., 2007).

The signal at 338.4 eV can be assigned to PdO/Pd^{2+} and the peak at 339.4 eV was attributed to the interactions between Pd and IO-Chitosan.

The O1s XPS spectrum of Pd@IO-Chitosan in Figure 3.6G exhibited a peak at binding energy of 529.99 eV attributed to Pd-O species and Pd-O-Fe interactions while peak at 531.7 eV was assigned to C-O of chitosan and 533.7eV to OH group (Shaw et al., 2017). Further, the deconvoluted N1s XPS spectra (Figure 3.6F) showed a peak at 399.8 eV ascribed to -NH_2 or -NH of chitosan, 400.5 eV to C-N and 402.2 eV to NH_2–Fe. The C 1s XPS spectrum (Figure 3.6E) exhibited deconvoluted peaks at binding energies 284.8, 286.5 eV and 288.2 eV assigned to C−C and C−H; C–NH and C-NH_2; (–C–OH) and C-O-C=O groups respectively.

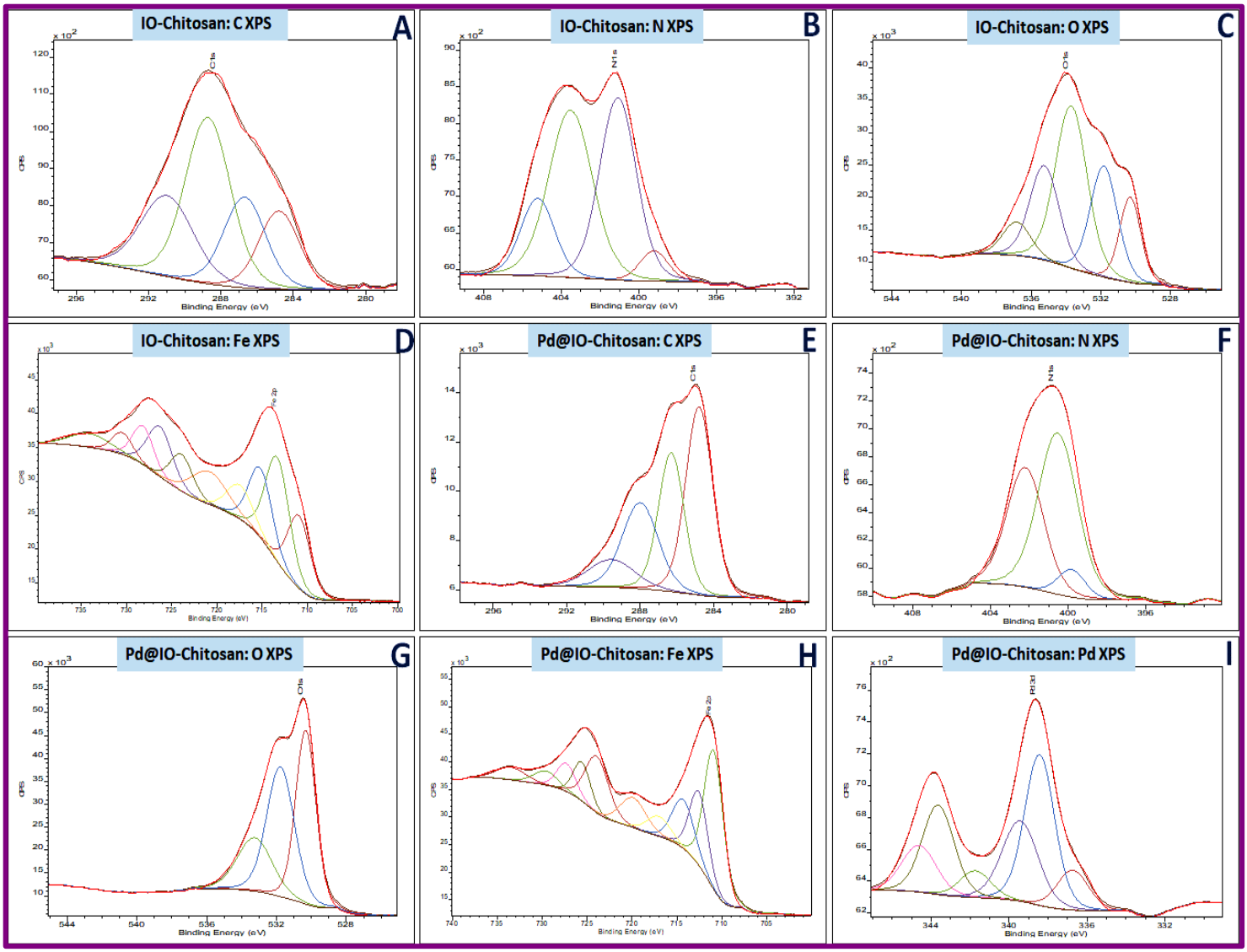

Figure 3.6: *(A-D) C, N, O, Fe XPS spectra of IO-Chitosan and (E-I) C, N, O, Fe, Pd XPS spectra of Pd@IO-Chitosan*

The de-convoluted C1s (27.21 At%), N1s (1.78 At%), O1s (52.24 At%), Fe2p (18.45 At%) and Ni2p (0.31 At%) XPS spectra of Ni@IO-Chitosan are shown in Figure 3.7. In the Fe2p XPS spectrum (Figure 3.7D), the signals at binding energies of about 710.16, 714.12, 723.23 and 727.23 eV were assigned to Fe2p3/2 and Fe 2p1/2 of Fe^{3+} of γ-Fe_2O_3 and α-Fe_2O_3 ions along with satellite peaks(Kong et al., 2010). The peak at 711.97 eV can be attributed to octahedral and tetrahedral Fe^{3+} in Fe_3O_4. The de-convoluted O 1s (Figure 3.7C) peak at binding energy 529.70 eV was attributed to lattice oxygen of iron oxide while the peak at 530.80 eV was attributed to N-C=O bond of chitosan and 532.38 to C-O-H. Further, the assignment for N1s de-convoluted peaks (Figure 3.7B) with binding energy 399.29 eV was made to -NH_2 or -NH of chitosan, 400.24 eV to C-N and 401.82 eV to NH_2–Fe (Unsoy et al., 2012). In the C 1s spectrum (Figure 3.7A) the peak with binding energy of 284.6 eV was attributed to C-C, while peak with binding energy 286.2 eV to C-OH, C-NH_2 and 288.299 eV to O-C-O of chitosan.

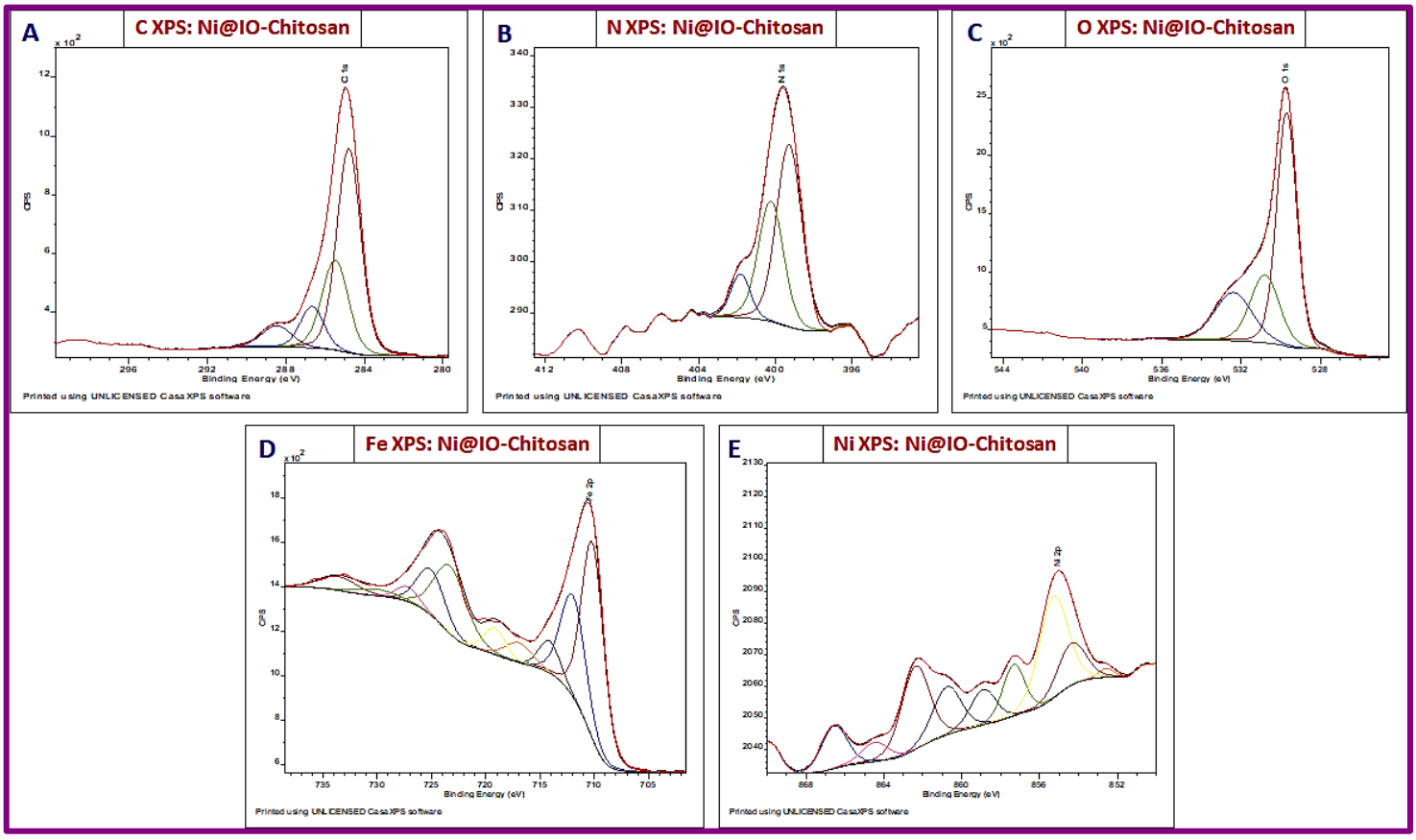

Figure 3.7: *C, N, O, Fe, Ni XPS spectra of Ni@IO-Chitosan*

The Ni 2p3/2 spectrum of Ni@IO-Chitosan in Figure 3.7E shows a complex structure with intense satellite signals of high binding energy adjacent to the main peaks due to multi-electron excitation. The binding energy of 852.58 eV may be attributed to metallic Ni. The most intense peak at 855.29 eV was due to Ni^{2+} in NiO while the second doublet at 860.77 eV could be

ascribed to Ni^{2+} in $Ni(OH)_2$. It should be noted that there are weak peaks related to NiO or $Ni(OH)_2$ in the XRD pattern. This is most likely because of the amorphous nature of resulting NiO and $Ni(OH)_2$ (Xia et al., 2016).

The de-convoluted C1s (29.30 At%), N1s (1.36 At%), O1s (50.40 At%), Fe2p (18.14 At%), Ni2p (0.20 At%) and Pd3d (0.59 At%) XPS spectra of Pd@Ni@IO-Chitosan are shown in Figure 3.8 (A-F). In Fe2p XPS spectrum (Figure 3.8D), characteristic peaks at 710.00 and 723 eV of Fe2p 3/2 and 1/2 of Fe^{3+} of γ- Fe_2O_3 and α- Fe_2O_3 are seen with the satellites at 719.85 eV (Kong et al., 2010). The Fe2p3/2 peak at 711.86 eV correspond to tetrahedral Fe^{3+} in Fe_3O_4 (Unsoy et al., 2012). In Pd 3d deconvoluted XPS spectrum (Figure 3.8F) the signals with binding energy 334.94 and 340.34 eV were assigned to Pd(0), 336.81 eV and 341.61 eV were assigned to charged metallic clusters. The signal at 337.79 eV can be attributed to PdO /Pd^{2+} and 339.4 eV to the interactions between Pd and Ni@IO-Chitosan (Tsyrul et al., 2007). From the Ni 2p3/2 spectrum (Figure 3.8E) it was observed that metallic character of Ni has increased after immobilization of Pd while the NiO content decreased.

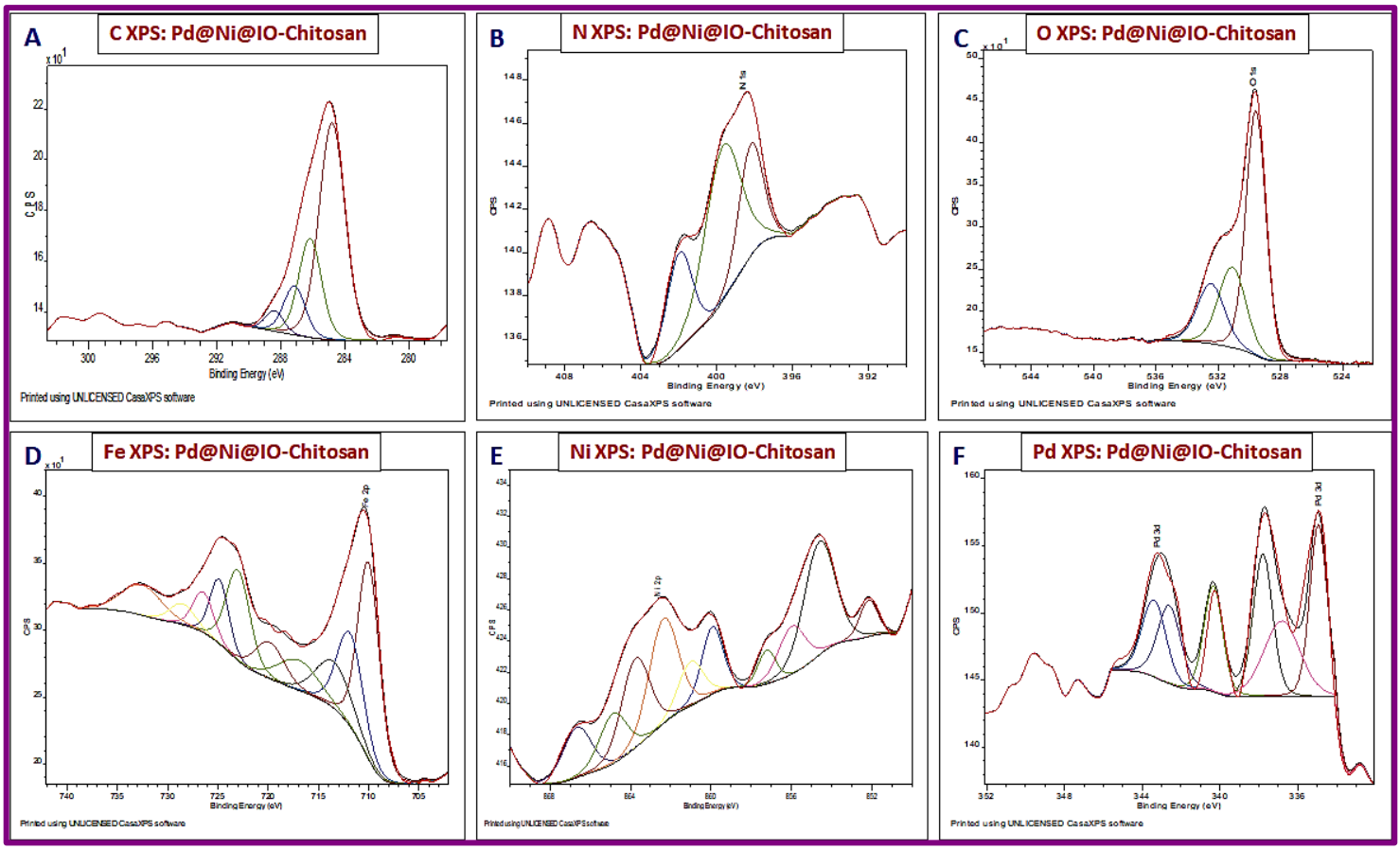

Figure 3.8: *C, N, O, Fe, Ni, Pd XPS spectra of Pd@Ni@IO-Chitosan*

The deconvoluted O1s XPS spectrum of Pd@Ni@IO-Chitosan depicted in Figure 3.8C exhibited a peak at binding energy of 529.59 eV was assigned to Pd-O species and Pd-O-Fe interactions while peak at binding energy 531.11 eV to C-O of chitosan and the peak at 532.47eV to OH group (Shaw et al., 2017). Further, N1s deconvoluted peaks with binding energy 398.2 eV was made to -NH_2 or -NH of chitosan, 399.68 eV to C-N and 401.97 eV to NH_2–Fe. (Figure 3.8B). The C 1s spectrum exhibited binding energies at 284.8, 286.17 eV and 288.39 eV attributed to C-C and C-H; C–NH and C-NH_2; (–C–OH) and C-O-C=O groups respectively (Figure 3.8A).

3.3.1.7. XANES analysis

X-ray absorption near edge spectra (XANES) technique was used to study the oxidation states of Fe and Ni further. (Figure 3.9)

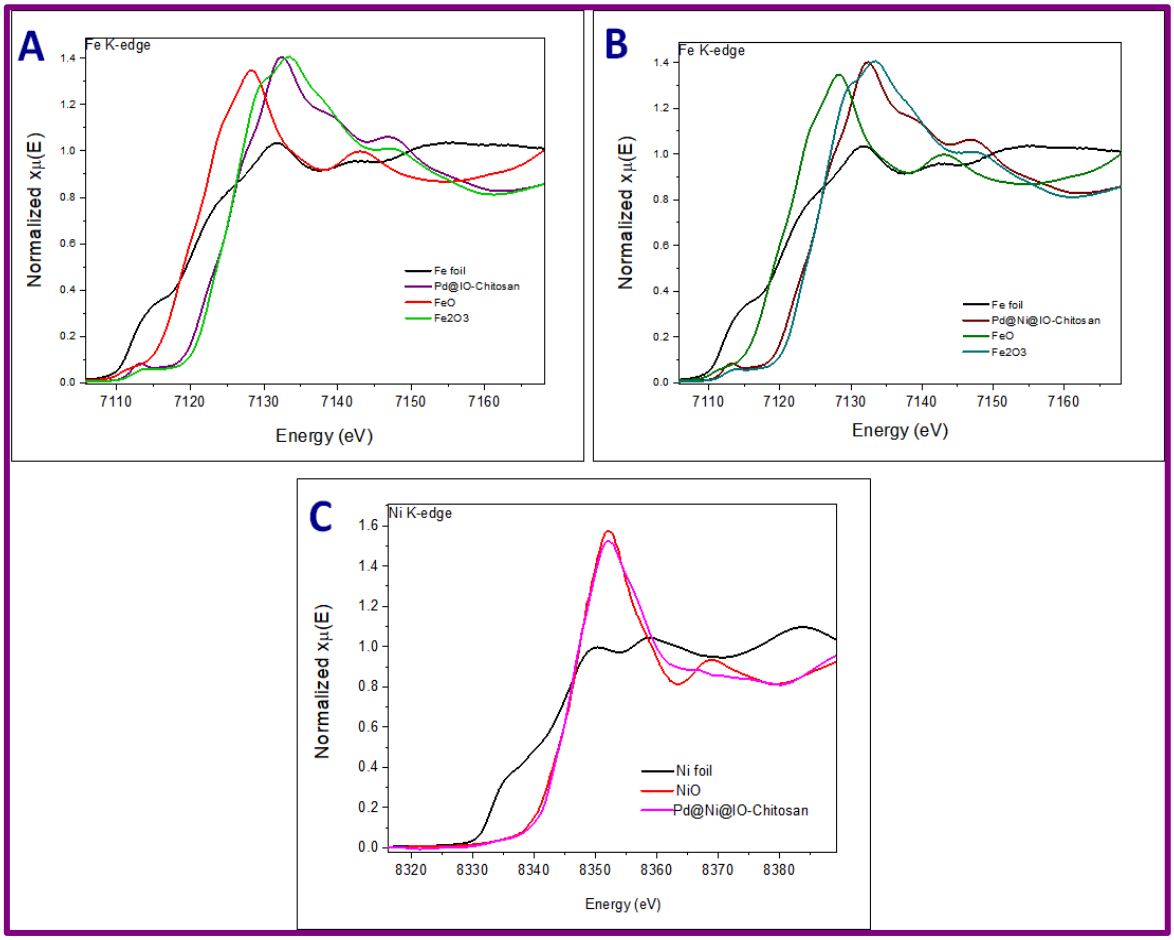

Figure 3.9: *(A) Fe K edge XANES spectra of Pd@IO-Chitosan, (B) Fe K edge XANES spectra of Pd@Ni@IO-Chitosan, (C) Ni K edge XANES spectra of Pd@Ni@IO-Chitosan*

The Fe K-edge XANES spectrum of Pd@IO-Chitosan and Pd@Ni@IO-Chitosan was matched with the the reference FeO and Fe_2O_3 spectrum (Figure 3.9(A&B)). It is clear from the figure that the XANES spectrum of both the compounds did not match with the reference spectra.

Further comparison with other iron oxides from literature was done. No exact correlation was found due to the complex nature as seen by XRD, HRTEM, SAED and XPS studies. (Piquer et al., 2014).

However, from literature it was inferred that a shoulder at ~7117 eV and a significant pre-edge excitation peak at ~7113 eV confirmed the presence of maghemite as the predominant phase. The hump at ~7139.3eV confirmed poorly ordered ferric compounds wherein the deposition of Pd/PdO may cause the disturbance in the structure (Baumgartner et al., 2013). The intense band at ~7133 eV can be assigned to the 1s–4p transition indicating the presence of maghemite(Hsu et al., 2010). The presence of a non-stoichiometric phase of maghemite was indicated from these observations.

The Ni K edge XANES spectra (Figure 3.9C), exhibited distinct absorption characteristics at 8351 eV resembling NiO (Mansour & Melendres, 1994) but with lower intensity due to presence of Ni metal component. Pd@Ni@IO-Chitosan show particularly distinct peaks at 8334 eV and 8366 eV indicating the presence of Ni and NiO in Pd@Ni@IO-Chitosan

3.3.1.8. TG-DTA analysis

The thermal stability of IO-Chitosan, Pd@IO-Chitosan, Ni@IO-Chitosan and Pd@Ni@IO-Chitosan were examined by TGA in the temperature range of 30 to 750 °C and are depicted in Figure 3.10.

The first weight loss of around 13 % in the range of ~100–250 °C in IO-Chitosan (Figure 3.10 A) was assigned to deacetylation of chitosan and release of hydroxyl groups, while the second weight loss of 12.4% (250 °C to 800 °C) may be attributed to degradation of chitosan as well as stabilisation of alpha form of iron oxide.

The TG-DTA curve of Pd@IO-Chitosan (Figure 3.10B) exhibited first weight loss of 2.3% in the temperature range of 30-150 °C, attributed to evaporation of adsorbed and bound water. In the second stage, weight loss of 5.1% occurred as a result of the release of hydroxyl ions and the breakage of the principal chains of chitosan at temperatures between 150 °C and 270 °C. Decomposition of acetylated and deacetylated units as well as amine and $–CH_2OH$ group of chitosan and oxidation of Fe_3O_4 to Fe_2O_3 may be responsible for the 5.6% weight loss in the third stage in the temperature range of 270 °C to 480 °C. In the temperature range of 480°C to 800°C, the final weight loss of 1.6% was due to the degradation of glucopyranose residues of chitosan (Parandhaman et al., 2017) as well as stabilisation of iron oxide in alpha form.

The thermal stability of Ni@IO-Chitosan and Pd@Ni@IO-Chitosan were investigated by TGA and are depicted in Figure 3.10(C and D) respectively in the temperature range 30 to 750 °C. The thermograms of Ni@IO-Chitosan and Pd@Ni@IO-Chitosan demonstrated 3 major weight loss steps. The weight loss of ~12.4 % in the temperature range of ~150–400 °C in Ni@IO-Chitosan may be attributed to degradation and deacetylation of Chitosan as well as release of hydroxyl groups while the gradual weight loss of 14.3% in the second stage (400 °C to 750 °C) may be attributed to final decomposition of chitosan as well as stabilisation of iron oxide in alpha form. The thermogram of Pd@Ni@IO-Chitosan exhibited an initial weight loss of 1.5% up to 150°C which was attributed to evaporation of both adsorbed and bound water. In the second stage, release of hydroxyl ions and degradation of principle chains of chitosan resulted in a weight loss of 9.0% in the temperature range 150 °C to 400 °C. The third stage weight loss of 2.3% in the temperature range 400 °C to 750 °C may be attributed to degradation of glucopyranose residues of chitosan as well as stabilisation of iron oxide in alpha form.

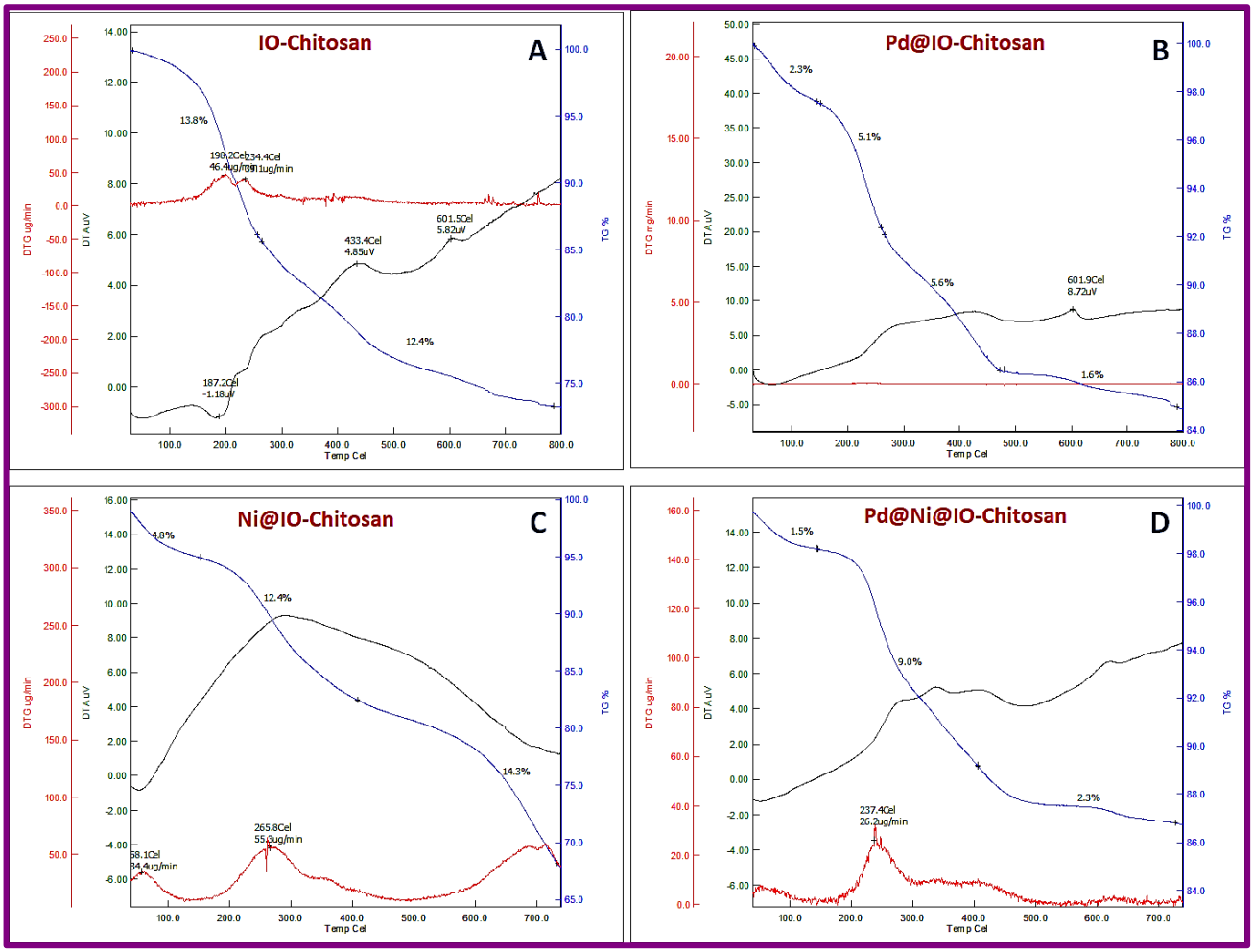

Figure 3.10: *(A) TG-DTA curve of IO-Chitosan, (B) TG-DTA curve of Pd@IO-Chitosan, (C) TG-DTA curve of Ni@IO-Chitosan, (D) TG-DTA curve of Pd@Ni@IO-Chitosan*

3.3.1.9. VSM analysis

The superparamagnetic behaviour of IO-Chitosan, Pd@IO-Chitosan, Ni@IO-Chitosan and Pd@Ni@IO-Chitosan systems were validated by vibrating sample magnetometer (VSM) analysis (Figure 3.11). Due to the small size of the particles and chitosan coating/support, or the existence of a little amount of magnetic material per gram of sample, the Ms values were low (Ahmadzadeh et al., 2018).

The saturation magnetization of IO-Chitosan was determined to be 52.91emu/g from the magnetization curve in Figure 3.11. The magnetic response of the Pd@IO-Chitosan catalyst was reduced to 39.037emu/g attributed to the loading of palladium nanoparticles on the IO-Chitosan surface. The saturation magnetization of Ni@IO-Chitosan was observed to be 81.07 emu/g, which was higher than IO-Chitosan due to presence of Ni species. Further, magnetic saturation of Pd@Ni@IO-Chitosan catalyst decreased to 74.38 emu/g.

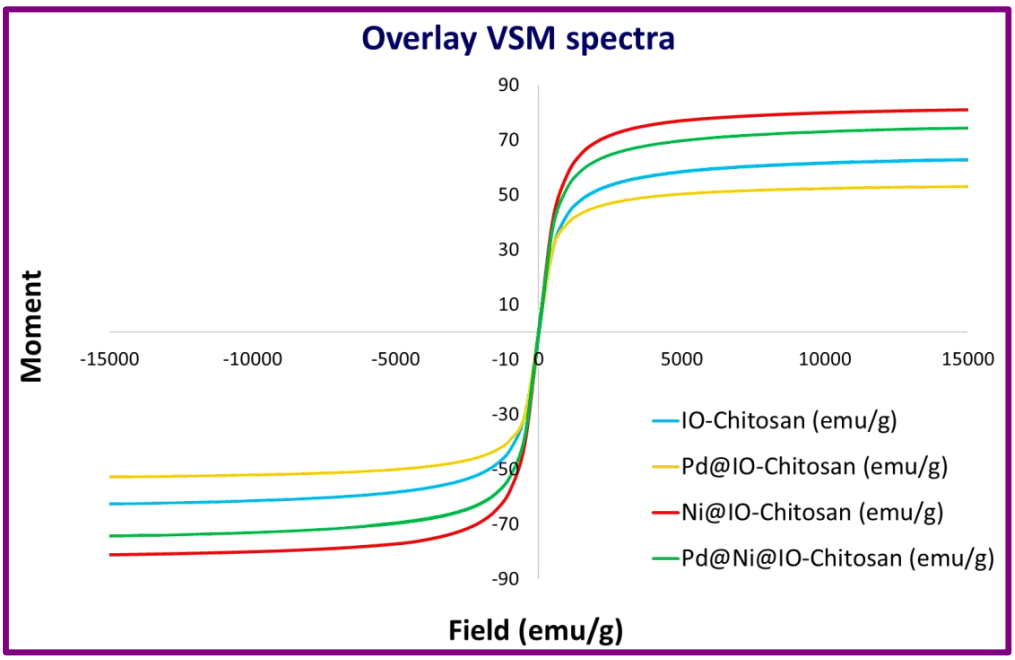

Figure 3.11: *Overlay VSM spectra of IO-Chitosan, Pd@ IO-Chitosan, Ni@ IO-Chitosan and Pd@Ni@IO-Chitosan*

3.3.2. Catalytic performance of Pd@IO-Chitosan and Pd@Ni@IO-Chitosan

3.3.2.1. Catalytic reduction of p-NP in the presence of Pd@IO-Chitosan and Pd@Ni@IO-Chitosan

Catalytic activity of the synthesized nanoacatalysts were evaluated by reduction of p-Nitrophenol (p-NP) to p-Aminophenol (p-AP) by sodium borohydride in aqueous system at room temperature (30-35 ℃) (Figure 3.12). Solution of p-NP exhibits a strong UV absorption peak at 305 nm,

which turns to dark yellow on addition of $NaBH_4$ and absorption peak red shifted to 402 nm due to the formation of p-nitrophenolate under alkaline conditions (Figure 3.12 (A&C)) (Baran & Nasrollahzadeh, 2019). The reaction was a thermodynamically feasible process and was kinetically restricted in the absence of a catalyst (Liu et al., 2016).

Upon the addition of Pd catalyst to the reaction medium, the p-NP absorption peak at 402 nm gradually decreased and completely disappeared after 10 mins with Pd@IO-Chitosan and 8 mins with Pd@Ni@IO-Chitosan. Further, a new absorption band was also observed at 300 nm. (Figure 3.12 (A&C)) At the end of the catalytic reduction, the deep yellow color of the solution changed to colorless. Figure 3.12 (B&D) show the linear relations of $\ln(At/A_0)$ and reaction time (t) in the p-NP reduction. Pseudo-first-order rate was calculated by the equation: $\ln(At/A_0) = -kt$ where A_0 and A_t correspond to the p-NP initial concentration and that at selected reaction time (t), respectively, and $k(min^{-1})$ is the reaction rate. The rate constant was determined as 0.3363 min^{-1} for Pd@IO-Chitosan and 0.4095 min^{-1} for Pd@Ni@IO-Chitosan.

Control experiment with Ni@IO-Chitosan was performed indicated a slight decrease (0.08%) in the concentration of p-NP due to reduction by Ni/NiO nanoparticles (Boonying et al., 2018; Xia et al., 2016). No reduction was observed with IO-Chitosan (Figure 3.12F).

Recyclability potential of both the nanoacatalysts was investigated. The Pd@IO-Chitosan catalyst could be readily recovered by a magnet after each catalytic cycle due to its superparamagnetic nature , was dried in oven and used for the next run. Recyclability experiments showed that Pd@IO-Chitosan has high recovery efficiency and can work up to twenty-four cycles for p-NP reduction. Recyclability experiments with Pd@Ni@IO-Chitosan showed higher recyclability of 27 cycles for p-NP reduction reaction than the Pd@IO-Chitosan. The time required for reduction increased to 14 min for 28 to 29 cycles and later increased to 20 minutes upto 31 cycles.

3.3.2.2. Application of the magnetic palladium catalyst Pd@IO-Chitosan and Pd@Ni@IO-Chitosan in Suzuki−Miyaura Cross-Coupling Reactions.

The potential of the synthesised catalysts was further checked with Suzuki Miyaura C-C coupling reaction. Carbon-carbon bond formation is one of the most important and fundamental reactions for the preparation of molecular scaffolds in organic chemistry. To the best of our knowledge, it is the first time that a Ni-Pd supported on magnetic chitosan is reported as catalyst for Suzuki Miyaura reactions.

In order to improve the yield of the reaction, the effect of different factors like base, solvent, temperature, catalyst amount and time (Figure 3.13) were tested for the model reaction. The cross coupling between iodobenzene and Phenyl boronic acid was selected as a model reaction.

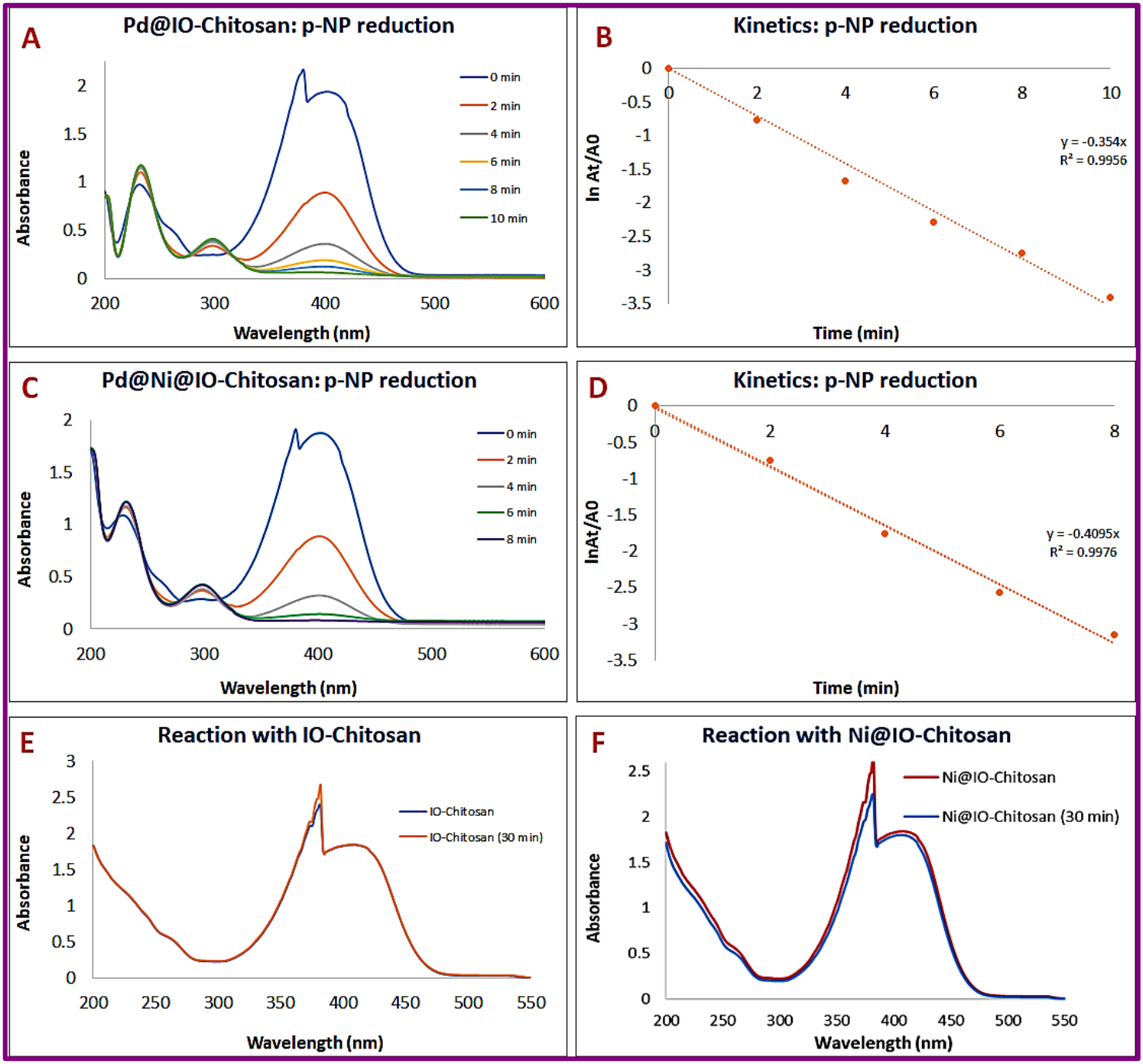

Figure 3.12: (*A) p-Nitrophenol reduction catalysed by Pd@IO-Chitosan, (B) Kinetic study of p-NP reaction catalysed by Pd@IO-Chitosan, (C) p-Nitrophenol reduction catalysed by Pd@Ni@IO-Chitosan, (D) Kinetic study of p-NP reaction catalysed by Pd@Ni@IO-Chitosan, (E) p-Nitrophenol reduction catalysed by IO-Chitosan, (F) p-Nitrophenol reduction catalysed by Ni@IO-Chitosan*

Initially, optimization studies were carried out in water. Different amounts of Phenylboronic acid, ranging from 2.38 to 1.59 mmol. (i.e., 2-1 mol%) was reacted with 1.59 mmol Iodobenzene. Quantitative aryl halide conversion and formation of biphenyl was accomplished using 1.59 mmol phenylboronic acid (i.e.,1 mol%). Use of increased amounts of Phenylboronic acid, led to the presence of unreacted boronic acid. Therefore 1 mol% of phenylboronic acid was used for further studies.

A solvent plays crucial role in improving the rate of coupling reaction. The effect of solvents on the Suzuki coupling reaction was investigated (Figure 3.13A). When water and water:alcohol mixture was used as solvents, good yields of the desirable product was obtained while trace amount of product was obtained in polar aprotic solvents like DMF & THF. Nevertheless, the product yield was 60% with Pd@IO-Chitosan and 5.6% with Pd@Ni@IO-Chitosan when the reaction was done in less polar solvent (toluene). Therefore, water was determined to be the most appropriate selection.

Subsequently the effect of temperature on the reaction yield was investigated. Reactions conducted at room temperature (30 ℃), 40℃, 60℃, 80℃ and 100℃ were most efficient in water and gave 100% yield at all the temperatures (Table 3.1A and 3.1B, entry 1) studied. The optimum reaction temperature for the catalytic conversion of Iodobenzene and Phenyl boronicacid was found to be at ambient temperature. When the temperature was raised to 100 °C, better catalytic performance with other aryl halides (Bromobenzene, Chlorobenzene and substituted Iodo benezene) were obtained (Table3.1A and 3.1B, entries 2-7).

Bases are known play a substantial role in coupling reactions; therefore, the reaction was conducted with different inorganic and organic bases (Figure 3.13B). K_2CO_3 was observed to be a suitable base for generating cross-coupling yield. Sodium hydroxide and potassium hydroxide were not effective under the reaction conditions studied. Different amounts of K_2CO_3 ranging from 5 to 0.1 equivalent were used in Suzuki coupling (Figure 3.13C). Complete conversion was obtained even when 1 mol equivalent of K_2CO_3 with Pd@Ni@IO-Chitosan was used in the reaction while Pd@IO-Chitosan required 2 mol equivalent of base for the completion of reaction. Reducing the K_2CO_3 amount to 1.5 equivalents decreased the yield of the product to ~24%.

Base free reaction in the presence of optimized catalyst and solvent did not yield any product (Table 3.A13 entry 8). The role of the base in these reactions may be to facilitate the formation of a more reactive boronate species or form a part of coordination sphere of Pd to facilitate intramolecular transmetallation which otherwise is reported to be slow (Turkmen et al., 2009).

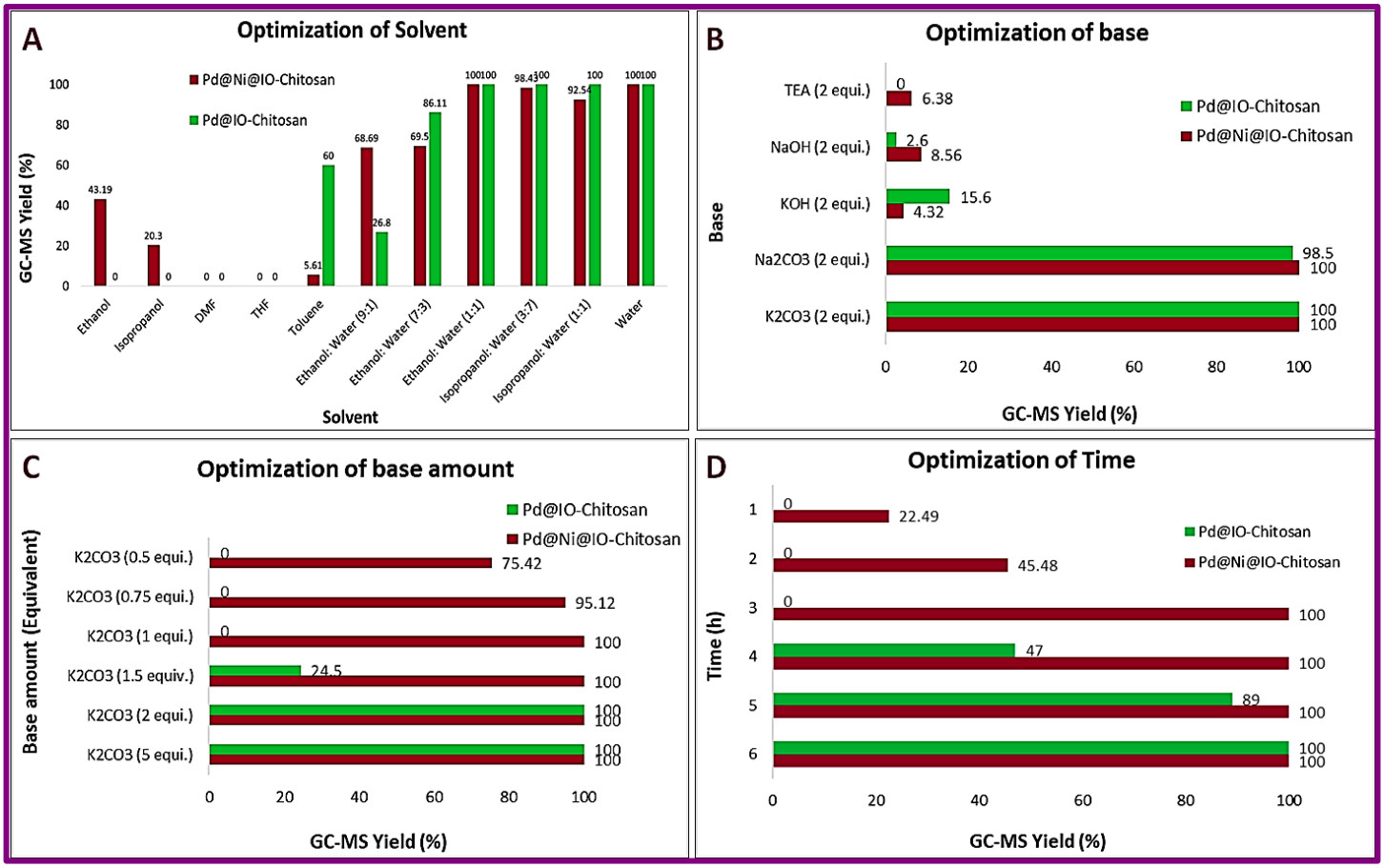

Figure 3.13: Optimization of Suzuki coupling reaction catalyzed by Pd@IO-Chitosan and Pd@Ni@IO-Chitosan, *(A)Optimizations of Solvent, (B) Optimizations of base, (C) Optimizations of base amount, and (D) Optimizations of time for reaction between Iodobenzene and Phenyboronic acid in aqueous medium.* ***Reaction condition:*** *Iodobenzene (1.59 mmol), Phenylboronic acid (1.59 mmol), catalyst dose:1 mg, solvent (10 ml water), Base-* K_2CO_3 (1 equi.), *TLC (n-hexane), GC-MS (HPLC grade chloroform)*

It was observed that quantitative yields were obtained with progressive decrease of catalyst (Pd@IO-Chitosan) loading from 0.275 mol% Pd to 0.00275% Pd (Table 3.A14, entries 1-8) in 12h at 100 °C with 1.59 mmol aryl halide. Monitoring of the reaction time indicated that the reaction was completed in 6 h from the start of the reaction at both 35 °C and 100 °C (Table 3.A15, entries 1-11 and Figures 3.A20-3.A21). The optimized reaction conditions for Pd@IO-Chitosan in water were determined as: iodobenzene,1.59 mmol; phenylboronic acid,1.59 mmol; 0.00275 mol% Pd present as Pd@IO-Chitosan, K_2CO_3, 2 mol equivalent; reaction time, 6h; water 10 mL.

The progress of coupling reaction was monitored by TLC and % conversion was detected using GC-MS. The highest conversion of Suzuki coupling reaction using 1 mg of Pd@Ni@IO-

Chitosan obtained within 3h with 1.59 mmol of starting materials (Table 3.A16, Entry 34). Suzuki coupling of 2.0 mmol Iodobenzene and Phenylboronic acid with 1 mg catalyst (0.0095 mol% Pd) gave 99.9% yield at 100°C as well as at room temperature (Table 3.A16, entry 35). On the other hand reaction performed with Ni@IO-Chitosan as catalyst did not yield any product at 100 ℃ (Table 3.A16, entry 36). The optimized reaction conditions for Pd@Ni@IO-Chitosan in water were determined as: iodobenzene,2 mmol; phenylboronic acid,2 mmol; 0.0095 mol% Pd present as Pd@Ni@IO-Chitosan, K_2CO_3, 2 mmol; reaction time, 3h; water 10 mL.

The applicability of the catalyst under study was further investigated for wider scope of Suzuki reactions. Different arylhalides incorporating electron-rich and electron-poor aromatic rings and Phenylboronic acids were converted into the corresponding biphenyl derivatives using very low amount of catalyst (1 mg), K_2CO_3 as base and water as solvent. This study revealed that Iodobenzene (Table3.1, entry 1) bromobenzene (Table 3.1, entry 6) had almost comparable yields but bromobenzene took a little longer time (7 h for Pd@IO-Chitosan and 6 h for Pd@Ni@IO-Chitosan) for completion of reaction. However, Chlorobenzene (Table3.1, entry 7) reacted slowly with phenylbronic acid (11 h for Pd@IO-Chitosan and 7 h for Pd@Ni@IO-Chitosan).

Researchers have reported three fundamental steps for the Suzuki C-C coupling reaction: oxidative addition, transmetalation, and reductive elimination as demonstrated in chapter 7 scheme 2. Oxidative addition is the rate-determining step in the Pd catalytic cycle and the relative reactivity decreases in the order of I> Br> Cl based mainly on the strength of the C-X bond.

Furthermore, the Iodobenzene having electron-withdrawing group (-CHO) can efficiently couple with phenylboronic acid in comparison to Iodobenzene containing electron-donating group (-CH_3). The electron withdrawing group (-CHO) facilitated the rate limiting oxidative addition step. On the other hand, the ortho-substituted iodobenzene gave slightly lower yields as compared to para substituted. Considering the above discussed reaction protocols, this magnetic catalyst was amenable to a wide range of aryl halides.

Table 3.1: Suzuki Coupling Reaction catalysed by Pd@IO-Chitosan at 30, 60 and 100 °C

Reaction condition For Pd@IO-Chitosan*: Aryl halide (1.59 mmol), phenylboronic acid (1.59 mmol), solvent (10 mL), catalyst (1 mg, 0.005 mol%), base (2 equi.), TLC (9:1 n-hexane: ethyl acetate), GC-MS (HPLC grade chloroform), Yields were obtained by GC-MS analysis*

Reaction condition For Pd@Ni@IO-Chitosan*: Aryl halide (2 mmol), phenylboronic acid (2 mmol), solvent (10 mL), catalyst (1 mg, 0.0095 mol%), base (1 equiv.), TLC (9:1 n-hexane: ethyl acetate), GC-MS (HPLC grade chloroform), Yields were obtained by GC-MS analysis*

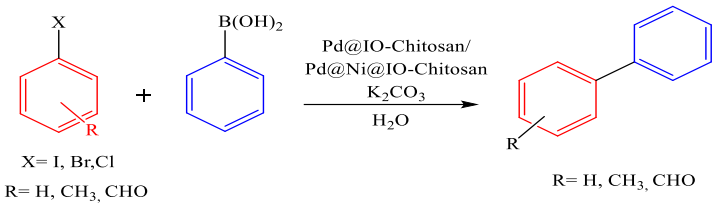

Sr. No.	X	R	At 30 °C Pd@IO-Chitosan/ Pd@Ni@IO-Chitosan		At 60°C Pd@IO-Chitosan/ Pd@Ni@IO-Chitosan		At 100°C Pd@IO-Chitosan/ Pd@Ni@IO-Chitosan		
			Time	GC-MS Yield (%)	Time	GC-MS Yield (%)	Time	GC-MS Yield (%)	Isolated Yield (%)
1	I	H	7 h	99.99	6 h	99.99	6 h.	99.99	99
			5h	100	4h	100	3h	100	99.99
2	I	p-CH_3	12 h	14.91	12 h	58.4	8 h	85.58	85.3
			12h	55.76	10h	75.28	7h	98.96	98.4
3	I	o-CH_3	12 h	7.93	12 h	76.4	9 h	83.10	83.05
			12h	52.938	12h	73.061	9h	92.10	91.8
4	I	o-CHO	20 h	4.52	15 h	78.38	12 h	99.99	99
			15h	54.28	13h	89.697	11h	100	99.99
5	I	p-CHO	12 h.	68.66	12 h	93.2	11 h	99.99	99

			12h	58.81	10h	96.87	8h	100	99.99
6	Br	H	10 h	53.41	8 h	99.5	7 h	99.99	99
			10h	57.98	8h	97.76	6h	100	99.99
7	Cl	H	12 h	10.19	12 h	92.41	11 h	93.65	93.2
			12h	24.51	10h	90.98	7h	100	99.99

A hot filtration experiment was carried out to investigate the heterogenous nature of the catalyst and to obtain information about the presence of leached metal species in our reaction (Figure 3.A51). Under optimized conditions using model coupling reaction between the Iodobenzene and phenylboronic acid, after 2 h the catalyst (Pd@Ni@IO-Chitosan) was separated and the reaction was then continued further for 10 h after catalyst removal. Products were isolated and analyzed with GC-MS. There was no further conversion of the desired product after magnetic removal of the catalyst is detected, ascertaining the heterogeneous nature of the catalyst under study.

3.3.2.3. Recyclability of catalyst

The recyclability and reusability of Pd@IO-Chitosan as catalyst in successive reactions was studied as it is an important requisite from economic, environmental and industrial point of view. The recycling of the catalyst was investigated under optimized reaction conditions using a reaction between Iodobenzene and Phenylboronic acid at 100°C. The catalyst was magnetically separated, washed with water and subsequently with acetone, dried in oven at 100 °C and employed for another round of reactions. Recycled catalysts were characterized by IR, VSM, SEM, TGA and XPS techniques and Pd leaching was tested by ICP-MS.

Pd@IO-Chitosan maintained its activity upto 12 cycles. A 3% decrease in yield was observed during the 13th cycle (Figures 3.A52) and the catalyst (Pd@Ni@IO-Chitosan) proved to be readily recyclable and no significant loss of catalytic activity is observed upto 17 cycles. Also no significant loss of palladium was observed from ICP-MS (Figure 3.17F). A 2.71% decrease in yield was observed during the 18th cycle (Figure 3.A53).

SEM images of Pd@IO-Chitosan revealed negligible change in morphology up to 4 cycles (Figure 3.14C). The SEM images of subsequent cycles exhibited a more porous morphology which could be due to gradual breakdown of chitosan chains.

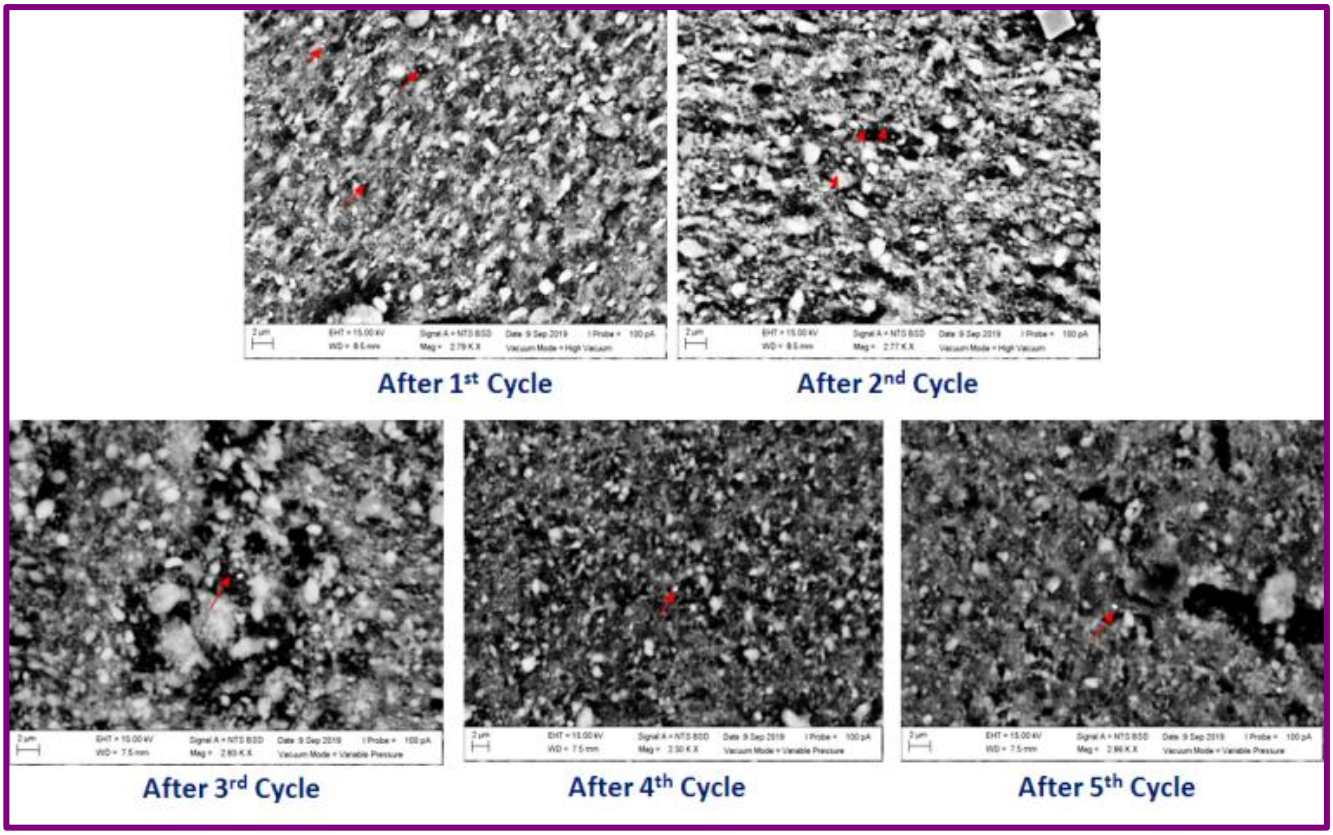

Figure 3.14: *SEM Images of recycled catalyst (Pd@IO-Chitosan)*

SEM images of Recycled Pd@Ni@IO-chitosan (Figure 3.15) catalyst after 17th cycle showed aggregation of nanoparticles.

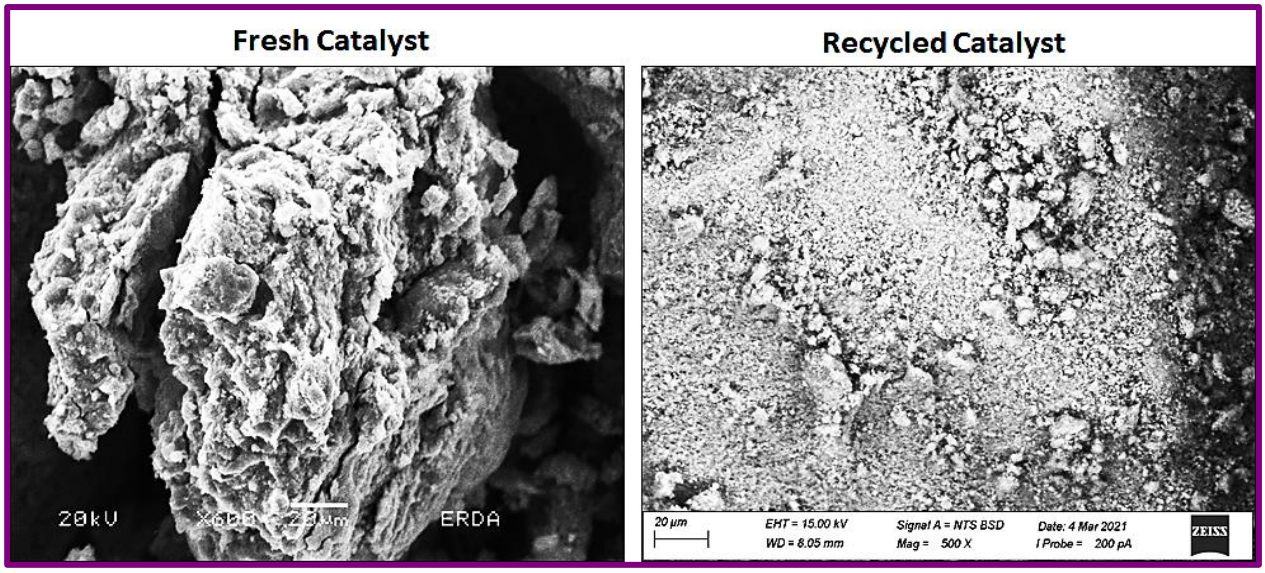

Figure 3.15: *SEM Images of recycled catalyst (Pd@Ni@IO-Chitosan)*

Superparamagnetic property of Pd@IO-Chitosan (Figure 3.16A) was retained even after the 10th cycle. Though the magnetic response decreased to 14 emu/g, the catalyst could be still be easily separated by a handheld magnet and could be uniformly dispersed in reaction system again after

the magnetic separation due to its superparamagnetism. VSM analysis of recycled Pd@Ni@IO-Chitosan catalyst (Figure 3.16B) revealed super paramagnetic response of the recycled catalyst was decreased to 49.49 emu/g from 74.38 emu/g.

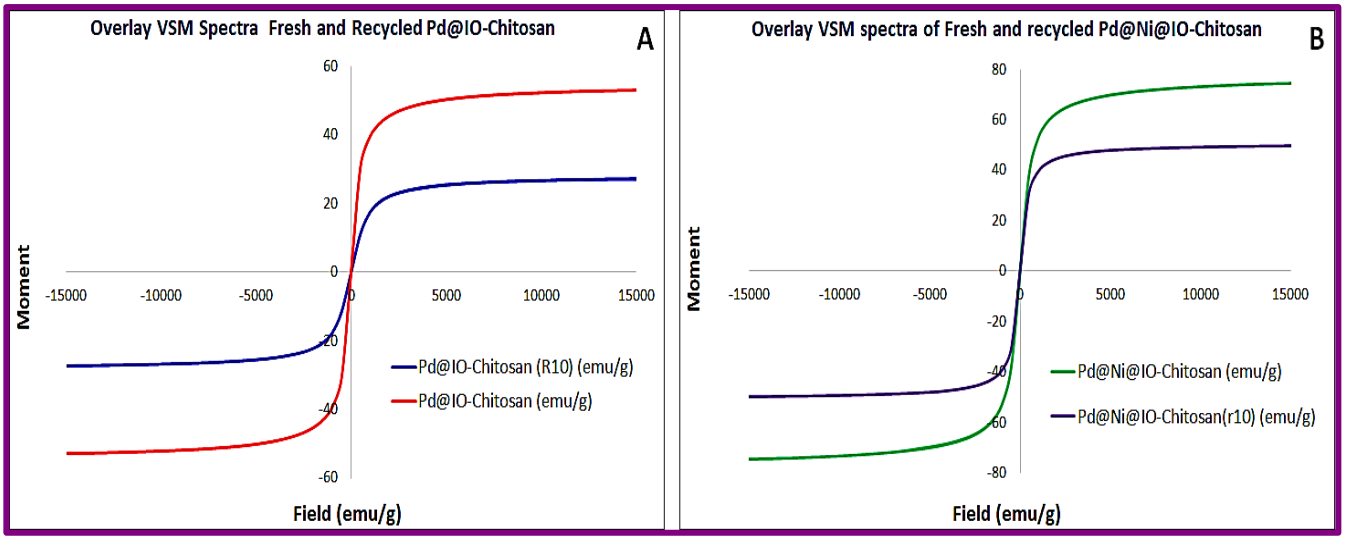

Figure 3.16: *(A) VSM spectra of recycled catalyst (Pd@IO-Chitosan), (B) VSM spectra of recycled catalyst (Pd@Ni@IO-Chitosan)*

The thermogram obtained during thermogravimetric analysis of Pd@IO-Chitosan and Pd@Ni@IO-Chitosan (Figure 3.17) showed 3 stages of weight loss. A total weight loss of about 25% was observed as compared to 25% and 15% in IO-Chitosan and Pd@IO-Chitosan respectively, suggesting loss in thermal stability (Figure 3.17A). While the TG-DTA analysis of fresh and recycled catalyst (Pd@Ni@IO-Chitosan) of 17th cycle ((Figure 3.17B) revealed a total weight loss of 12.8% in and 60.93% respectively in the temperature range of ~30-750 °C.

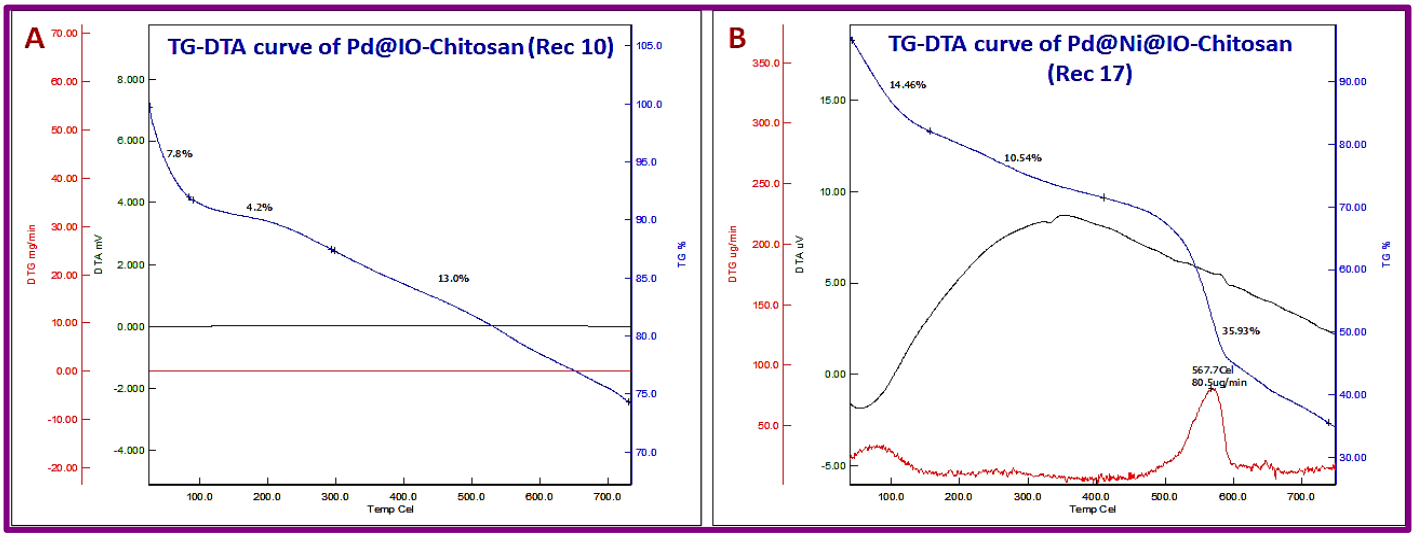

Figure 3.17: *(A) TG-DTA Curve of recycled catalyst (Pd@IO-Chitosan), (B) TG-DTA Curve of recycled catalyst (Pd@Ni@IO-Chitosan)*

The recycled catalyst (Pd@IO-Chitosan) after the 10th run was further investigated by XPS. The Fe and Pd spectra (Figure 3.18(A & B)) exhibited the same characteristic peaks as observed in the fresh catalyst. There was 8% decrease in Fe content and 0.02% decrease in Pd content. There was 3% decrease in nitrogen and 11% increase in C content suggesting a disruption of the chitosan backbone and poisoning of the catalyst with reactants (Figure 3.18 (C&D)). Detailed XPS assignment of the fresh and recycled catalysts is given in Tables 3.A1-3.A5.

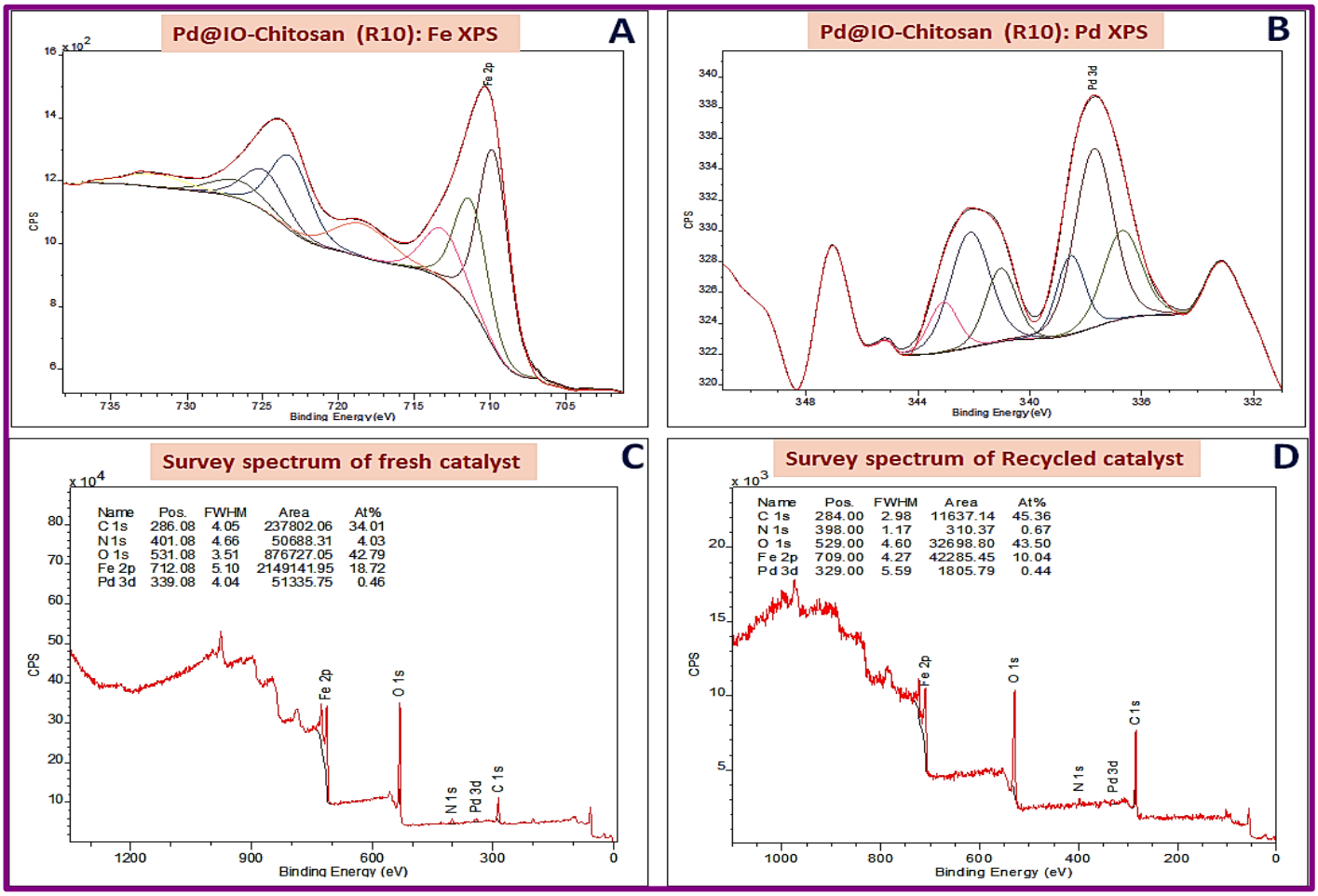

Figure 3.18: *(A&B) Fe and Pd XPS spectra of recycled catalyst after 10th cycle, (C&D) Survey spectrum of fresh and recycled catalyst*

The recycled catalyst Pd@Ni@IO-Chitosan (after the 17th run) was further investigated by XPS (Figure 3.19). The Fe, Ni and Pd spectra (Figure 3.19 (C-E)) exhibited the same characteristic peaks as observed in the fresh catalyst. There was 7.92% decrease in Fe content, 1.29% decrease in nitrogen, 0.01% decrease in Pd, 0.07% decrease in Ni, 4% decrease in O. There was 22% increase in C content suggesting a poisoning of the catalyst with reactants. Detailed XPS assignment of the fresh and recycled catalyst are given in Tables (3.A6-3.A11)

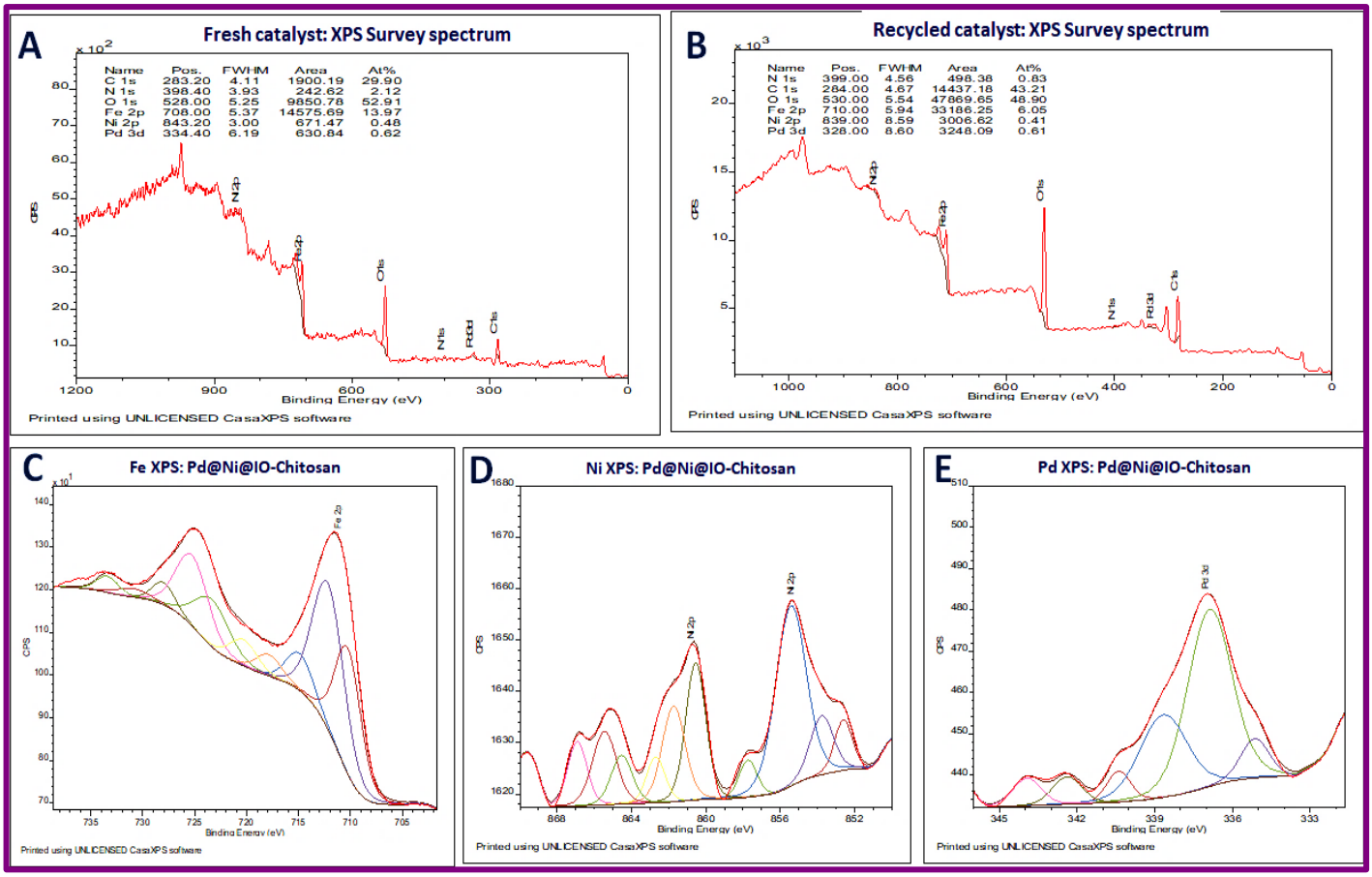

Figure 3.19:*(A) XPS survey spectrum of Fresh catalyst (B) XPS survey spectrum of Recycled catalyst (C) Fe2p XPS spectra of Recycled catalyst (D) Ni2p XPS spectra of Recycled catalyst (E) Pd3d XPS spectra of Recycled catalyst*

3.4. Conclusions

In conclusion, we have fabricated a novel catalytic system comprising Pd nanoparticles supported on Chitosan stabilized Iron oxide nanoparticles (Pd@IO- Chitosan) and Ni dopped Chitosan stabilized Iron oxide nanoparticles (Pd@Ni@IO-Chitosan) at room temperature in aqueous medium without using reducing agent.

Characterization studies of Pd@IO-Chitosan revealed that Pd, Pd^{2+} and PdO dispersed on IO-Chitosan. While characterisation of Pd@Ni@IO-Chitosan confirmed the presence of well dispersed Pd, Pd^{2+}, PdO, Ni, NiO and $Ni(OH)_2$ on support. Both the catalyst showed the excellent catalytic activity for Suzuki coupling reaction and p-Nitrophenol reduction with very high recoverability.

Superparamagnetic property of IO-Chitosan (52.91 emu/g) has increased after loading of Nickel on IO-Chitosan (Ni@IO-Chitosan) (81.07 g/emu). Because of that Pd@Ni@IO-Chitosan (74.38 emu/g) catalyst separation become faster and easier than the Pd@IO-Chitosan (39.037 emu/g).

Therefore, recyclability of the catalyst had increased and Pd@Ni@IO-Chitosan can be reuse for 31 times in p-NP reduction and 17 times in Suzuki coupling reaction. While Pd@IO-DTPA can be reuse upto 24 times in p-NP reduction and 12 times for Suzuki coupling reaction.

Furthermore, combining non noble metal Ni with noble metal Pd can affect the electronic structure of Pd by the electron transfer which can disturb the highest occupied and lowest unoccupied molecular orbitals of Pd and this further reduces the activation energies. So, fabrication of Pd@Ni@IO-DTPA catalyst is potential strategy to enhance the catalytic activity and reusability.

3.5. References

Ahmad, T., Bae, H., Iqbal, Y., Rhee, I., & Hong, S. (2015). Chitosan-coated nickel-ferrite nanoparticles as contrast agents in magnetic resonance imaging. *Journal of Magnetism and Magnetic Materials*, *381*, 151–157. https://doi.org/10.1016/j.jmmm.2014.12.077

Ahmadzadeh, M., Romero, C., & Mccloy, J. (2018). Magnetic analysis of commercial hematite, magnetite, and their mixtures. *AIP ADVANCES*, *8*, 056807. https://doi.org/10.1063/1.5006474

Amendola, V., Meneghetti, M., Granozzi, G., Agnoli, S., Polizzi, S., Riello, P., Boscaini, A., Anselmi, C., Fracasso, G., Colombatti, M., Innocenti, C., Gatteschid, D., & Sangregorio, C. (2011). Top-down synthesis of multifunctional iron oxide nanoparticles for macrophage labelling and manipulation. *J. Mater. Chem.*, *21*, 3803–3813. https://doi.org/10.1039/c0jm03863f

Arumugam, S., Toku, Y., & Ju, Y. (2020). Fabrication of γ -Fe2O3 Nanowires from Abundant and Low-cost Fe Plate for Highly Effective Electrocatalytic Water Splitting. *Scientific Reports*, *10*(1), 5407. https://doi.org/10.1038/s41598-020-62259-6

Bao, G., Bai, J., & Li, C. (2019). Synergistic effect of the Pd–Ni bimetal/carbon nano fiber composite catalyst in Suzuki coupling. *Org. Chem. Front.*, *6*(3), 352–361. https://doi.org/10.1039/c8qo01100a

Baran, T., & Nasrollahzadeh, M. (2019). Facile synthesis of palladium nanoparticles immobilized on magnetic biodegradable microcapsules used as effective and recyclable catalyst in Suzuki-Miyaura reaction and p -nitrophenol reduction. *Carbohydrate Polymers*, *222*, 115029. https://doi.org/10.1016/j.carbpol.2019.115029

Baumgartner, J., Morin, G., Menguy, N., Perez, T., Widdrat, M., Cosmidis, J., & Faivre, D. (2013). Magnetotactic bacteria form magnetite from a phosphate-rich ferric hydroxide via nanometric ferric (oxyhydr) oxide intermediates. *Proc Natl AcadSci*, *1*(20), 14883–14888. https://doi.org/10.1073/pnas.1307119110

Boonying, P., Martwiset, S., & Amnuaypanich, S. (2018). Highly catalytic activity of nickel nanoparticles generated in poly (methylmethacrylate)@ poly (2 - hydroxyethylmethacrylate) (PMMA @ PHEMA) core – shell micelles for the reduction

of 4 - nitrophenol (4 - NP). *Applied Nanoscience*, *8*, 475–488. https://doi.org/10.1007/s13204-018-0669-0

Dong, Y., Bi, J., Ming, S., Zhang, S., Zhu, D., Meng, D., & Li, T. (2021). Functionalized chitosan as a novel support for stabilizing palladium in Suzuki reactions. *Carbohydrate Polymers*, *260*, 117815. https://doi.org/10.1016/j.carbpol.2021.117815

Ghanbari, N., Hoseini, S. J., & Bahrami, M. (2017). Ultrasonic assisted synthesis of palladium-nickel/iron oxide core-shell nanoalloys as effective catalyst for Suzuki-Miyaura and p - nitrophenol reduction reactions. *Ultrasonics - Sonochemistry*, *39*, 467–477. https://doi.org/10.1016/j.ultsonch.2017.05.015

Han, Y. C., Cha, H. G., Kim, C. W., Kim, Y. H., & Kang, Y. S. (2007). Synthesis of Highly Magnetized Iron Nanoparticles by a Solventless Thermal Decomposition Method. *J. Phys. Chem. C*, *111*, 6275–6280. https://doi.org/10.1021/jp0686285

Hsu, T., Hsiung, T., Wang, J., Huang, C., & Wang, H. P. (2010). In situ XANES studies of TiO2/Fe3O4@C during photocatalytic degradation of trichloroethylene. *Nuclear Instruments and Methods in Physics Research A*, *619*, 98–101. https://doi.org/10.1016/j.nima.2009.10.136

Jang, S., Kim, T., & Park, K. H. (2017). Fabrication of crumpled ball-like nickel doped palladium-iron oxide hybrid nanoparticles with controlled morphology as effective catalyst for suzuki-miyaura coupling reaction. *Catalysts*, *7*(9), 247. https://doi.org/10.3390/catal7090247

Jiao, Z. F., Tian, Y. M., Zhang, B., Hao, C. H., Qiao, Y., Wang, Y. X., Qin, Y., Radius, U., Braunschweig, H., Marder, T. B., Guo, X. N., & Guo, X. Y. (2020). High photocatalytic activity of a NiO nanodot-decorated Pd/SiC catalyst for the Suzuki-Miyaura cross-coupling of aryl bromides and chlorides in air under visible light. *Journal of Catalysis*, *389*, 517–524. https://doi.org/10.1016/j.jcat.2020.06.025

Jie, Z., Ying, X., Nian, B., & Wu, C. (2008). Hydrothermal synthesis and self-assembly of magnetite (Fe3O4) nanoparticles with the magnetic and electrochemical properties. *Journal of Crystal Growth*, *310*, 5453–5457. https://doi.org/10.1016/j.jcrysgro.2008.08.064

Kim, W., Suh, C., Cho, S., Roh, K., Kwon, H., Song, K., & Shon, I. (2012). A new method for the identification and quantification of magnetite – maghemite mixture using conventional X-ray diffraction technique. *Talanta*, *94*, 348–352. https://doi.org/10.1016/j.talanta.2012.03.001

Kolen, Y. V, Ban, M., Rodr, C., Carbo, E., Sailsman, A., Pin, Y., Fa, M., Petrovykh, D. Y., Kovnir, K., Lebedev, O. I., & Rivas, J. (2014). Large-Scale Synthesis of Colloidal Fe3O4 Nanoparticles Exhibiting High Heating Efficiency in Magnetic Hyperthermia. *J. Phys. Chem. C*, *118*, 8691–8701. https://doi.org/10.1021/jp500816u |

Kong, H., Song, J., & Jang, J. (2010). One-step fabrication of magnetic c-Fe2O3/polyrhodanine nanoparticles using in situ chemical oxidation polymerization and their antibacterial properties. *Chem. Commun.*, *46*, 6735–6737. https://doi.org/10.1039/c0cc00736f

Liu, L., Chen, R., Liu, W., Wu, J., & Gao, D. (2016). Catalytic reduction of 4-nitrophenol over Ni-Pd nanodimers supported on nitrogen-doped reduced graphene oxide. *Journal of Hazardous Materials*, *320*, 96–104. https://doi.org/10.1016/j.jhazmat.2016.08.019

Nan, L., Yalan, C., Jixiang, L., Dujuan, O., Wenhui, D., Rouhi, J., & Mustapha, M. (2020). Carbonylative Suzuki – Miyaura cross-coupling by immobilized Ni@Pd NPs supported on carbon nanotubes. *RSC Adv.*, *10*, 27923–27931. https://doi.org/10.1039/d0ra03915b

Neelabh, S., & Srivastava, P. C. (2010). Realizing NiO nanocrystals from a simple chemical method. *Bull. Mater. Sci.*, *33*(6), 653–656. https://doi.org/10.1007/s12034-011-0142-0

Parandhaman, T., Pentela, N., Ramalingam, B., Samanta, D., & Das, S. K. (2017). Metal Nanoparticle Loaded Magnetic-Chitosan Microsphere: Water Dispersible and Easily Separable Hybrid Metal Nano-biomaterial for Catalytic Applications. *ACS Sustainable Chem. Eng*, *5*, 489–501. https://doi.org/10.1021/acssuschemeng.6b01862

Park, J., Kang, E., Son, S. U., Park, H. M., Lee, M. K., Kim, J., Kim, K. W., Noh, H. J., Park, J. H., Bae, C. J., Park, J. G., & Hyeon, T. (2005). Monodisperse nanoparticles of Ni and NiO: Synthesis, characterization, self-assembled superlattices, and catalytic applications in the suzuki coupling reaction. *Advanced Materials*, *17*(4), 429–434. https://doi.org/10.1002/adma.200400611

Piquer, C., Roca, A. G., Boada, R., Guglieri, C., & Chaboy, J. (2014). Fe K - Edge X - ray Absorption Spectroscopy Study of Nanosized Nominal Magnetite. *J. Phys. Chem. C*, *118*, 1332–1346. https://doi.org/10.1021/jp4104992

Rai, R. K., Gupta, K., Behrens, S., Li, J., Xu, Q., & Singh, S. K. (2015). Highly Active Bimetallic Nickel – Palladium Alloy Nanoparticle Catalyzed Suzuki – Miyaura Reactions. *ChemCatChem*, *7*, 1806–1812. https://doi.org/10.1002/cctc.201500145

Rai, R. K., Gupta, K., Tyagi, D., Mahata, A., Behrens, S., Yang, X., Xu, Q., Pathak, B., & Singh, S. K. (2016). Access to highly active Ni-Pd bimetallic nanoparticle catalysts for C-C coupling reactions. *Catalysis Science and Technology*, *6*(14), 5567–5579. https://doi.org/10.1039/c6cy00037a

Richardson, J. T., Scates, R., & Twigg, M. V. (2003). X-ray diffraction study of nickel oxide reduction by hydrogen. *Applied Catalysis A : General*, *246*, 137–150. https://doi.org/10.1016/S0926-860X(02)00669-5

Sedghi, R., Heidari, B., Shahmohamadi, H., Zarshenas, P., & Varma, R. S. (2019). Pd nanocatalyst adorned on magnetic chitosan@N-Heterocyclic carbene: Eco-compatible suzuki cross-coupling reaction. *Molecules*, *24*(17), 3048. https://doi.org/10.3390/molecules24173048

Seth, K., Purohit, P., & Chakraborti, A. K. (2014). Cooperative Catalysis by Palladium−Nickel Binary Nanocluster for Suzuki−Miyaura Reaction of Ortho -Heterocycle-Tethered Sterically Hindered Aryl Bromides. *Organic Letters*, *16*, 2334–2337. https://doi.org/10.1021/ol500587m

Shaw, S. K., Alla, S. K., Meena, S. S., Mandal, R. K., & Prasad, N. K. (2017). Stabilization of temperature during magnetic hyperthermia by Ce substituted magnetite nanoparticles. *Journal of Magnetism and Magnetic Materials*, *434*, 181–186.

https://doi.org/10.1016/j.jmmm.2017.03.055

Su, N., Chen, X., Ren, Y., Yue, B., Wang, H., Cai, W., & He, H. (2015). The facile synthesis of single crystalline palladium arrow-headed tripods and their application in formic acid electro-oxidation. *Chem. Commun.*, *51*, 7195–7198. https://doi.org/10.1039/C5CC00353A

Tsyrul, P. G., Afonasenko, T. N., Koshcheev, S. V, & Boronin, A. I. (2007). State of Palladium in Palladium–Aluminosilicate Catalysts As Studied by XPS and the Catalytic Activity of the Catalysts in the Deep Oxidation of Methane. *Kinetics and Catalysis*, *48*(5), 778–784. https://doi.org/10.1134/S0023158407050187

Turkmen, H., Can, R., & Bekir Cetinkaya. (2009). Aqueous-phase Suzuki–Miyaura cross-coupling reactions catalyzed by Pd-NHC complexes. *Dalton Transactions*, *35*, 7039–7044. https://doi.org/10.1039/B907032J

Unsoy, G., Yalcin, S., Khodadust, R., Gunduz, G., & Gunduz, U. (2012). Synthesis optimization and characterization of chitosan- coated iron oxide nanoparticles produced for biomedical applications. *J Nanopart Res*, *14*, 964. https://doi.org/10.1007/s11051-012-0964-8

Veisi, H., Najafi, S., & Hemmati, S. (2018). Pd(II)/Pd(0) anchored to magnetic nanoparticles (Fe3O4) modified with biguanidine-chitosan polymer as a novel nanocatalyst for Suzuki-Miyaura coupling reactions. *International Journal of Biological Macromolecules*, *113*(1), 186–194. https://doi.org/10.1016/j.ijbiomac.2018.02.120

Verma, C. J., Pandey, R. K., & Prakash, R. (2018). In situ one step synthesis of Fe inserted octaethylporphyrin / polyindole : A multifunctional hybrid material with improved electrochemical and electrical properties. *Materials Science & Engineering B*, *227*, 80–88. https://doi.org/10.1016/j.mseb.2017.10.015

Xia, J., He, G., Zhang, L., Sun, X., & Wang, X. (2016). Hydrogenation of nitrophenols catalyzed by carbon black-supported nickel nanoparticles under mild conditions. *Applied Catalysis B: Environmental*, *180*, 408–415. https://doi.org/10.1016/j.apcatb.2015.06.043

Yang, F., Chi, C., Dong, S., Wang, C., Jia, X., Ren, L., Zhang, Y., Zhang, L., & Li, Y. (2015). Pd/PdO nanoparticles supported on carbon nanotubes: A highly effective catalyst for promoting Suzuki reaction in water. *Catalysis Today*, *256*, 186–192. https://doi.org/10.1016/j.cattod.2015.02.026

Zhou, J., Dong, Z., Yang, H., Shi, Z., Zhou, X., & Li, R. (2013). Pd immobilized on magnetic chitosan as a heterogeneous catalyst for acetalization and hydrogenation reactions. *Applied Surface Science*, *279*, 360–366. https://doi.org/10.1016/j.apsusc.2013.04.113

Appendix

XPS data of Pd@IO-chitosan

Table 3.A1: XPS Spectral assignment of Carbon

ReElement	IO-Chitosan		Fresh Pd@IO-chitosan		Recycled(10) Pd@IO-chitosan		Assignment
	Binding energy (eV)	Area%	Binding energy (eV)	Area%	Binding energy (eV)	Area%	
C 1s	284.8	16.88	284.8	39.06	284.76	59.23	C-C/C-H
C 1s	286.69	20.20	286.32	27.40	285.95		C-O-C , C-OH, C-O, C-NH_2
C 1s					287.07	8.94	C=O
C 1s	288.73	40.21	288.01	23.68	288.54	6.88	O-C-O, O-C=O
C 1s	290.99	22.72	289.57	9.87			N-C=O

Table 3.A2: XPS Spectral assignment of Nitrogen

Re Element	IO-Chitosan		Fresh Pd@IO-chitosan		Recycled(10) Pd@IO-chitosan		Assignment
	Binding energy (eV)	Area%	Binding energy (eV)	Area%	Binding energy (eV)	Area%	
N1s	399.47	38.95	399.81	38.45	399.2	33.43	O=C-NH
N1s	401.52	6.63	400.54	54.97	400.6	65.75	C-N
N1s	402.75	38.95	402.21	38.45	402.77	0.82	NH_2-Fe

Table 3.A3: XPS Spectral assignment of Oxygen

ReElement	IO-Chitosan		Fresh Pd@IO-chitosan		Recycled(10) Pd@IO-chitosan		Assignment
	Binding energy (eV)	Area%	Binding energy (eV)	Area%	Binding energy (eV)	Area%	
O 1s	528.14	14.28					Surface oxygen
O 1s	529.60	17.91	530.32	39.21	529.99	57.53	Bulk Fe-O, Pd-O
O 1s	531.49	38.60	531.77	40.00	531.82	28.44	N-C=O
O 1s	533.25	29.21	533.24	20.79	533.17	14.03	C-OH, C-O-C

Table 3.A4: XPS Spectral assignment of Iron

ReElement	IO-Chitosan		Fresh Pd@IO-chitosan		Recycled(10) Pd@IO-chitosan		Assignment
	Binding Energy (eV)	Area%	Binding Energy (eV)	Area%	Binding Energy (eV)	Area%	
Fe2p3/2	710.90	14.10	710.92	27.78	709.77 711.28	9.58 5.58	Fe^{3+}
Fe2p3/2	713.29	21.27	712.60	14.02	713.12	3.18	Fe^{3+}
Fe2p3/2	715.17	13.90	714.32	11.27			Satellite
Fe2p3/2	717.46	7.61	717.05	4.88			Satellite
Fe2p3/2	720.80	10.13	719.89	8.09	718.47	51.04	Satellite
Fe2p1/2					723.17	4.79	
Fe2p1/2	723.90	7.05	723.92	13.89	724.86	2.79	
Fe2p1/2	726.29	10.64	725.60	7.01	726.59	1.59	
Fe2p1/2	728.17	6.95	727.32	5.64			
Fe2p1/2	730.46	3.80	729.61	3.58			Satellite
Fe2p1/2	734.11	4.55	733.48	3.84	732.14	21.45	Satellite

Table 3.A5: XPS Spectral assignment of Palladium

Element	Fresh Pd@IO-chitosan		Recycled(10) Pd@IO-chitosan		Assignment
	Binding Energy (eV)	Area%	Binding Energy (eV)	Area%	
Pd3d5/2	336.73	9.02	336.70	16.20	Charged Pd metallic nanoclusters
			337.70	33.17	Pd-O
Pd3d5/2	338.44	32.40	338.64	10.63	PdO, Pd^{2+}
Pd3d5/2	339.43	20.67			Strong Pd –IO chitosan interactions
Pd3d3/2	341.73	6.01	341.04	10.80	
Pd3d3/2	343.64	20.36	342.14	22.11	
Pd3d3/2	344.62	11.53	343.09	7.09	

XPS data of Pd@Ni@IO-chitosan

Table 3.A6: XPS Spectral assignment of Carbon

Element	Ni@IO-Chitosan		Pd@Ni@IO-Chitosan		Pd@Ni@IO-Chitosan (r10)		Interpretation
C1s	Peak	Area%	Peak	Area%	Peak	Area%	
C1s	284.80	55.11	284.79	60.39	284.80	43.36	C-C/C-H
C1s	285.49	26.78	286.17	24.24	285.60	33.84	C-O-C, C-OH, C-O, C-NH_2
C1s	286.67	11.02	287.15	11.37	286.79	13.85	C=O
C1s	288.47	7.09	288.39	4.00	288.27	8.95	O-C-O, O-C=O

Table 3.A7: XPS Spectral assignment of Nitrogen

Element	Ni@IO-Chitosan		Pd@Ni@IO-Chitosan		Pd@Ni@IO-Chitosan (r10)		Interpretation
N1s	Peak	Area%	Peak	Area%	Peak	Area%	
N1s	399.29	54.33	398.20	24.95	398.24	21.29	O=C-NH
N1s	400.24	35.74	399.68	52.09	400.14	17.82	C-N
N1s	401.82	9.93	401.97	22.96	402.82	60.89	NH_2-Fe

Table 3.A8: XPS Spectral assignment of Oxygen

Element	Ni@IO-Chitosan		Pd@Ni@IO-Chitosan		Pd@Ni@IO-Chitosan (r10)		Interpretation
O 1s	Peak	Area%	Peak	Area%	Peak	Area%	
O 1s	529.70	55.36	529.59	55.95	529.60	19.72	Bulk Fe-O, Pd-O
O 1s	530.80	23.21	531.11	25.27	531.24	52.11	N-C=O
O 1s	532.38	21.43	532.47	18.78	532.85	28.18	C-OH, C-O-C

Table 3.A9: XPS Spectral assignment of iron

Element	Ni@IO-Chitosan		Pd@Ni@IO-Chitosan		Pd@Ni@IO-Chitosan (r10)		Interpretation
	Peak	Area%	Peak	Area%	Peak	Area%	
Fe2p3/2	710.16	33.00	710.00	25.91	710.25	16.53	Fe^{3+} octahedral
Fe2p3/2	711.97	19.00	711.86	14.55	712.12	22.98	Fe^{3+} octahedral
Fe2p3/2	714.13	5.10	713.48	10.00	714.93	5.00	Fe^{3+} Tetrahedral
Fe2p3/2	716.99	4.01	716.99	7.32	717.88	2.87	Fe^{2+} octahedral
Fe2p3/2	719.19	4.35	719.85	6.49	720.33	3.61	Satellite peak of Fe^{3+} 2p3/2
Fe2p1/2	723.26	16.50	723.00	12.95	723.35	15.97	Fe^{3+} octahedral
Fe2p1/2	725.07	9.50	724.86	7.27	725.25	22.20	Fe^{3+} octahedral
Fe2p1/2	727.23	2.55	726.48	5.00	728.03	4.83	Fe^{3+} Tetrahedral
Fe2p1/2	730.09	2.01	728.54	3.16	730.98	2.65	Fe^{2+} octahedral 2p3/2
Fe2p1/2	733.60	3.98	732.61	7.34	733.43	3.48	Satellite peak of Fe^{3+} 2p3/2

Table 3.A10: XPS Spectral assignment of Nickel

Elememt	Ni@IO-Chitosan		Pd@Ni@IO-Chitosan		Pd@Ni@IO-Chitosan (r10)		Interpretation
	Peak	Area%	Peak	Area%	Peak	Area%	
Ni2p3/2	852.58	1.18	852.18	3.87	852.60	4.92	Ni metal
Ni2p3/2	854.35	10.22	854.62	20.68	853.76	7.54	NiO
Ni2p3/2	855.29	25.16	855.99	7.57	855.42	30.02	
Ni2p3/2	857.33	9.77	857.23	3.55	857.73	3.65	
Ni2p3/2	858.90	7.85	859.94	8.39	860.54	15.07	$Ni(OH)_2$
Ni2p3/2	860.77	11.77	861.00	6.48	861.73	12.03	satellite (Ni metal)
Ni2p3/2	862.38	20.13	862.36	17.93	862.69	4.66	satellite (higher oxidation state of Ni
Ni2p3/2	864.47	4.45	863.74	14.99	864.52	5.68	satellite
Ni2p3/2			864.86	8.12	865.45	9.65	
Ni2p3/2	866.54	9.48	866.64	8.42	866.91	6.78	satellite (NiO)

Table 3.A11: XPS Spectral assignment of Palladium

	Pd@Ni@IO-Chitosan		Pd@Ni@IO-Chitosan (r10)		Interpretation
	Peak	Area%	Peak	Area%	
Pd3d5/2	334.94	21.09	335.14	7.3	Pd (0)
Pd3d5/2	336.81	19.39	336.88	51.51	Pd (2+)
Pd3d5/2	337.79	19.52	338.67	25.75	PdO
Pd3d3/2	340.34	14.06	340.40	4.87	Pd (0)
Pd3d3/2	342.61	12.93	342.38	5.35	Pd (2+)
Pd3d3/2	343.39	13.01	343.93	5.22	PdO

GC –MS Spectra of standard Biphenyl

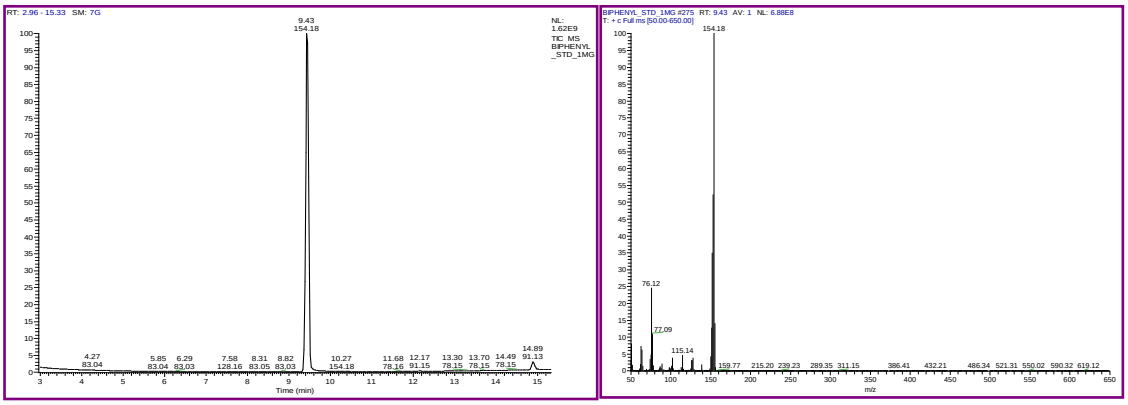

Figure 3.A1 *GC –MS Spectra of standard Biphenyl;* **RT:** 9.49 min **Molecular weight:** 154.18 gm/mol

GC –MS Spectra of standard Iodobenzene

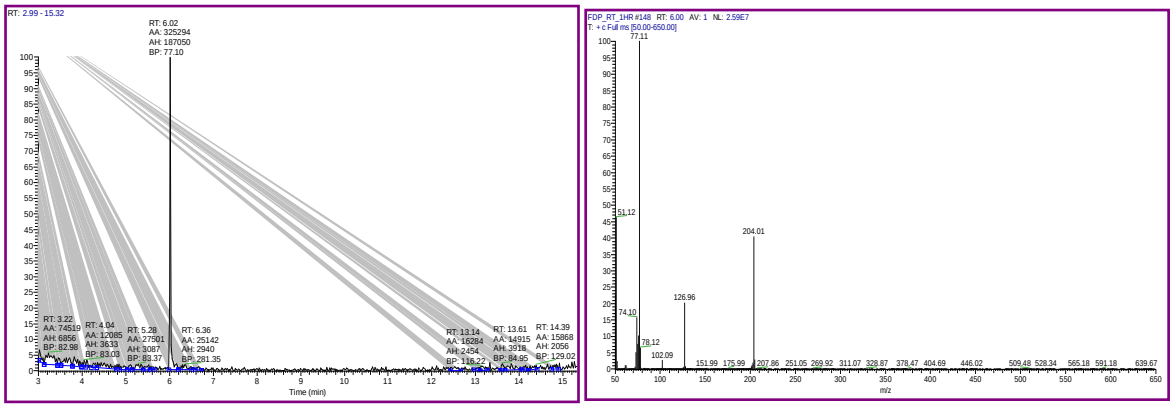

Figure 3.A2 *GC –MS Spectra of Iodobenzene;* **RT:** 6.02 min **Molecular weight:** 204.01 gm/mol

GC-MS spectra of optimization of Suzuki coupling reaction using Pd@IO-Chitosan

GC MS spectra during screening of solvent for the reaction between Iodobenzene and phenylboronic acid (Figures 3.A3-12)

Polar aprotic and alcoholic solvent was not showing a good yield. However, alcoholic solvents with water showing a good quantitative yield. It was observed that reaction in water as a solvent leading to quantitative yield (>99%) of biphenyl after 6 h. Ethanol and isopropanol as co-solvents with water in the ratio 9:1, 7:3, 1:1, 3:7 respectively also gave quantitative yield of biphenyl.

Table 3.A12 Optimization of solvent and temperature

Entry	Catalyst [mg(mol%)]	Solvent	Base	Temp °C	Time (h)	GC-MS Yield
1.	1	Ethanol	K_2CO_3 (2 equiv.)	60	12	0%
2.	1	Isopropanol	K_2CO_3 (2 equiv.)	60	12	0%
3.	1	Toluene	K_2CO_3 (2 equiv.)	60	12	60%
4.	1	Toluene	K_2CO_3 (2 equiv.)	35	12	0%
5.	1	DMF	K_2CO_3 (2 equiv.)	60	12	0%
6.	1	THF	K_2CO_3 (2 equiv.)	60	12	0%
7.	1	Ethanol:water(9:1)	K_2CO_3 (2 equiv.)	60	12	>99%
8.	1	Ethanol:water(7:3)	K_2CO_3 (2 equiv.)	60	12	>99%
9.	1	Ethanol:water(1:1)	K_2CO_3 (2 equiv.)	60	12	>99%
10.	1	Ethanol:water(3:7)	K_2CO_3 (2 equiv.)	60	12	>99%
11.	1	Ethanol:water(9:1)	K_2CO_3 (2 equiv.)	35	12	26.28%
12.	1	Ethanol:water(7:3)	K_2CO_3 (2 equiv.)	35	12	86.11%
13.	1	Ethanol:water(1:1)	K_2CO_3 (2 equiv.)	35	12	>99%
14.	1	Isopropanol: water (1:1)	K_2CO_3 (2 equiv.)	60	12	>99%
15.	1	Isopropanol: water (7:3)	K_2CO_3 (2 equiv.)	60	12	>99%
16.	1	Isopropanol: water (1:1)	K_2CO_3 (2 equiv.)	35	12	>99%
17.	1	Water	K_2CO_3 (2 equiv.)	100	12	>99%
18.	1	Water	K_2CO_3 (2 equiv.)	100	6	>99%
19.	1	Water	K_2CO_3 (2 equiv.)	75	6	>99%
20.	1	Water	K_2CO_3 (2 equiv.)	60	6	>99%
21.	1	Water	K_2CO_3 (2 equiv.)	50	6	>99%
22.	1	Water	K_2CO_3 (2 equiv.)	35	6	>99%

Reaction conditions: Iodobenzene (1.59 mmol), phenylboronic acid (1.59 mmol), solvent (10 ml), catalyst (1 mg), base (2 equiv.), TLC (n-hexane), GC-MS (HPLC grade chloroform), Yields were obtained by GC-MS analysis (Figs. S7 to S16 show the representative GC MS spectra of standard biphenyl and products obtained in respective solvents)

Toluene (Figure 3.A3)

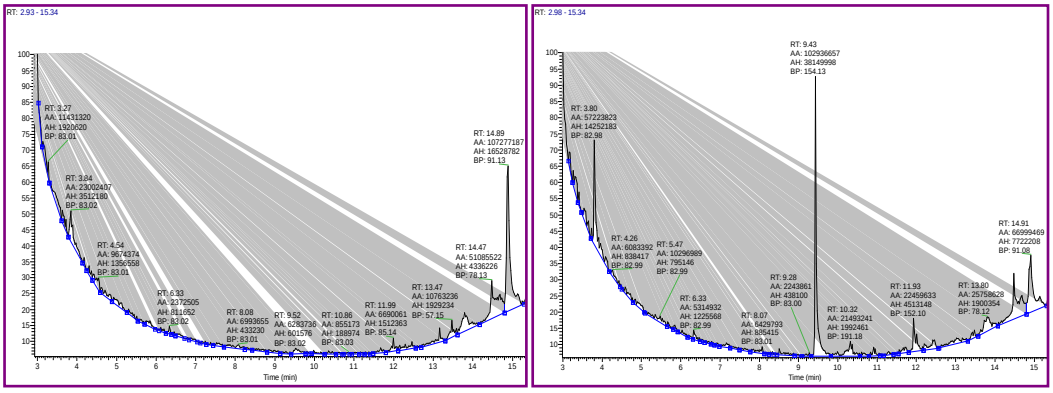

At 60 C At 35°C

Figure 3.A4: THF

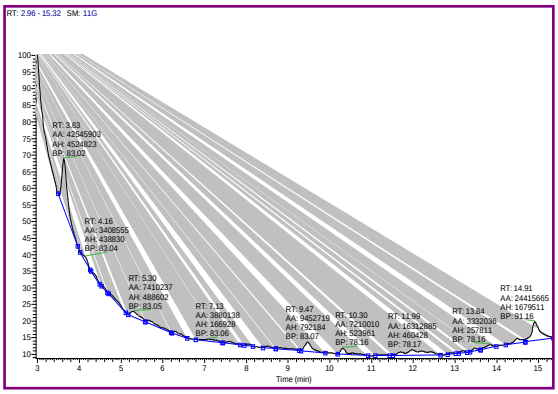

Figure 3.A5: Ethanol

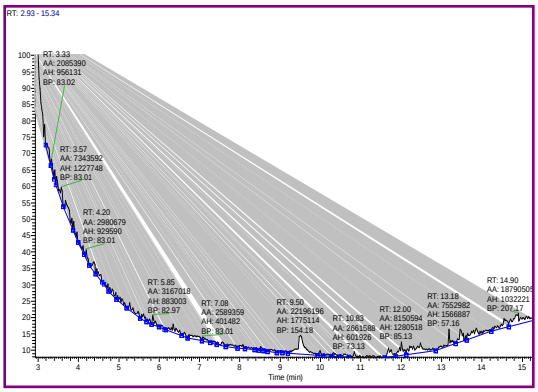

Figure 3.A6: Isopropropanol

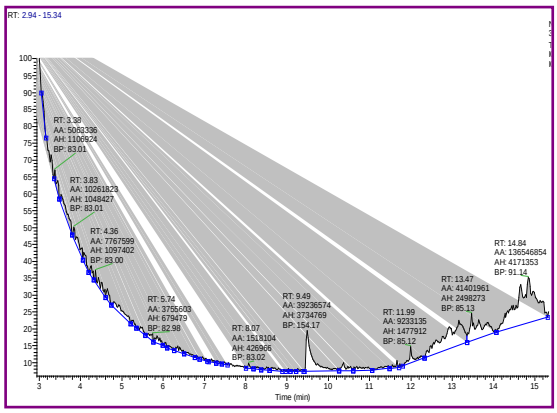

Ethanol:Water

It was observed that as the amount of water increases formation of biphenyl increases Figure 3.A7-3.A9. In the absence of water negligible amount of yield was obtained. Temperature also played an important role, as the temperature increases selectively biphenyl is formed.

Figure 3.A7: EtOH: H_2O (9:1)

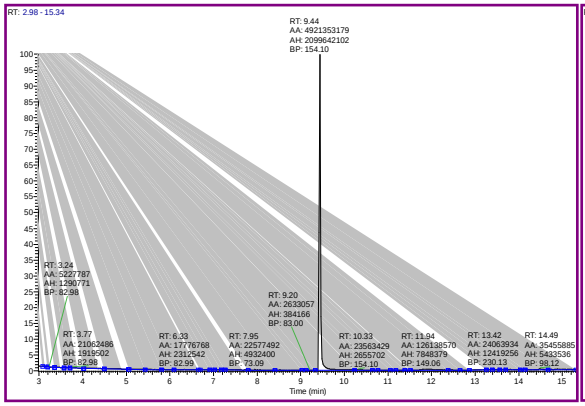

At 60 C

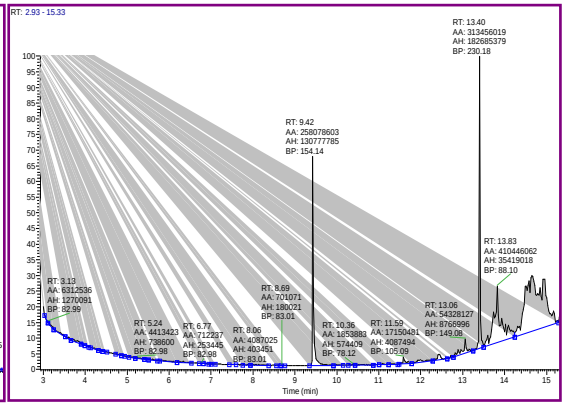

At 35°C

Figure 3.A8: EtOH: H_2O (7:3)

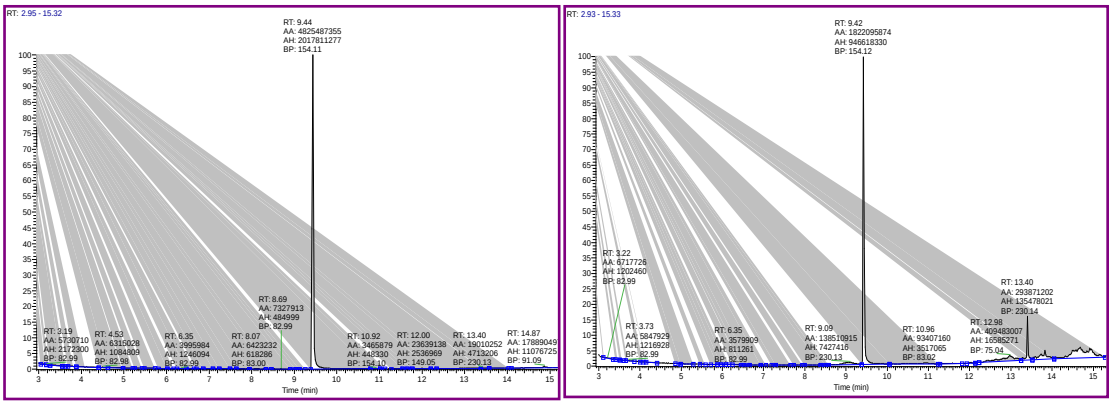

At 60°C At 35°C

Figure 3.A9: EtOH: H_2O (5:5)

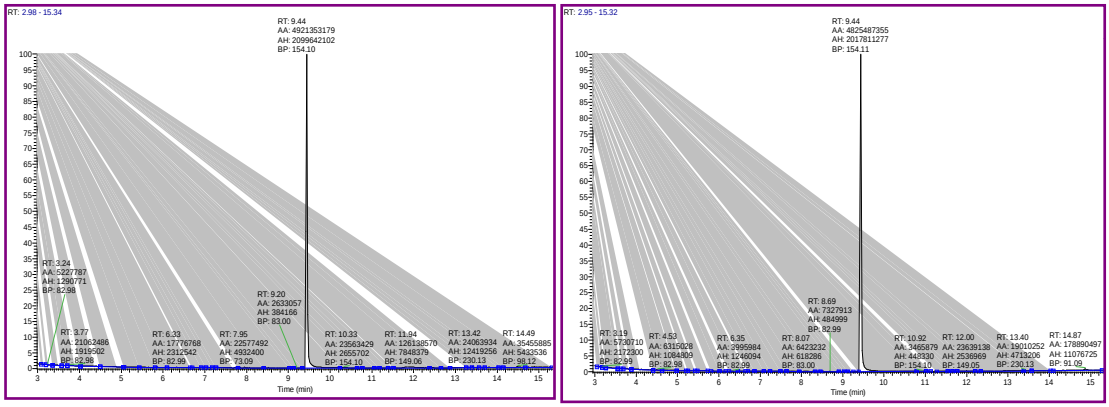

At 60°C At 35°C

Figure 3.A10: EtOH: H_2O (3:7)

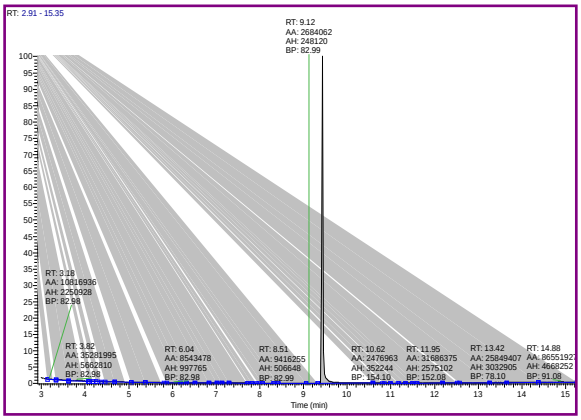

Figure 3.A11: Isopropanol:Water (6:4)

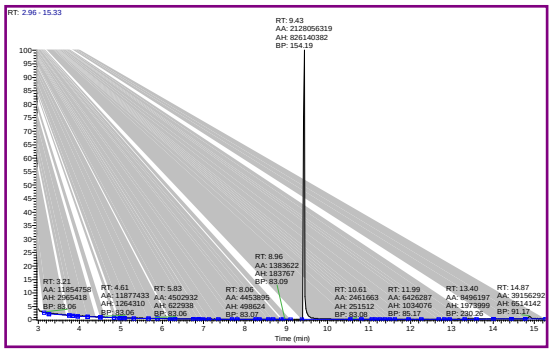

Figure 3.A12: Water

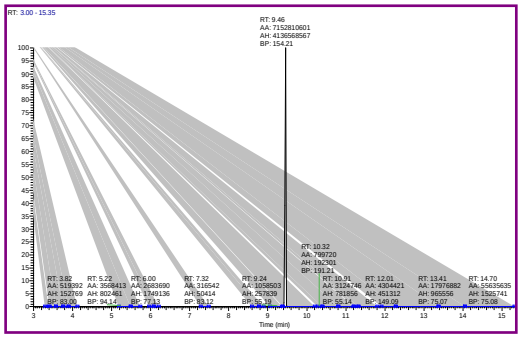

At 100 ℃

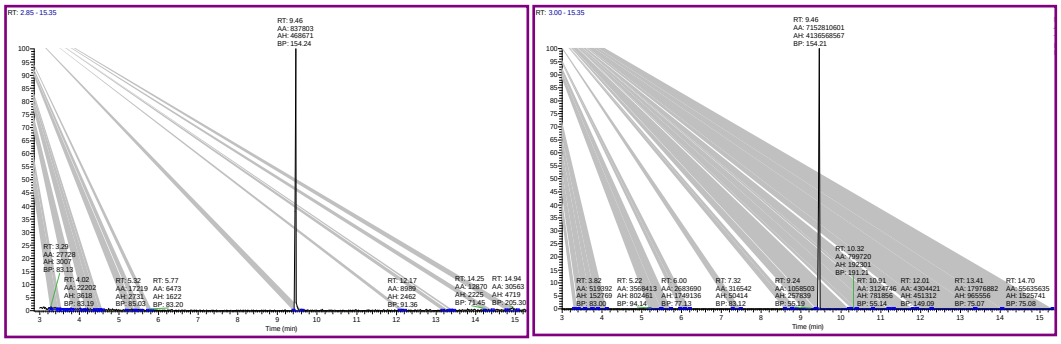

At 60°C At 35°C

Reaction in absence of iodobenzene

Recycling of catalyst was carried out using Phenyl boronic acid (1.59 mmol), K_2CO_3 (3.18 mmol), Pd@IO-chitosan (1 mg) and H_2O (10 ml) at 60°C and at 35°C under stirring for 6 h. Figure 3.A13 show that homocoupling of phenylboronic acid was not observed which is reported to be a dominant reaction, which gradually subsides as the temperature rises.

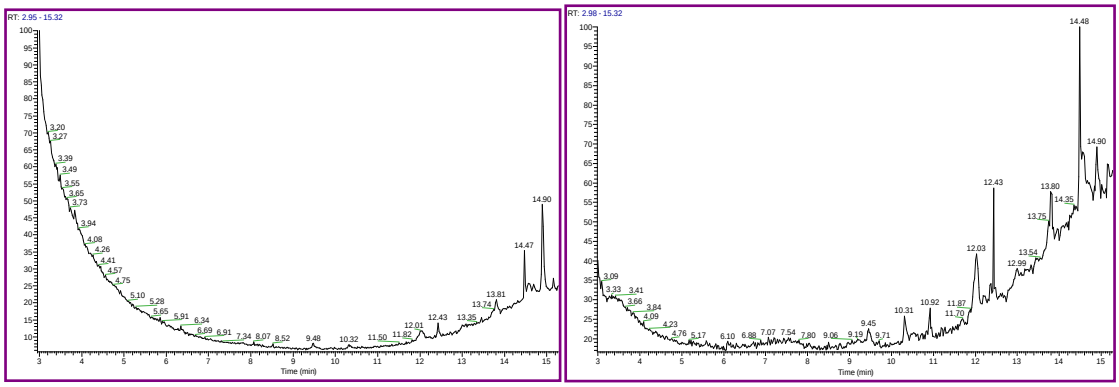

At 60°C *At 35°C*

Figure 3.A13*: GC-MS spectra of the product for Pd@IO-Chitosan catalysed reaction in absence of iodobenzene performed at 60 °C and at 35 °C*

GC MS spectra during screening of base for the reaction between iodo benzene and phenylboronic acid (Figures 3.A14 to 3.A18)

Screening of bases such as K_2CO_3, Na_2CO_3, NaOH, KOH and Et_3N was performed and it revealed that highest yield could be obtained by the use of 2 equiv. K_2CO_3 and Na_2CO_3 as base.

Table 3.A13: Optimization of Base

Entry	Catalyst [mg(mol%)]	Solvent	Base	Temp °C	Time (h)	GC-MS Yield
1.	1	Water	K_2CO_3 (2 equiv.)	100	6	>99%
2.	1	Water	Na_2CO_3 (2 equiv.)	100	6	98.5%
3.	1	Water	KOH (2 equiv.)	100	6	15.6%
4.	1	Water	NaOH (2 equiv.)	100	6	2.6%
5.	1	Water	Et_3N (2 equiv.)	100	6	0%
6.	1	Water	K_2CO_3 (1.5 equiv.)	35	6.5	24.5%
7.	1	Water	K_2CO_3 (1 equiv.)	35	6.5	0%
8.	1	Water	No base	100	12	0%

Figure 3.A14: KOH

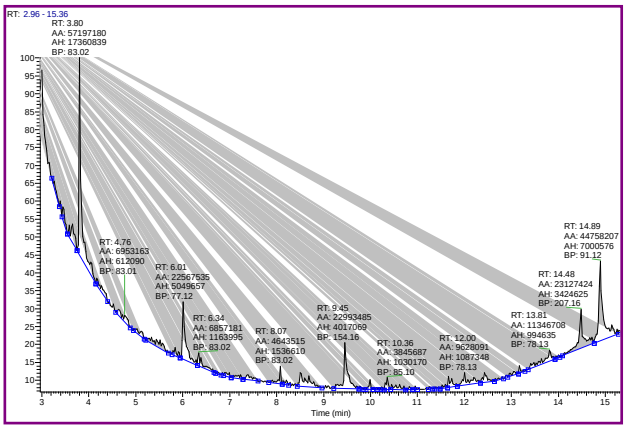

Figure 3.A15 NaOH

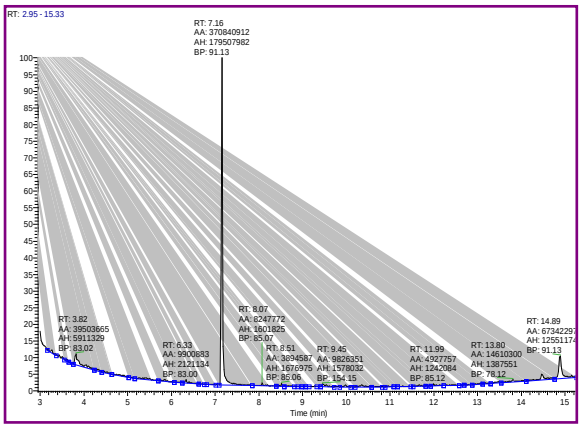

Figure 3.A16: Na_2CO_3

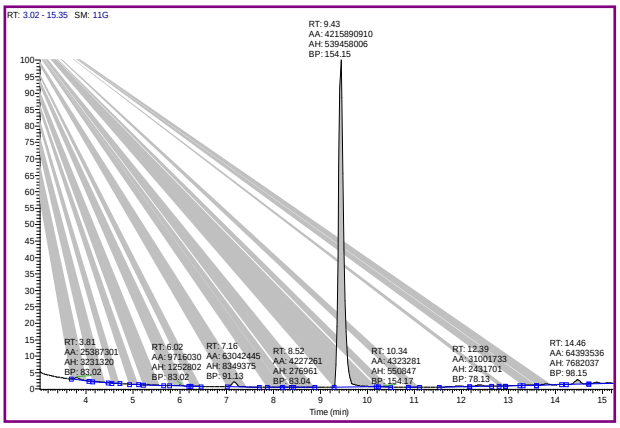

Figure 3.A17 Triethylamine

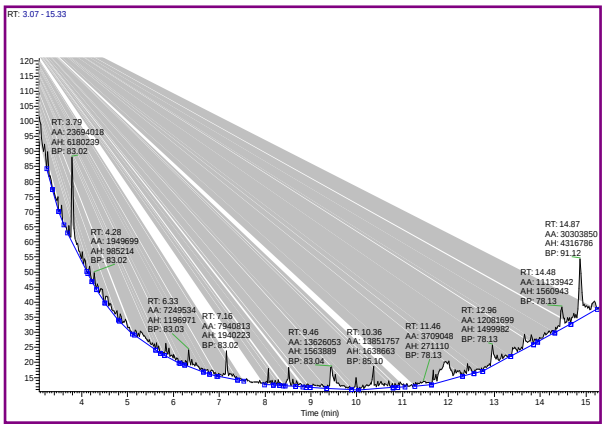

Figure 3.A18: K_2CO_3

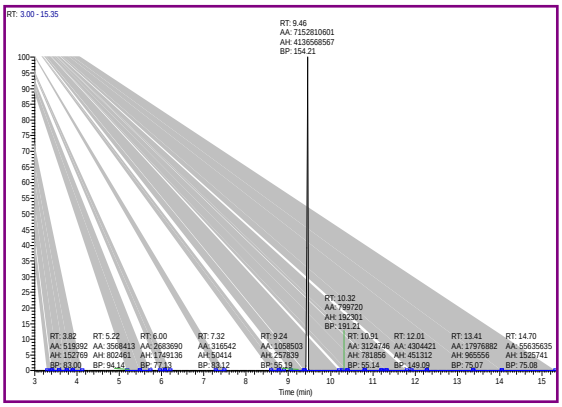

Optimization of amount of catalyst.

It was observed that coupling of 1.59 mmol Iodobenzene and 1.59 mmol Phenylboronic acid gave same results at 100 to 35 °C (i.e, Room temperature) with 1 mg of Catalyst. Reaction with 2 mmol Iodobenzene and Phenylboronic acid requires more catalyst for the completion of the

reaction at room temperature but 1 mg catalyst is enough for the reaction at 100 °C and gave 99% yield.

Table 3.A14: Optimization of amount of catalyst

Entry	Catalyst [mg(mol%)]	Solvent	Base	Temp (°C)	Time (h)	GC-MS Yield
1.	50 (0.27 mol% Pd)	Water	K_2CO_3 (5 equiv.)	100	12	>99%
2.	25 (0.13 mol% Pd)	Water	K_2CO_3 (5 equiv.)	100	12	>99%
3.	10 (0.05 mol% Pd)	Water	K_2CO_3 (5 equiv.)	100	12	>99%
4.	5 (0.027 mol% Pd)	Water	K_2CO_3 (5 equiv.)	100	12	>99%
5.	2 (0.01 mol% Pd)	Water	K_2CO_3 (5 equiv.)	100	12	>99%
6.	1 (0.0055 mol% Pd)	Water	K_2CO_3 (5 equiv.)	100	12	>99%
7.	0.5 (0.00275 mol% Pd)	Water	K_2CO_3 (5 equiv.)	100	12	>99%
8.	0.5 (0.00275 mol% Pd)	Water (N_2 atmosphere)	K_2CO_3 (2 equiv.)	100	12	>99%
9.	1 mg IO-Chitosan	Water	K_2CO_3 (2 equiv.)	100	12	0%
10.	1 mg $PdCl_2$	Water	K_2CO_3 (2 equiv.)	100	12	>99%
11.	1 mg $PdCl_2$	Water	K_2CO_3 (2 equiv.)	35	12	>99%
12.	No Catalyst	Water	K_2CO_3 (2 equiv.)	100	12	0%

Reaction conditions: Iodobenzene (1.59 mmol), phenylboronic acid (1.59 mmol), solvent (10 ml), temperature (100 C), reaction time (12h), TLC (n-hexane), GC-MS (HPLC grade chloroform), Yields were obtained by GC-MS analysis

Reaction with 2 mmol Starting material and 1 mg catalyst at 100 °C (Figure 3.A19)

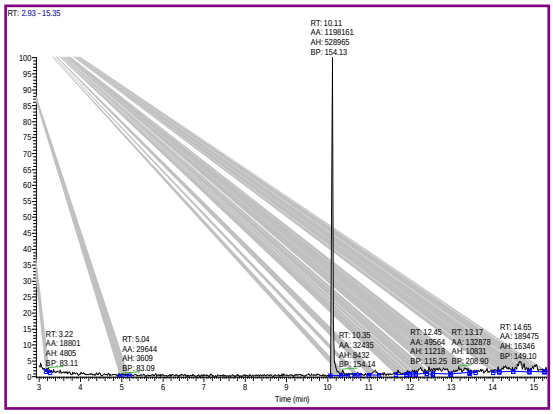

Optimization of Time:

Time study of Pd@IO-Chitosan catalysed reaction between iodobenzene and phenyl boronic acid performed at 35°C and at 100 °C. It was observed that reaction takes 6 hours for completion (Figures 3.A20-21)

Table 3.A15: Optimization of Time for C-C Coupling

Entry	Catalyst [mg(mol%)]	Solvent	Base	Temp (°C)	Time (h)	GC-MS Yield
1.	1	Water	K_2CO_3 (2 equiv.)	100	7	>99%
2.	1	Water	K_2CO_3 (2 equiv.)	100	6	>99%
3.	1	Water	K_2CO_3 (2 equiv.)	100	5	96.51%
4.	1	Water	K_2CO_3 (2 equiv.)	100	4	49.45%
5.	1	Water	K_2CO_3 (2 equiv.)	100	1	0%
6.	1	Water	K_2CO_3 (2 equiv.)	35	6	>99%
7.	1	Water	K_2CO_3 (2 equiv.)	35	5	89%
8.	1	Water	K_2CO_3 (2 equiv.)	35	4	47%
9.	1	Water	K_2CO_3 (2 equiv.)	35	3	0%
10.	1	Water	K_2CO_3 (2 equiv.)	35	2	0%
11.	1	Water	K_2CO_3 (2 equiv.)	35	1	0%

Reaction conditions: Iodobenzene (1.59 mmol), phenylboronic acid (1.59 mmol), solvent (10 mL), temperature (100°C& RT), TLC (n-hexane), GC-MS (HPLC grade chloroform), Yields were obtained by GC-MS analysis

Time study

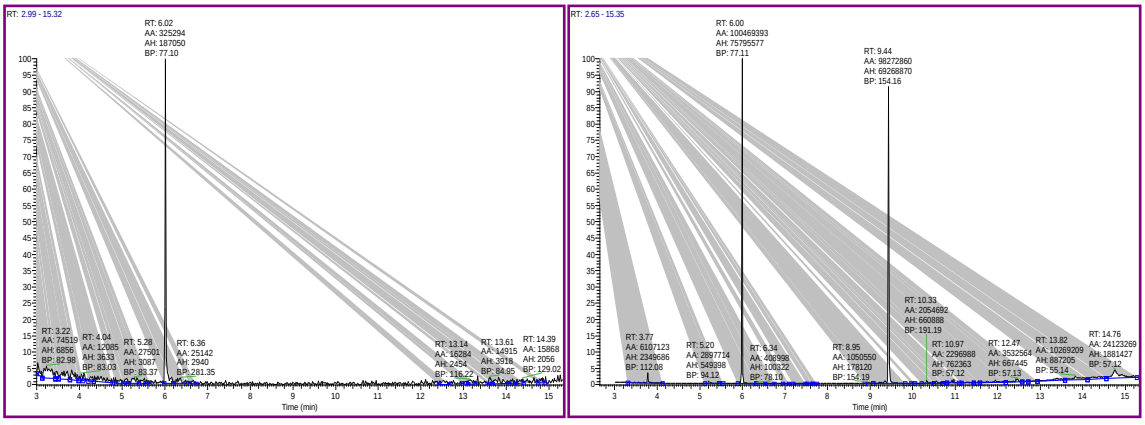

1 hour **4 hours**

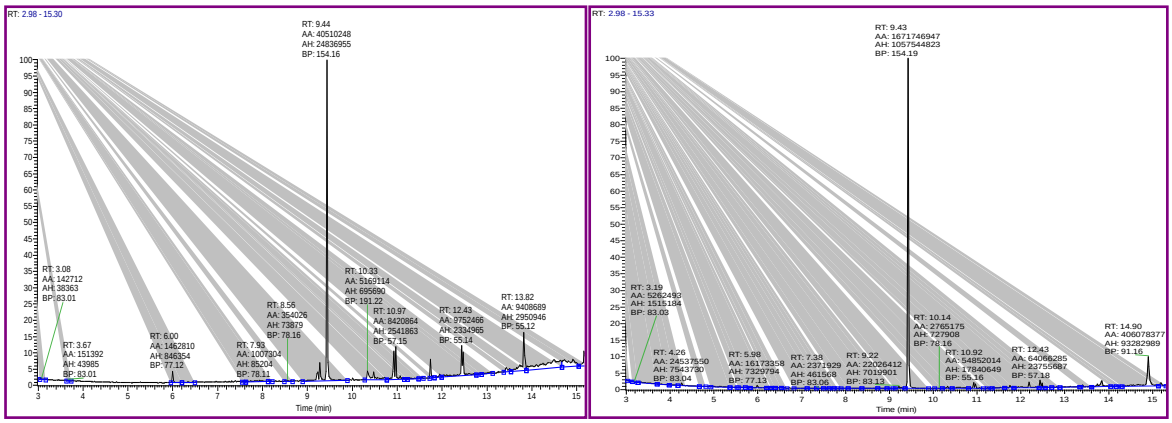

5 hours **6 hours**

Figure 3.A21: *GC-MS spectra of the product for Pd@IO-Chitosan catalysed reaction between iodobenzene and phenyl boronic acid performed at 100 °C in the time range 1 to 6 hours*

GC-MS spectra of the product for Pd@IO-Chitosan catalysed reaction between 2-methyliodobenzene and phenyl boronic acid performed at 100 °C for 15 hours.

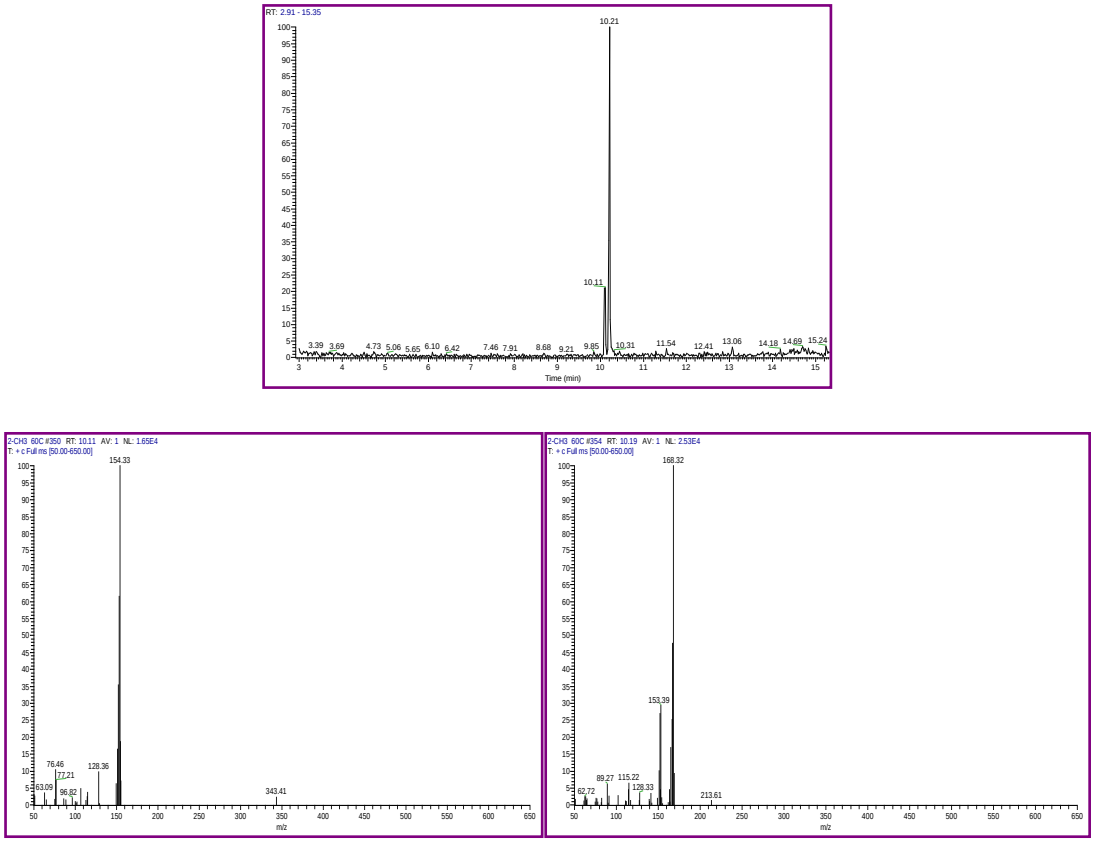

Figure 3.A22: GC-MS spectra of the(2-methyl-1,1'-Biphenyl) at 100°C for 15 h

GC-MS spectra of the product for Pd@IO-Chitosan catalysed reaction between 4-methyliodobenzene and phenyl boronic acid performed at 100 °C for 15 hours

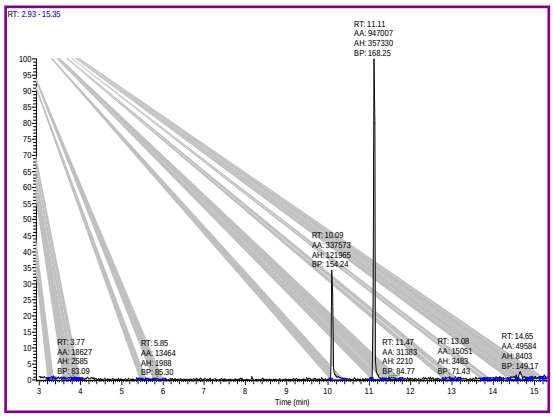

***Figure* 3.A23**: GC-MS spectra of the (4-methyl-1,1'-Biphenyl) at 100°C for 15 h

GC-MS spectra of optimization of Suzuki coupling reaction using Pd@Ni@IO-Chitosan

Table 3.A16: Optimization of Suzuki coupling reaction

Sr. No.	Catalyst (mg)	Solvent	Base	Temp (°C)	Time (h)	GC-MS Yield
Optimization of Solvent						
1.	1	Ethanol	K_2CO_3 (2 equi.)	80	12	43.19
2.	1	Isopropanol	K_2CO_3 (2 equi.)	80	12	20.30
3.	1	DMF	K_2CO_3 (2 equi.)	100	12	trace
4.	1	THF	K_2CO_3 (2 equi.)	80	12	trace
5.	1	Toluene	K_2CO_3 (2 equi.)	100	12	5.61
6.	1	Ethanol: Water (3:7)	K_2CO_3 (2 equi.)	80	12	68.69
7.	1	Ethanol: Water (1:1)	K_2CO_3 (2 equi.)	80	12	69.50
8.	1	Isopropanol: Water (3:7)	K_2CO_3 (2 equi.)	80	12	98.43
9.	1	Isopropanol: Water (1:1)	K_2CO_3 (2 equi.)	80	12	92.54
10.	1	Water	K_2CO_3 (2 equi.)	80	12	100
Optimization of temperature						
11.	1	Water	K_2CO_3 (2 equi.)	100	12	100
12.	1	Water	K_2CO_3 (2 equi.)	80	12	100
13.	1	Water	K_2CO_3 (2 equi.)	60	12	100
14.	1	Water	K_2CO_3 (2 equi.)	40	12	100
15.	1	Water	K_2CO_3 (2 equi.)	30	12	100
Optimization of Base						
16.	1	Water	K_2CO_3 (2 equi.)	30	12	100
17.	1	Water	Na_2CO_3 (2 equi.)	30	12	100
18.	1	Water	KOH (2 equi.)	30	12	0
19.	1	Water	NaOH (2 equi.)	30	12	0

20.	1	Water	TEA (2 equi.)	30	12	0
Optimization of amount of base						
21.	1	Water	K_2CO_3 (5 equi.)	30	12	100
22.	1	Water	K_2CO_3 (2 equi.)	30	12	100
23.	1	Water	K_2CO_3 (1 equi.)	30	12	100
24.	1	Water	K_2CO_3 (0.75 equi.)	30	12	95.12
25.	1	Water	K_2CO_3 (0.5 equi.)	30	12	75.42
Optimization of Time						
26.	1	Water	K_2CO_3 (1 equi.)	30	12	100
27.	1	Water	K_2CO_3 (1 equi.)	30	10	100
28.	1	Water	K_2CO_3 (1 equi.)	30	8	100
29.	1	Water	K_2CO_3 (1 equi.)	30	6	100
30.	1	Water	K_2CO_3 (1 equi.)	30	4	100
31.	1	Water	K_2CO_3 (1 equi.)	30	3	100
32.	1	Water	K_2CO_3 (1 equi.)	30	2	45.48
33.	1	Water	K_2CO_3 (1 equi.)	30	1	22.49
Optimization of amount of catalyst						
34.	1 mg (0.012 mol%) (with 1.59 mmol starting material	Water	K_2CO_3 (2 equi.)	30	4	100
35.	1 mg (with 2 mmol starting material)	Water	K_2CO_3 (2 equi.)	30	4	100
36.	1 mg Ni@IO-Chitosan	Water	K_2CO_3 (2 equi.)	100	12	0
37.	No catalyst	Water	K_2CO_3 (2 equi.)	100	12	0

Reaction conditions: Iodobenzene (2 mmol), phenylboronic acid (2 mmol), solvent (10 ml), catalyst (1 mg), base (1 equiv.), TLC (n-hexane), GC-MS (HPLC grade chloroform), Yields were obtained by GC-MS analysis

GC MS spectra during screening of solvent for the reaction between Iodobenzene and phenylboronic acid (Figures 3.A24)

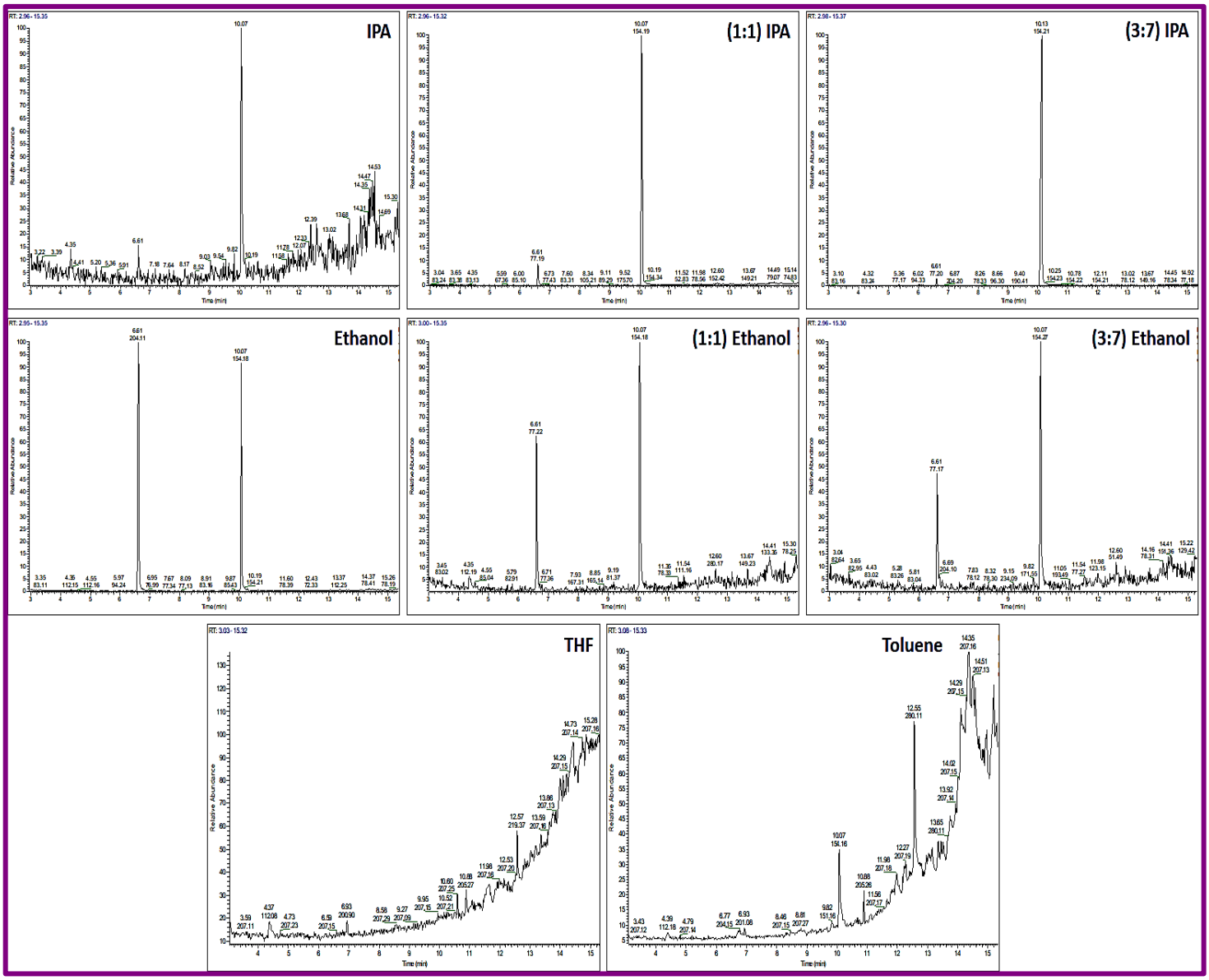

Figure 3.A24: *GC-MS spectra of the product for Pd@Ni@IO-Chitosan catalysed reaction between iodobenzene and phenylboronic acid performed using K_2CO_3 as a base at 100°C and at 80°C*

GC MS spectra during Optimization of temperature for the reaction between Iodobenzene and phenylboronic acid (Figure 3.A25)

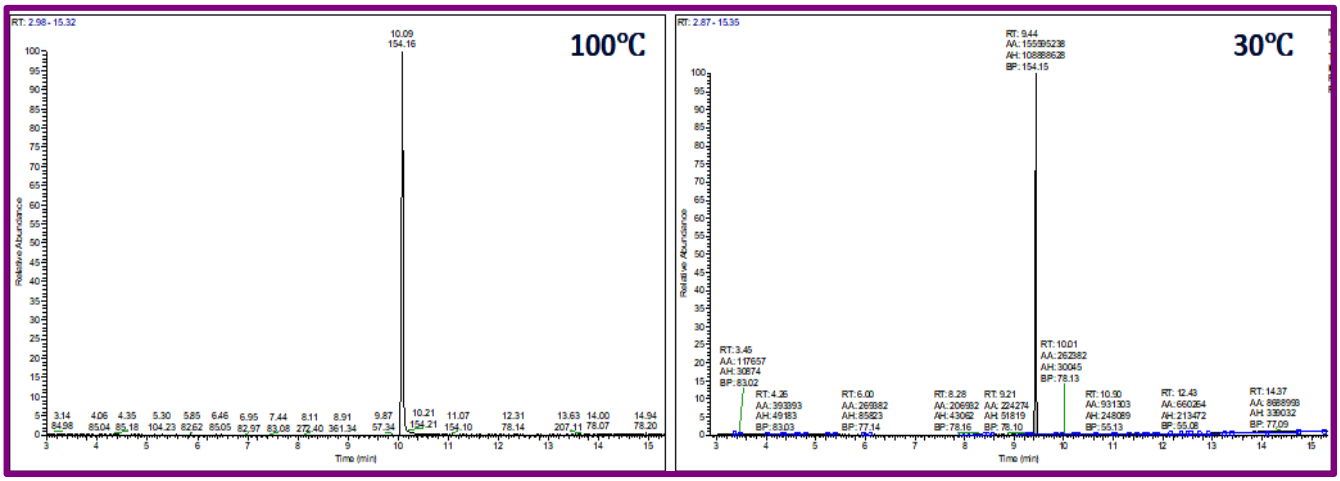

Figure 3.A25*: GC-MS spectra of the product for Pd@Ni@IO-Chitosan catalysed reaction between iodobenzene and phenylboronic acid performed using K_2CO_3 as a base and water as a solvent at 100°C and at 30°C*

GC MS spectra during Optimization of Base for the reaction between Iodobenzene and phenylboronic acid (Figures 3.A26) Screening of bases such as K_2CO_3, Na_2CO_3, NaOH, KOH and Et_3N was performed and it revealed that highest yield could be obtained by the use of 2 equiv. K_2CO_3 and Na_2CO_3 as base.

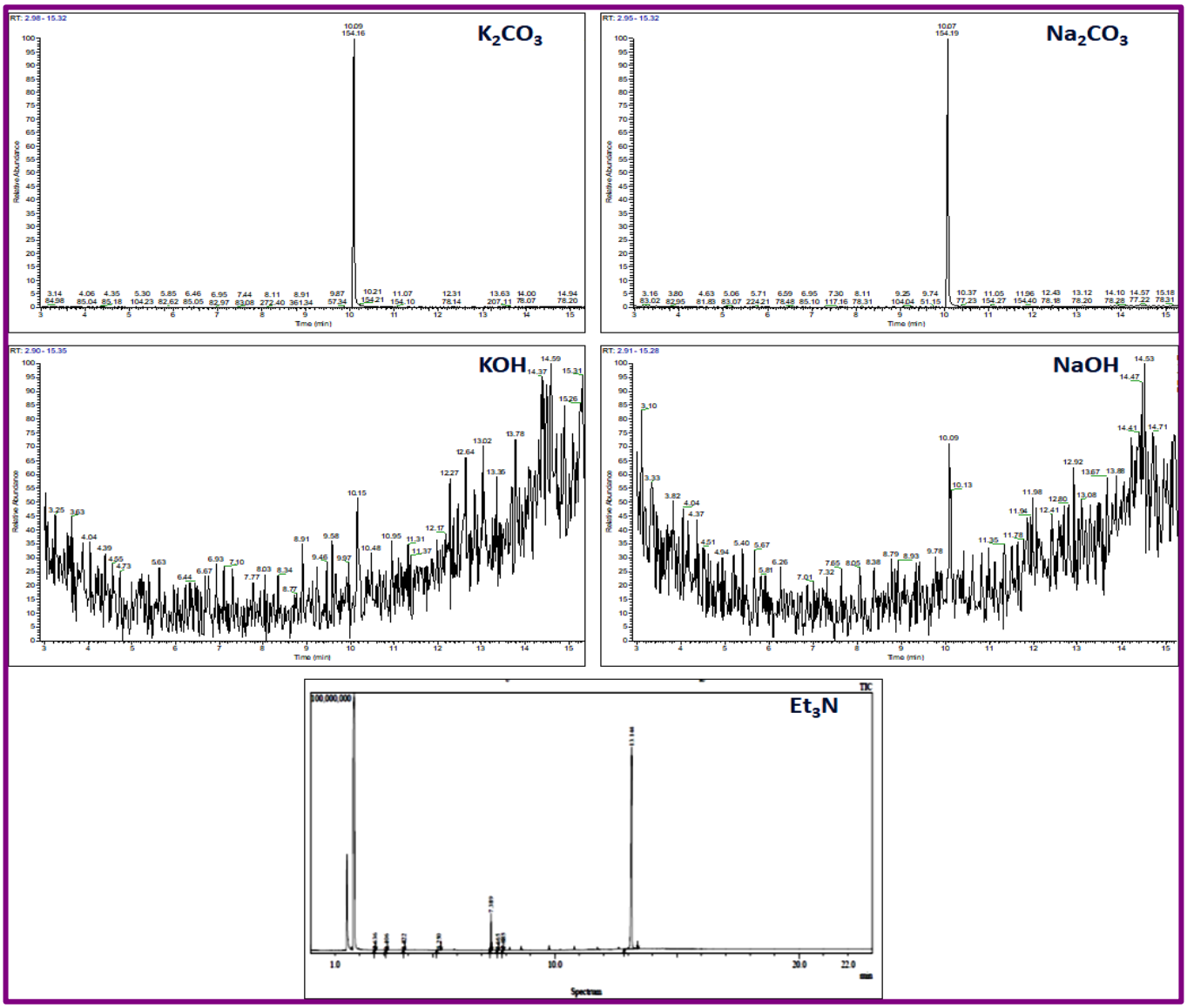

Figure 3.A26: GC-MS spectra of the product for Pd@Ni@IO-Chitosan catalysed reaction between iodobenzene and phenylboronic acid performed in water at 30 °C.

GC MS spectra during Optimization of Base amount for the reaction between Iodobenzene and phenylboronic acid (Figures 3.A27)

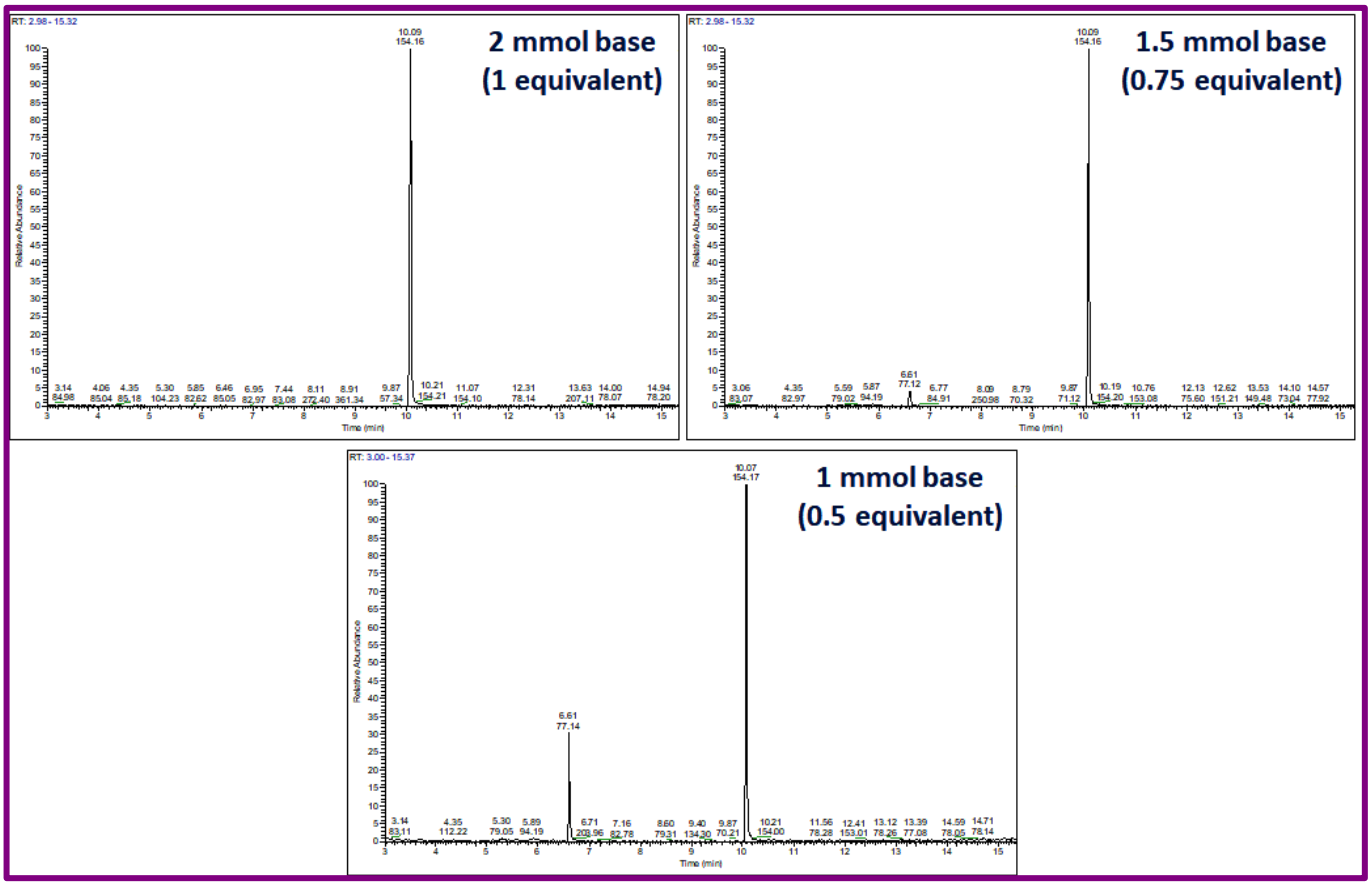

Figure 3.A27: GC-MS spectra of the product for Pd@Ni@IO-Chitosan catalysed reaction between iodobenzene and phenylboronic acid performed using K_2CO_3 as a base water as a solvent at 30 °C.

GC MS spectra during Optimization of Time for the reaction between Iodobenzene and phenylboronic acid (Figures 3.A28)

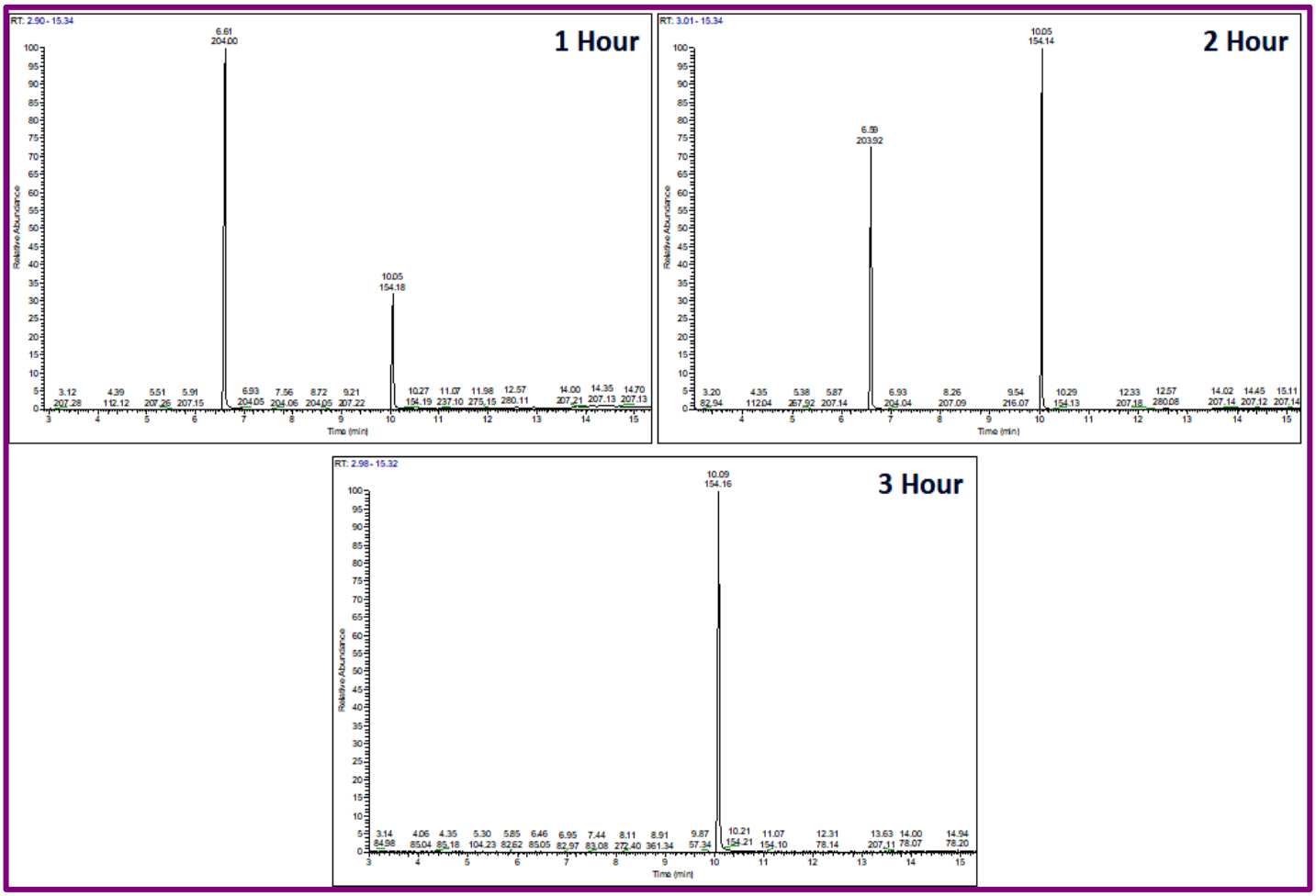

Figure 3.A28: GC-MS spectra of the product for Pd@Ni@IO-Chitosan catalysed reaction between iodobenzene and phenyl boronic acid performed at 35 °C in the time range 1 to 4 hours

Optimization of amount of catalyst.

It was observed that coupling of 2 mmol Iodobenzene and 2 mmol Phenylboronic acid using 1 equivalent K_2CO_3 gave same results at 100 to 30 °C (i.e, Room temperature) with 1 mg of Catalyst. (Figure 3.A29)

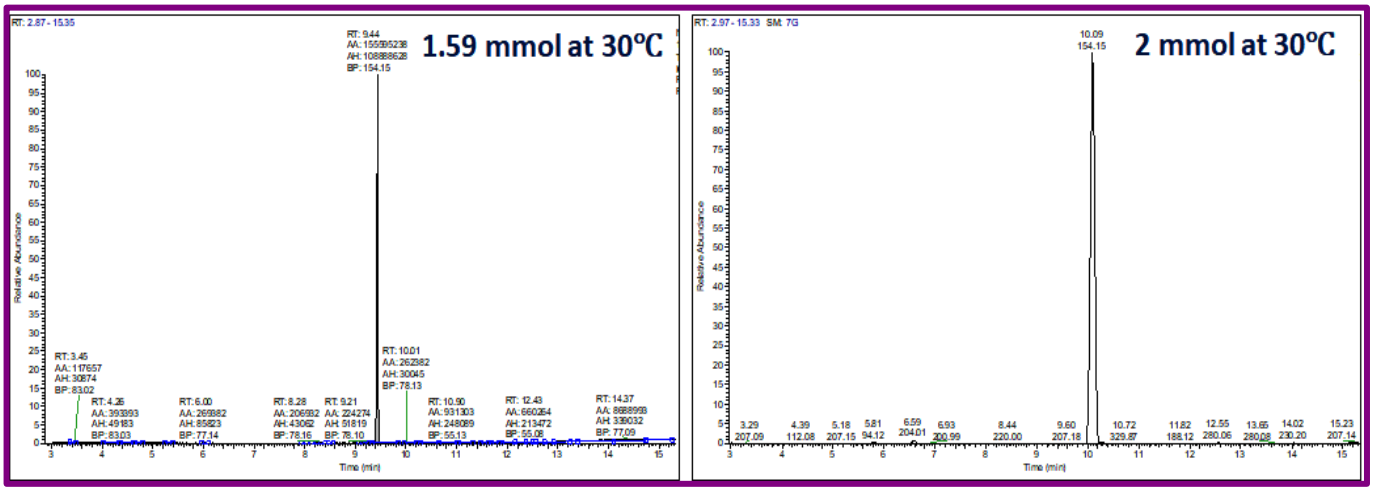

Figure 3.A29: GC-MS spectra of the product for Pd@Ni@IO-Chitosan catalysed reaction between 2 mmol iodobenzene and phenyl boronic acid performed in water using K_2CO_3 as a Base at 30 °C

GC-Ms and NMR spectra of biphenyl derivatives

1.

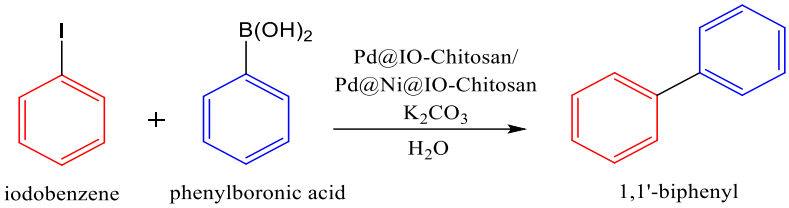

M.P: 70 °C

Molecular weight: 154.21 gm/mol

Pd@IO-Chitosan

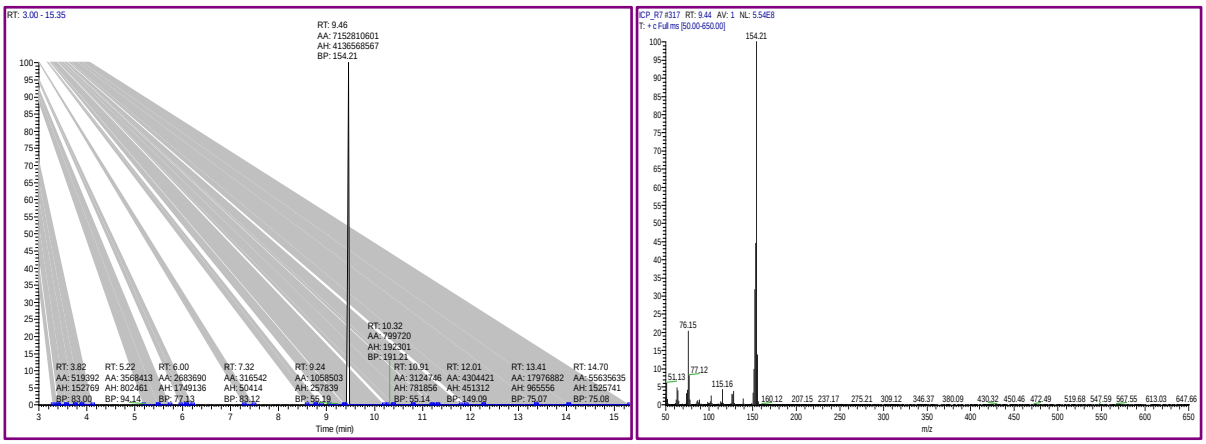

At 100°C

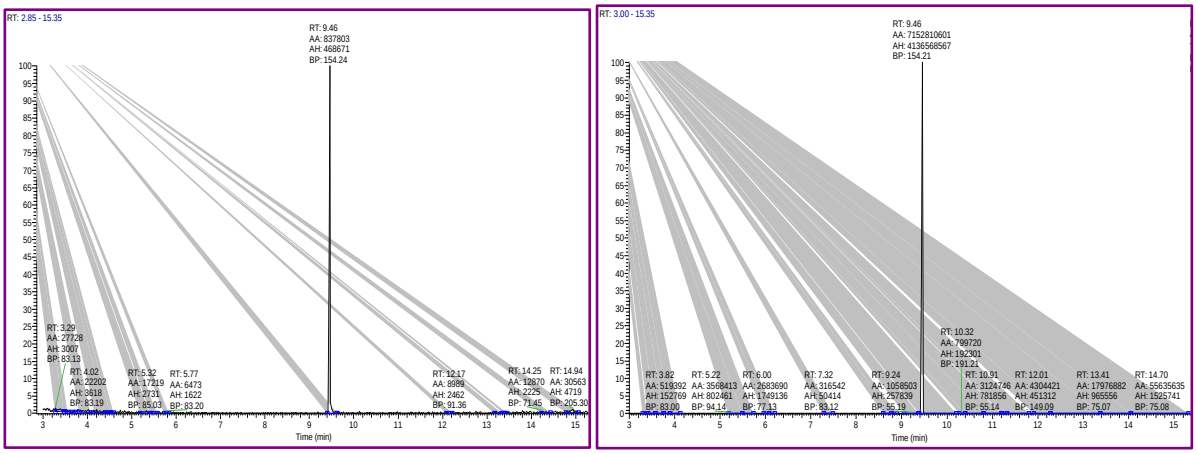

At 60 °C At room temperature

Figure 3.A30: *GC-Ms spectra of crude product (Biphenyl) synthesized From Iodobenzene at RT, 60°C and 100 °C*

Pd@Ni@IO-Chitosan

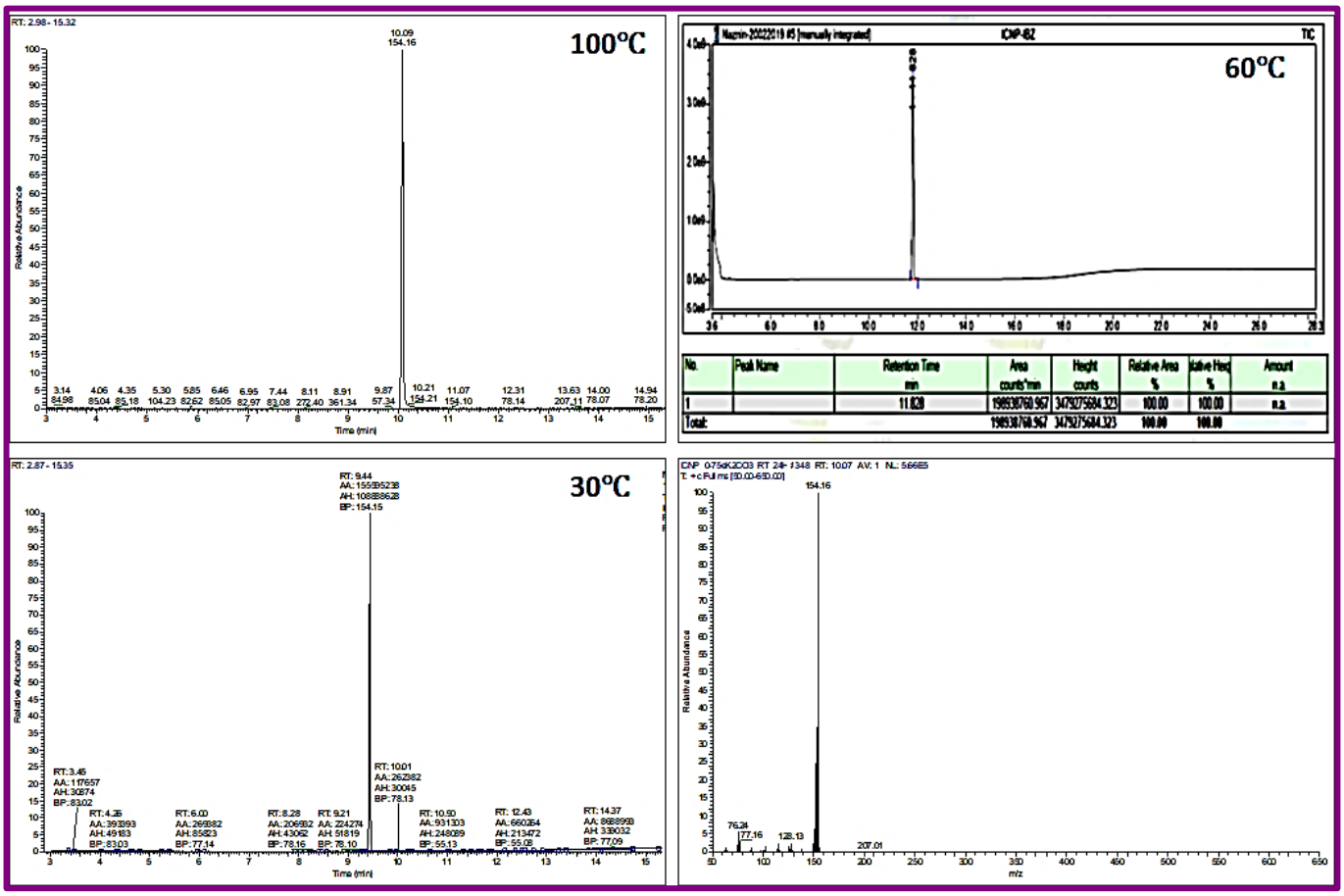

Figure 3.A*31* GC-Ms spectra of crude product (Biphenyl) synthesized From Iodobenzene at RT, 60°C and 100 °C

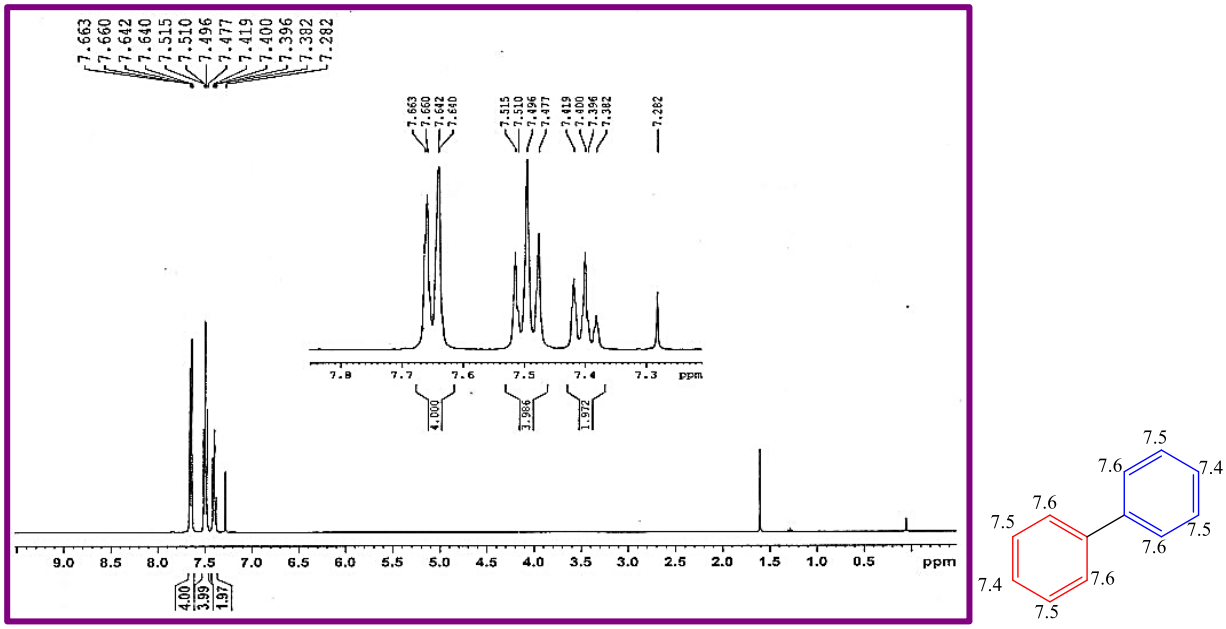

Figure 3.A*32*: NMR spectra of column purified (Biphenyl) synthesized From Iodobenzene

2.

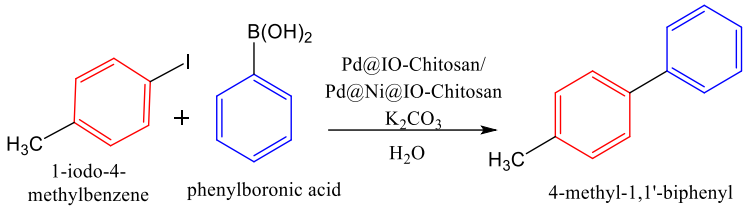

M.P: 49 °C

Molecular weight: 168.24 gm/mol`

Pd@IO-Chitosan

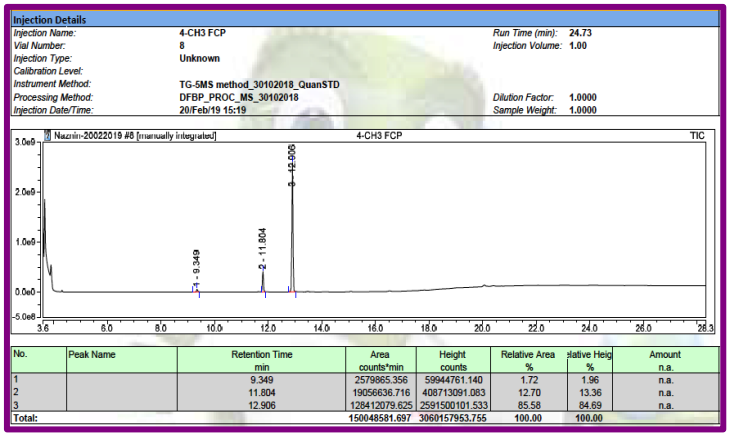

No.	Peak Name	Retention Time min	Area counts*min	Height counts	Relative Area %	Relative Height %	Amount n.a.
1		9.349	2579865.356	59944761.140	1.72	1.96	n.a.
2		11.804	19056636.716	408713091.083	12.70	13.36	n.a.
3		12.906	128412079.625	2591500101.533	85.58	84.69	n.a.
Total:			150048581.697	3060157953.755	100.00	100.00	

At 100 °C

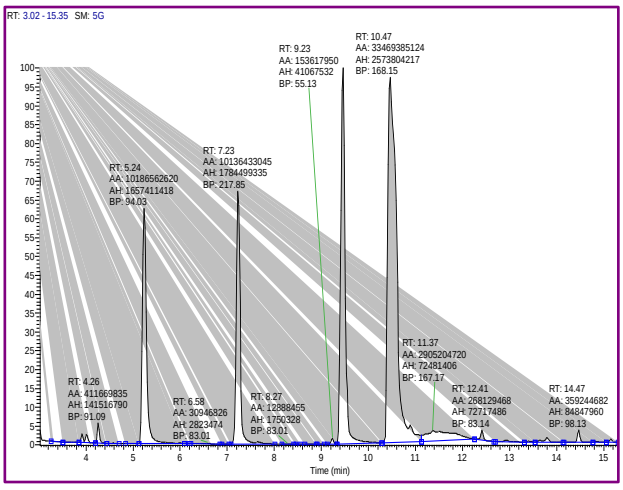

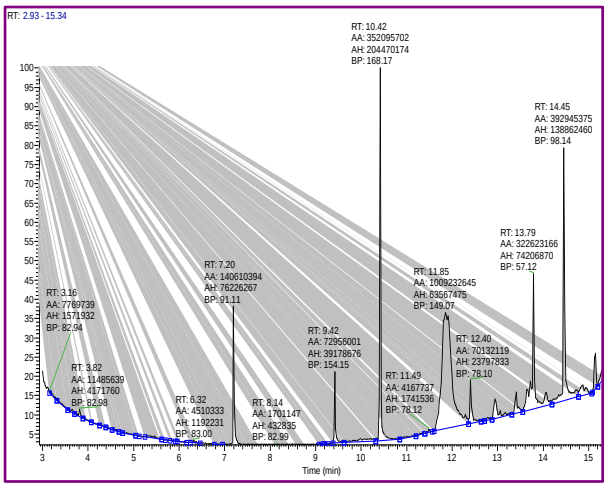

At 60°C At room temperature

Figure 3.A33: *GC-Ms spectra of crude product (4-methyl-1,1'-Biphenyl) synthesized at RT, 60°C and 100 °C*

Pd@Ni@IO-Chitosan

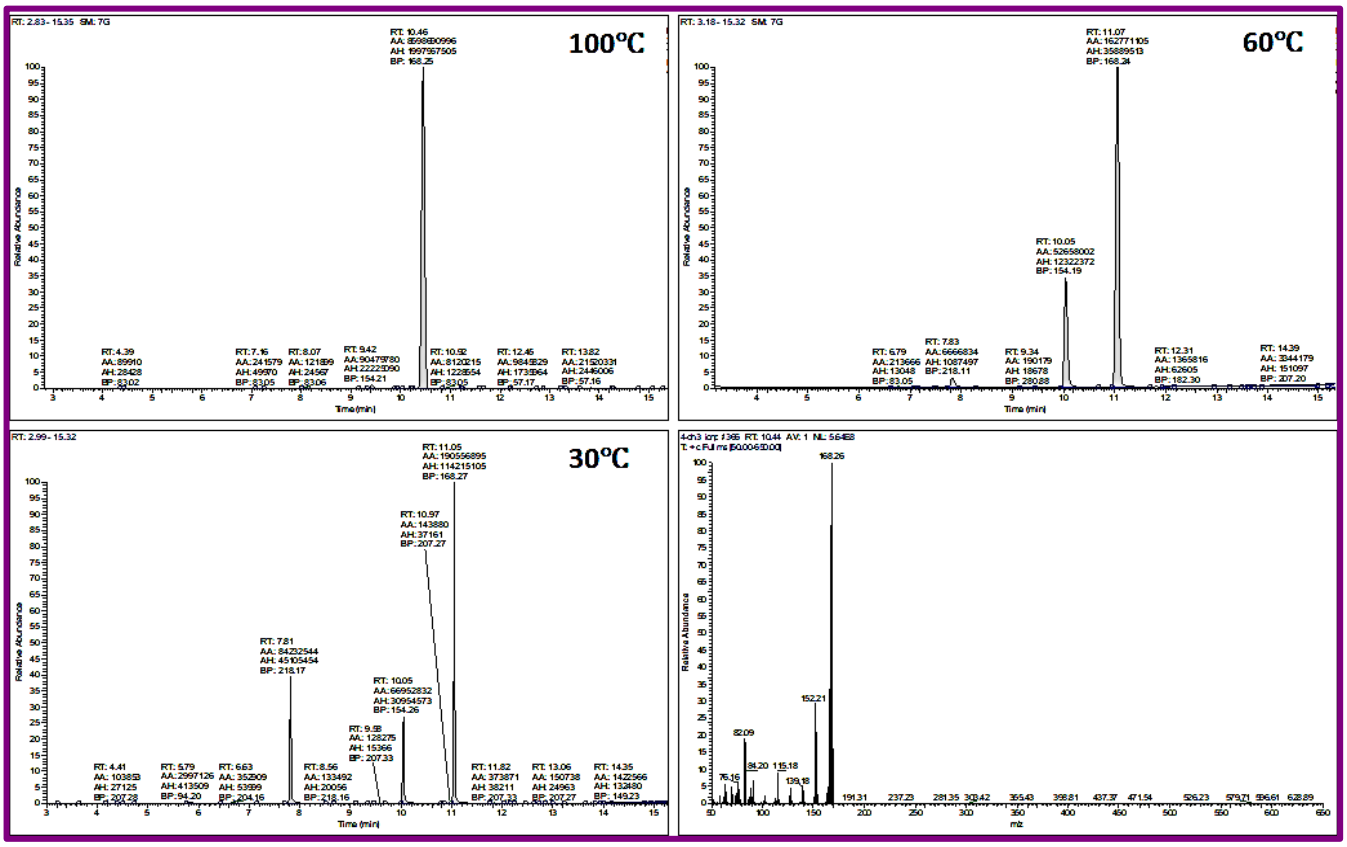

Figure 3.A*34* GC-Ms spectra of crude product (4-methyl-1,1'-Biphenyl) synthesized at RT, 60°C and 100 °C

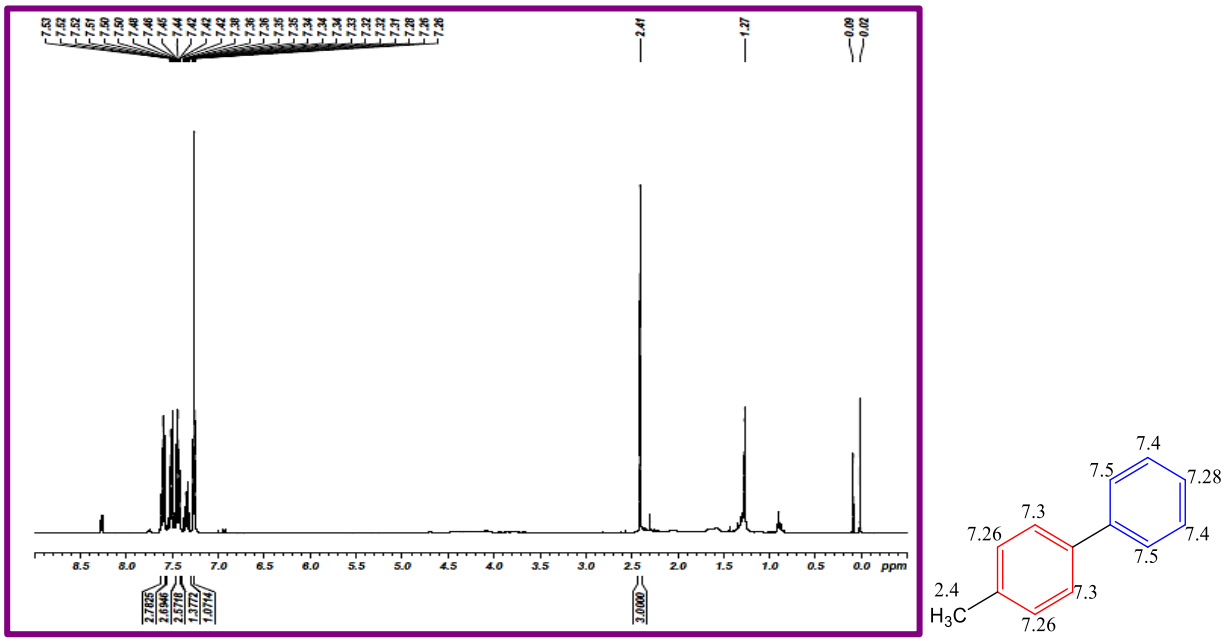

Figure 3.A35: *NMR spectra of column purified (4-methyl-1,1'-Biphenyl)*

3.

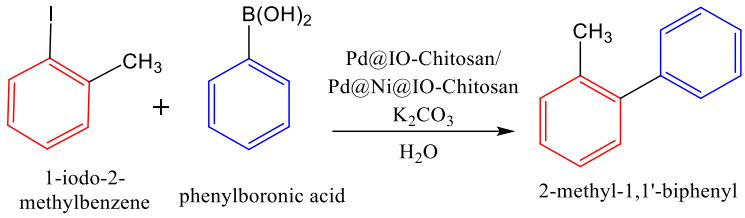

B.P: 255 °C

Molecular weight: 168.24 gm/mol

Pd@IO-Chitosan

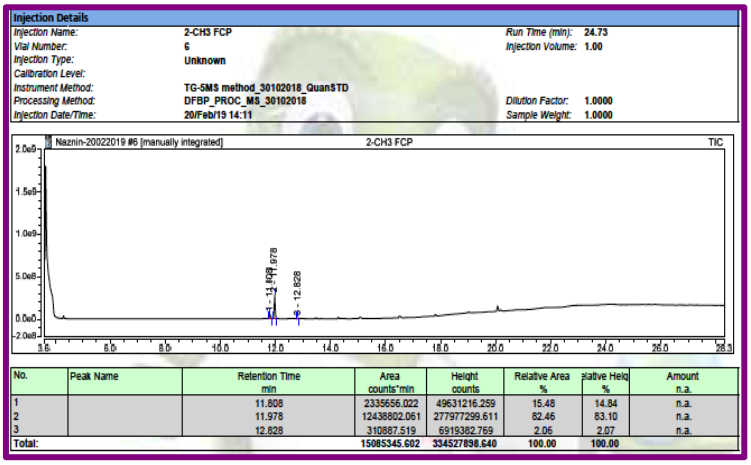

At 100 °C

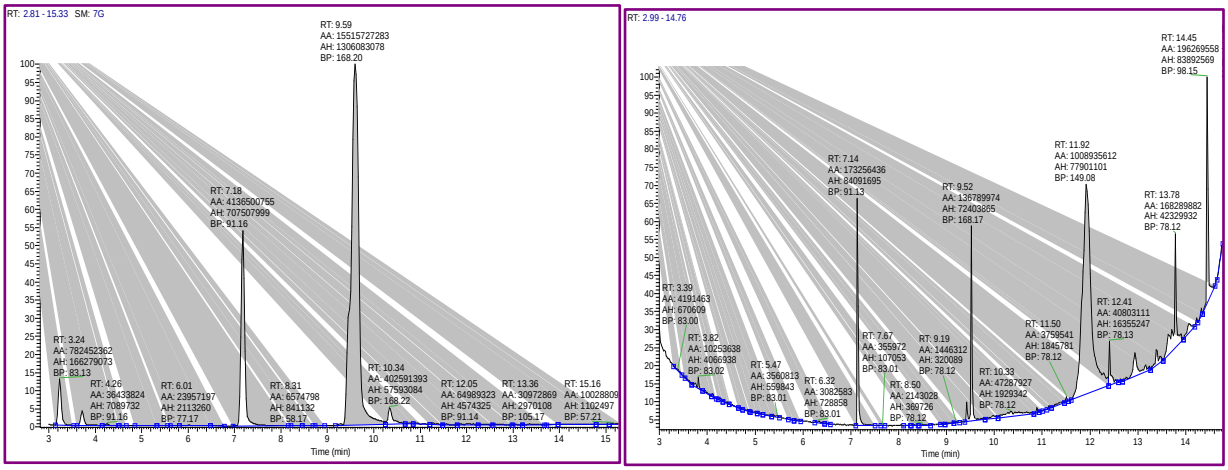

At 60 °C At Room temperature

Figure 3.A36: *GC-Ms spectra of crude product (2-methyl-1,1'-Biphenyl) synthesized at RT, 60°C and 100 °C*

Pd@Ni@IO-Chitosan

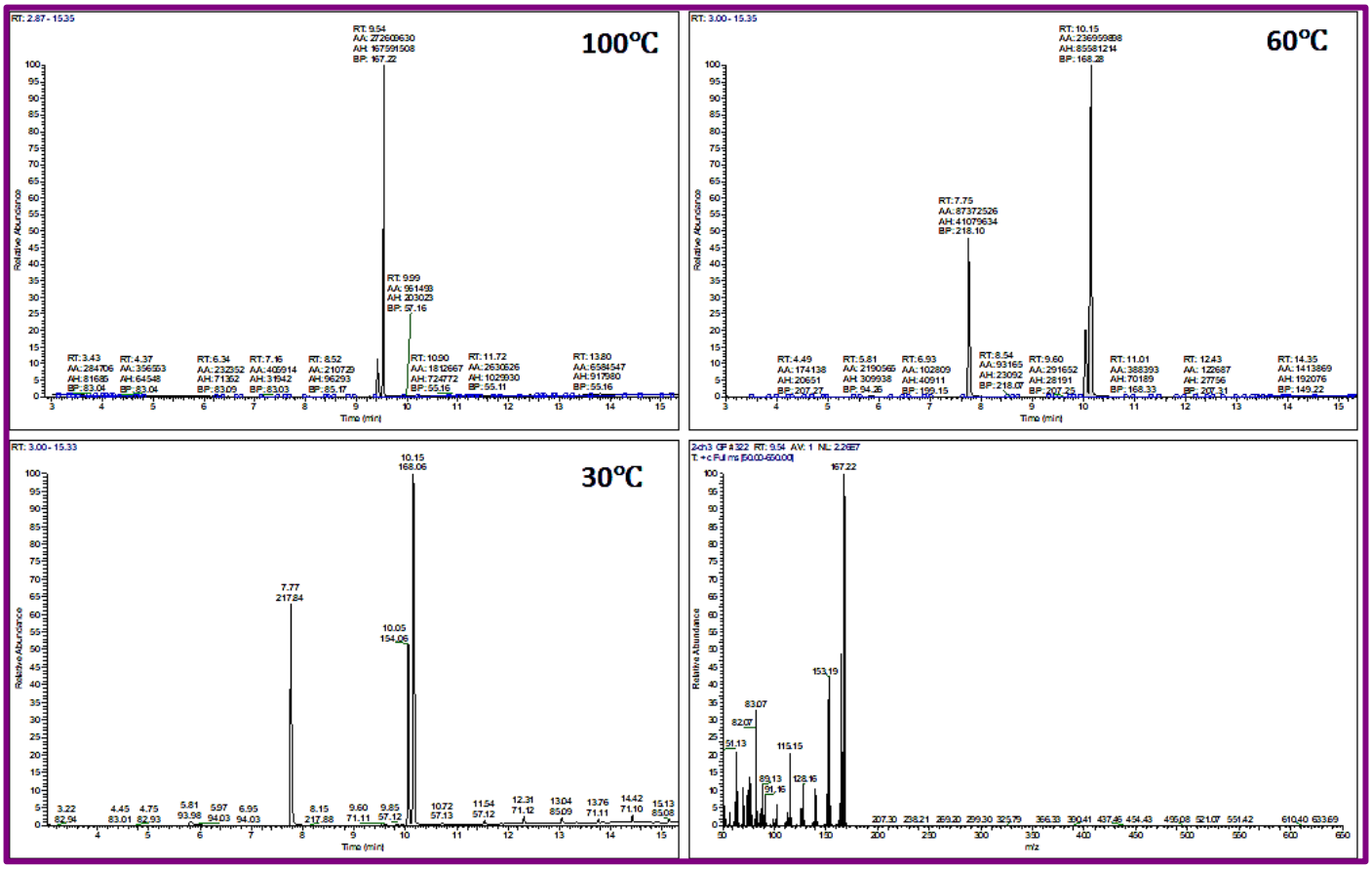

Figure 3.A37 GC-Ms spectra of crude product (2-methyl-1,1'-Biphenyl) synthesized at RT, 60°C and 100 °C

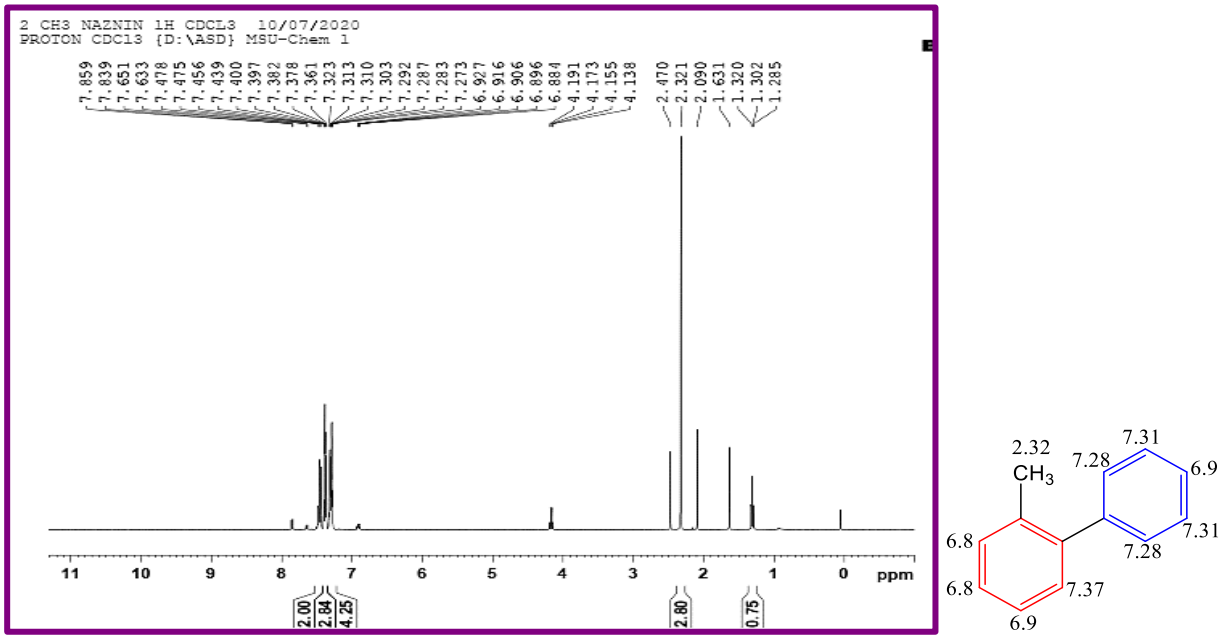

Figure 3.A*38:* NMR spectra of column purified (2-methyl-1,1'-Biphenyl)

4.

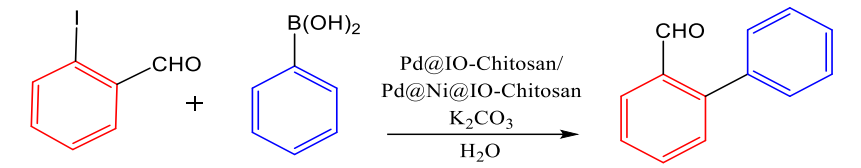

2-iodobenzaldehyde phenylboronic acid [1,1'-biphenyl]-2-carbaldehyde

B.P: 90 °C

Molecular weight: 182.2 gm/mol

Pd@IO-Chitosan

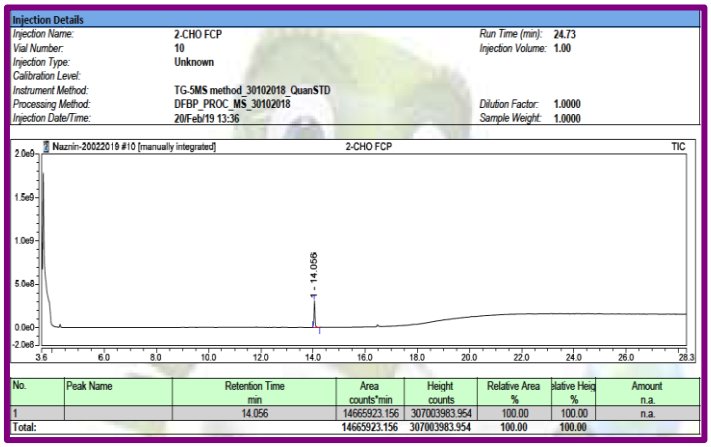

At 100°C

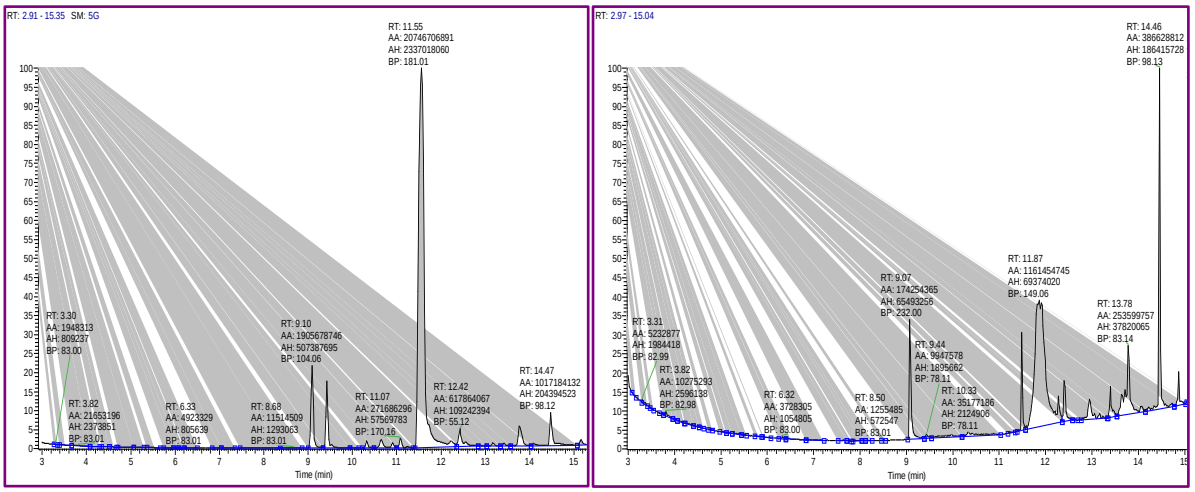

At 60°C At Room temperature

Figure 3.A39: *GC-MS spectra of crude product ([1,1'-biphenyl]-2-carbaldehyde) synthesized at RT, 60°C and 100 °C*

Pd@Ni@IO-Chitosan

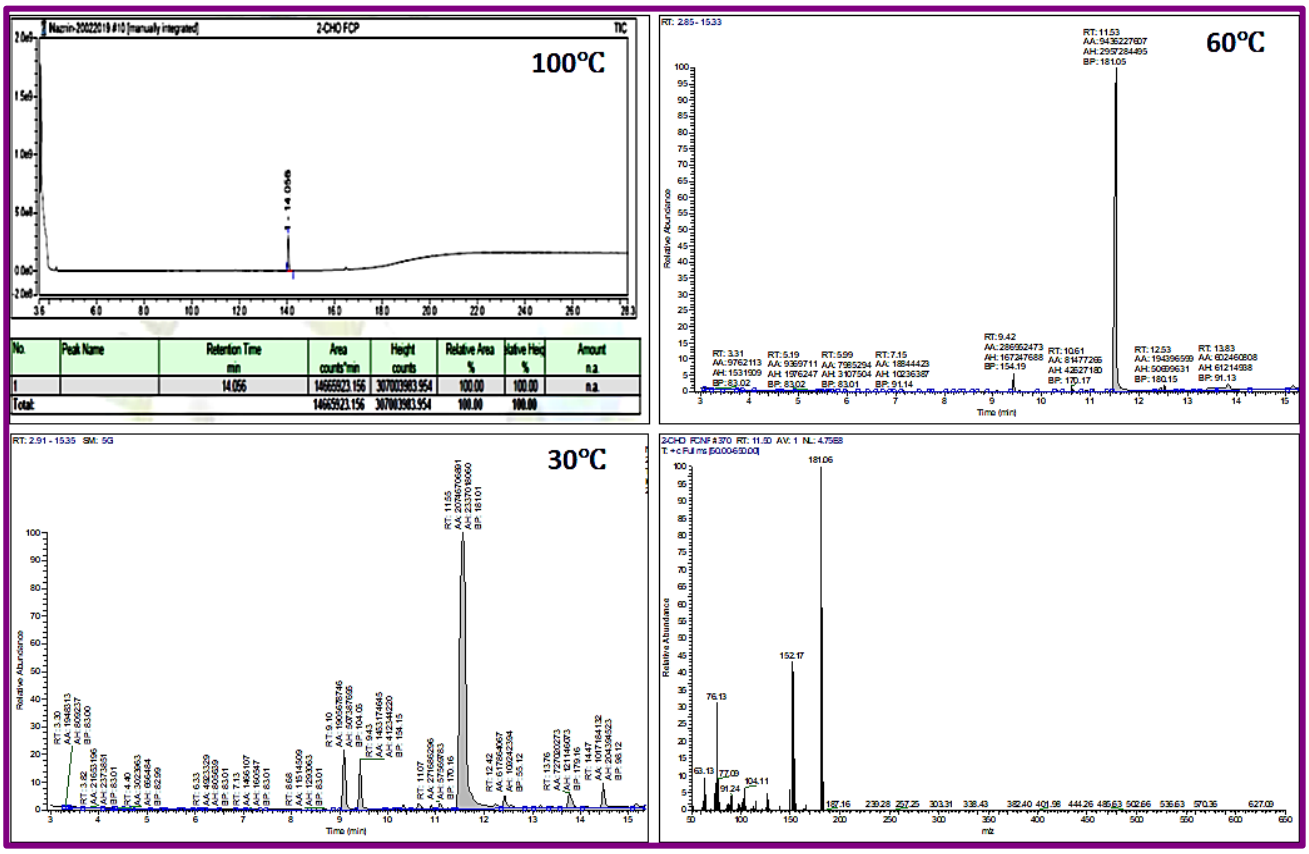

Figure 3.A40: GC-MS spectra of crude product ([1,1'-biphenyl]-2-carbaldehyde) synthesized at RT, 60°C and 100 °C

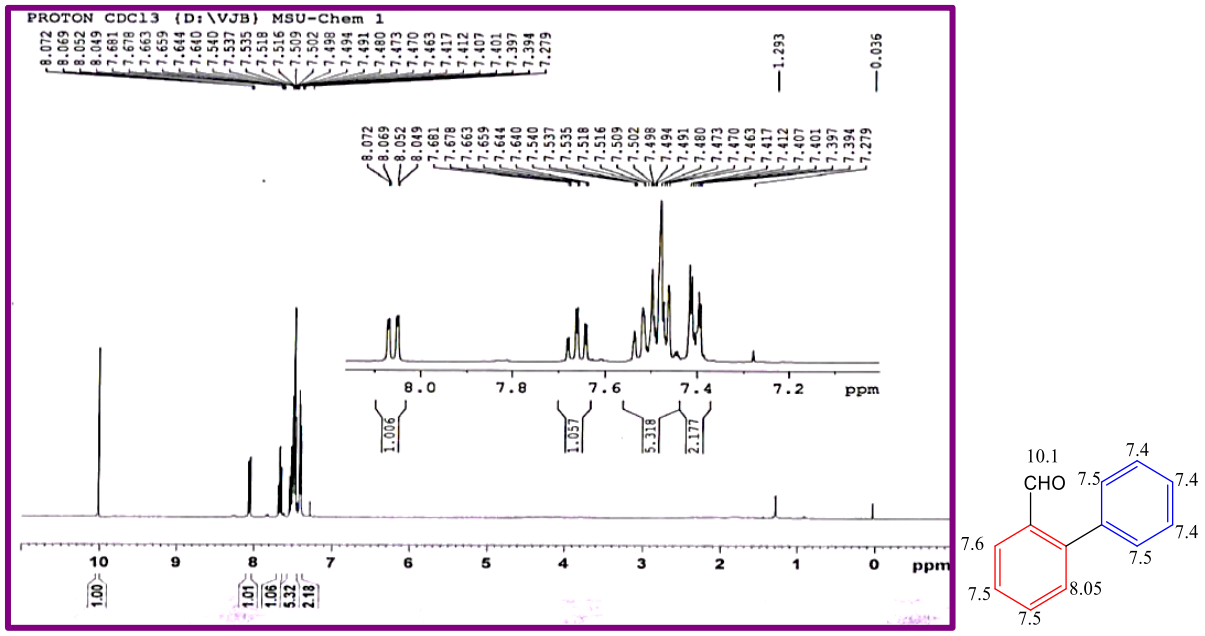

Figure 3.A41: NMR spectra of column purified ([1,1'-biphenyl]-2-carbaldehyde)

5.

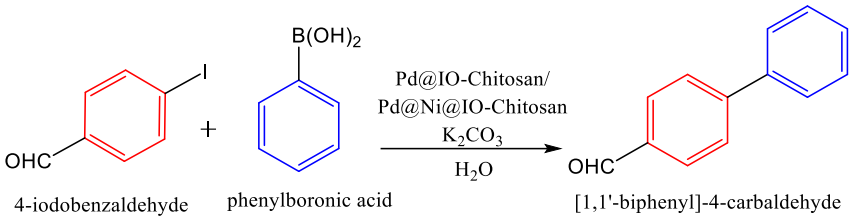

M.P. 60 °C

Molecular weight: 182.2 gm/mol

Pd@IO-Chitosan

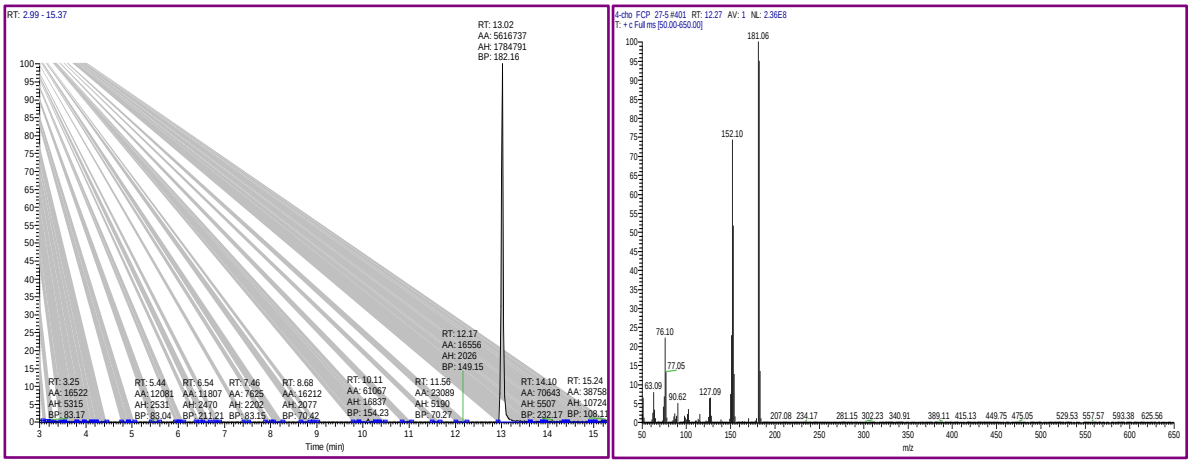

At 100 °C

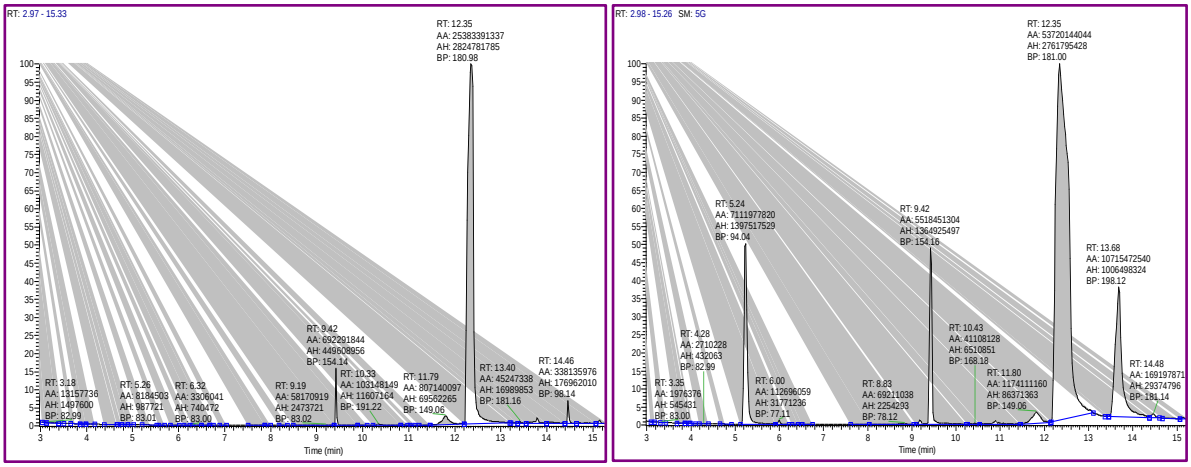

At 60 °C At room temperature

Figure 3.A42: *GC-Ms spectra of crude product ([1,1'-biphenyl]-4-carbaldehyde) synthesized at RT, 60°C and 100 °C*

Pd@Ni@IO-Chitosan

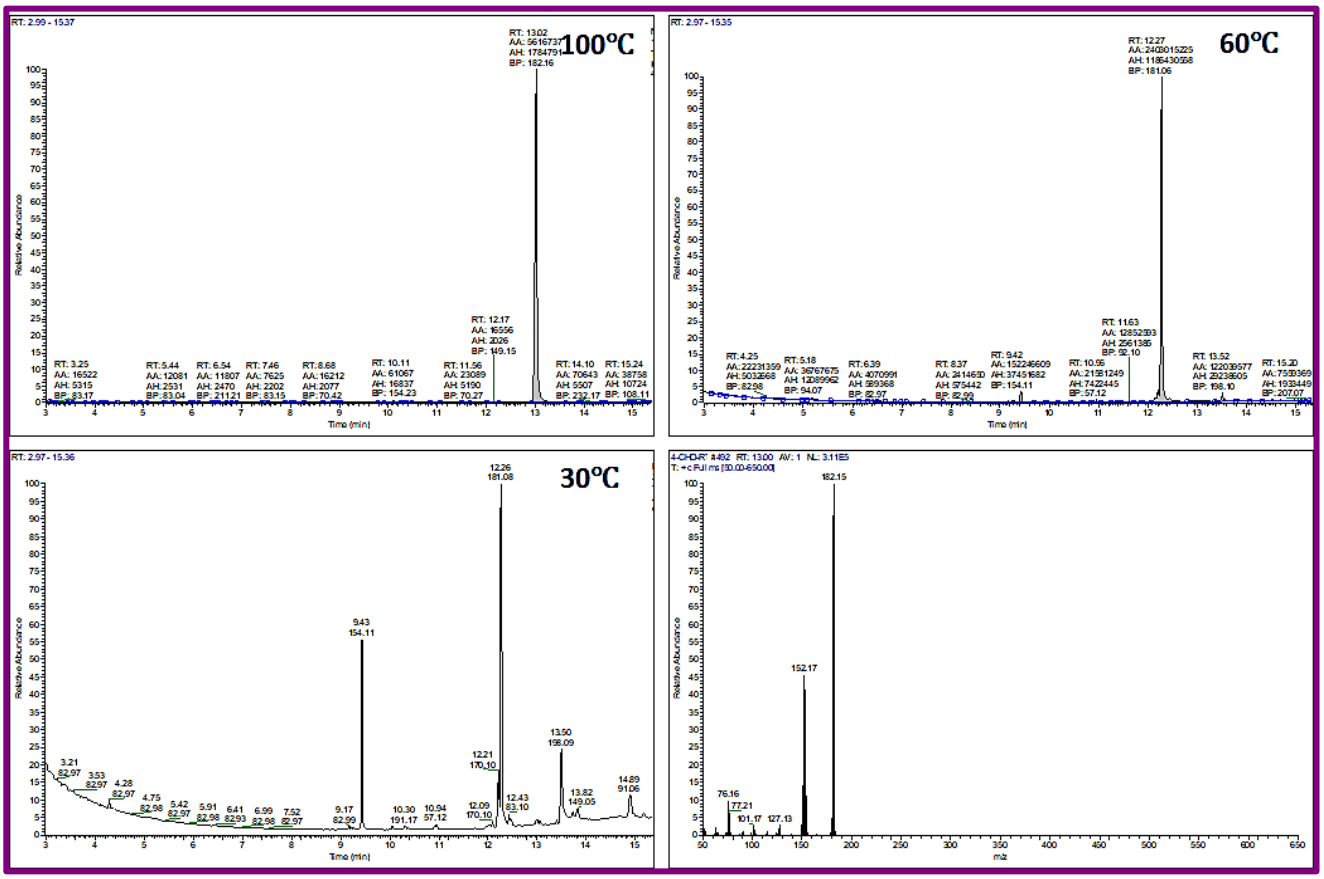

Figure 3.A43: GC-Ms spectra of crude product ([1,1'-biphenyl]-4-carbaldehyde) synthesized at RT, 60°C and 100 °C

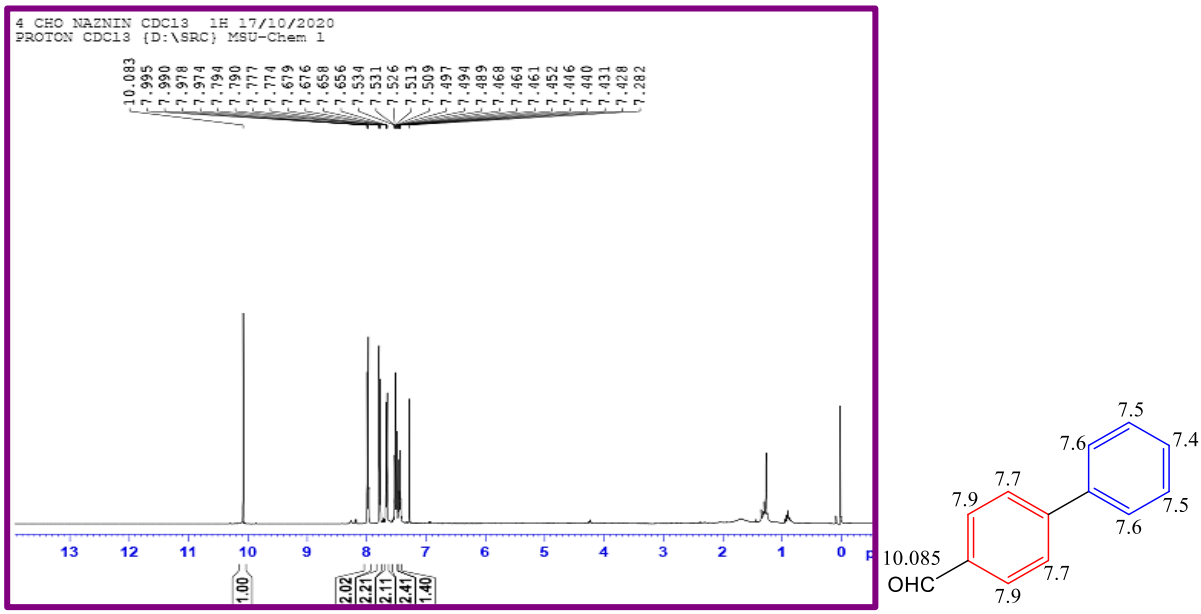

Figure 3.A44: *NMR spectra of column purified ([1,1'-biphenyl]-4-carbaldehyde)*

6.

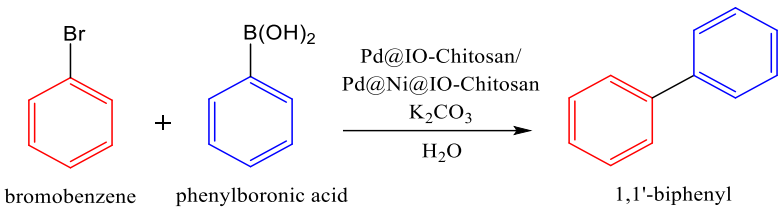

M.P: 70 °C;

Molecular weight: 154.21 gm/mol

Pd@IO-Chitosan

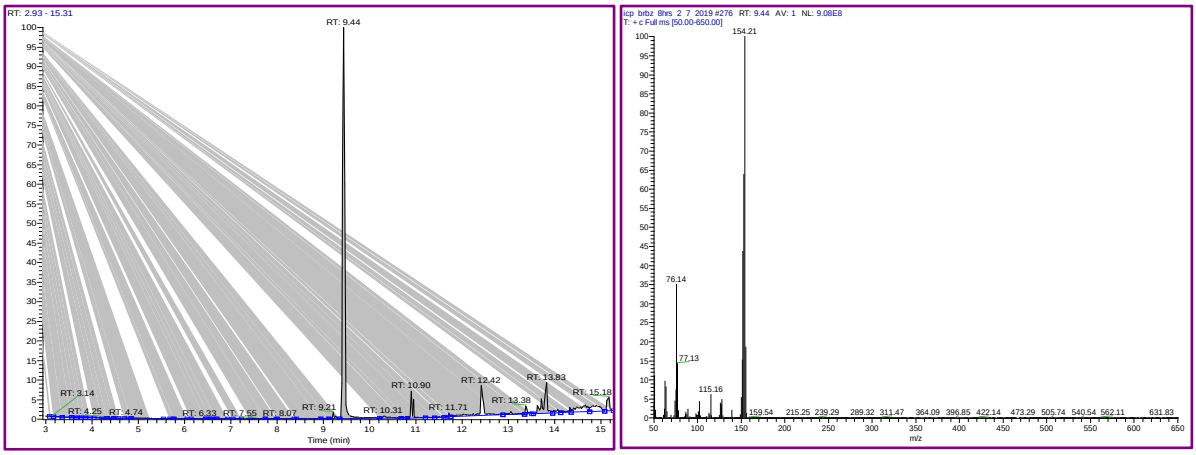

At 100 ℃

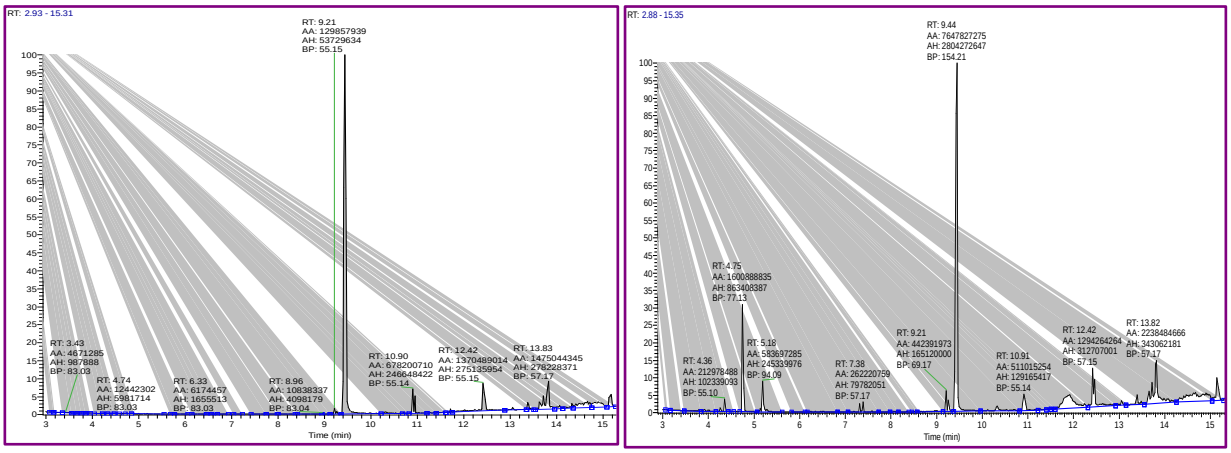

At 60 ℃ At room temperature

Figure 3.A45: *GC-MS spectra of crude product (Biphenyl) synthesized From Bromobenzene at RT, 60℃ and 100 °C*

Pd@Ni@IO-Chitosan

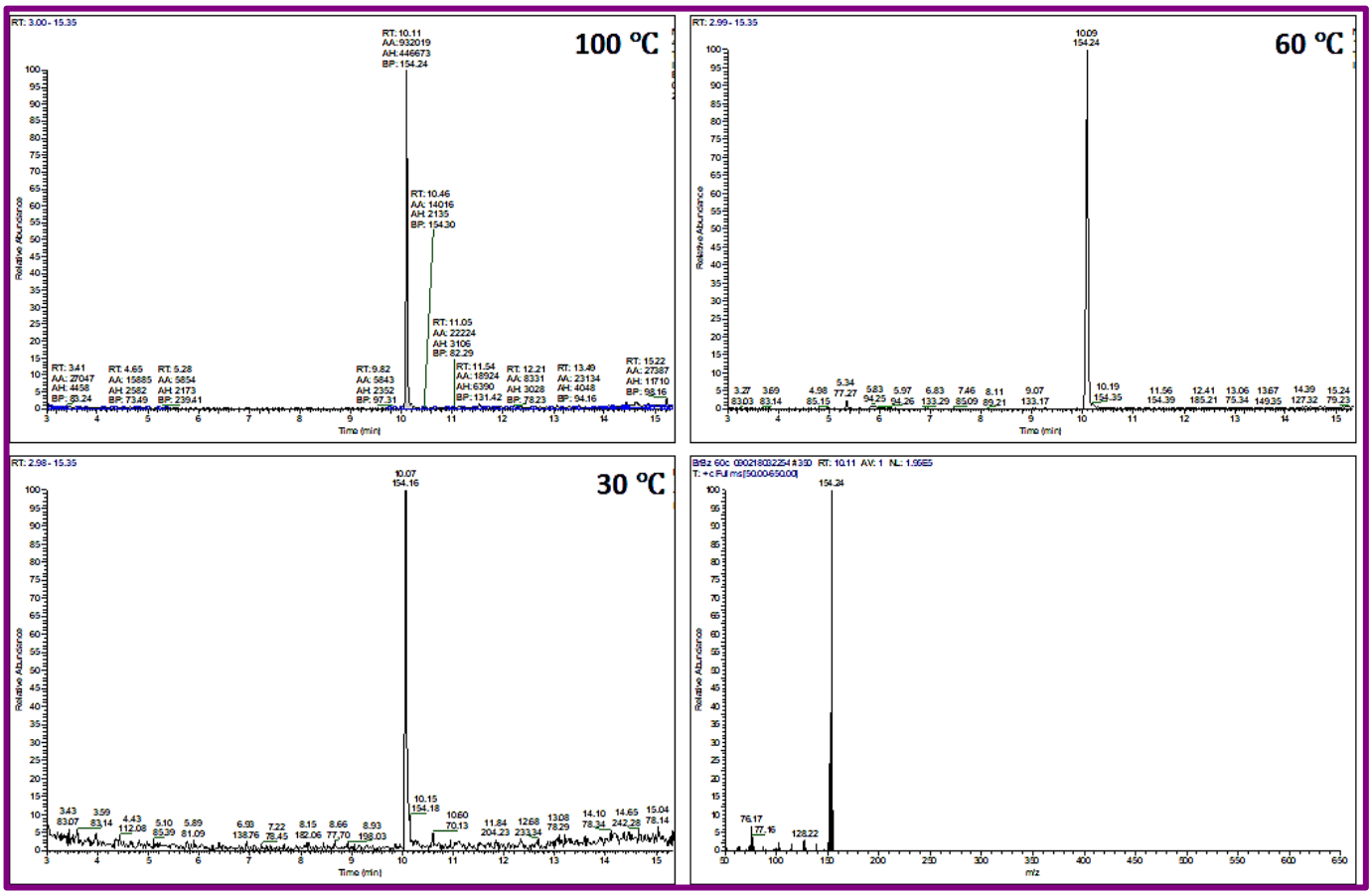

Figure 3.A46: GC-MS spectra of crude product (Biphenyl) synthesized From Bromobenzene at RT, 60°C and 100 °C

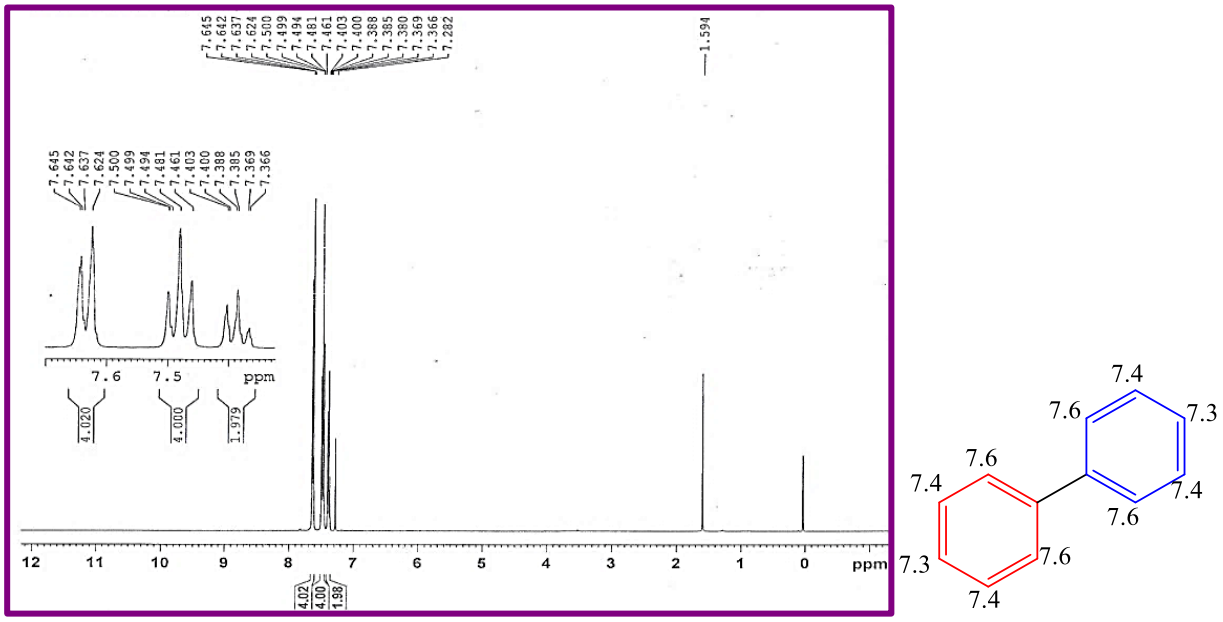

Figure 3.A47: *NMR spectra of column purified Biphenyl synthesized From Bromobenzene*

7.

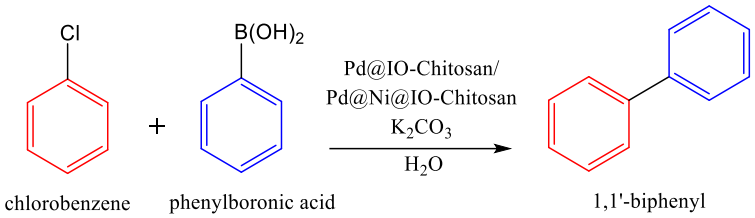

M.P: 70 °C

Molecular weight: 154.21 gm/mol

Pd@IO-Chitosan

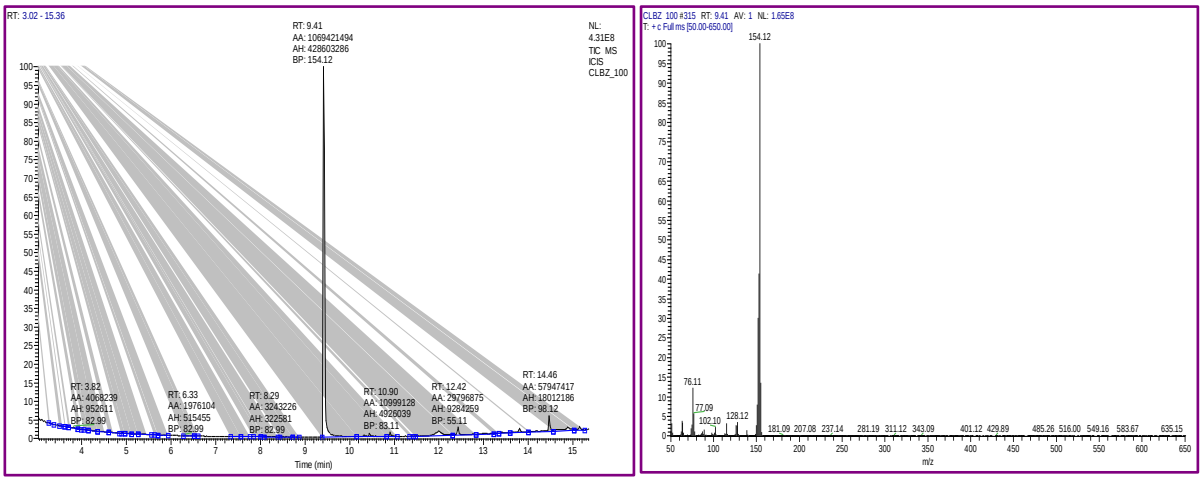

At 100 °C

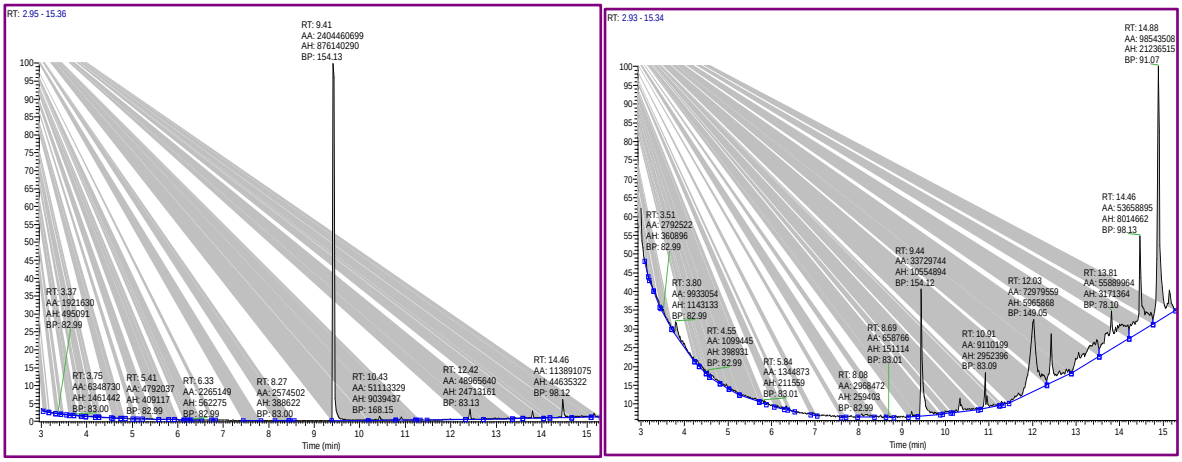

At 60 °C At room temperature

Figure 3.A48*:* GC-Ms spectra of crude product (Biphenyl) synthesized From Chlorobenzene at RT, 60°C and 100 °C

Pd@Ni@IO-Chitosan

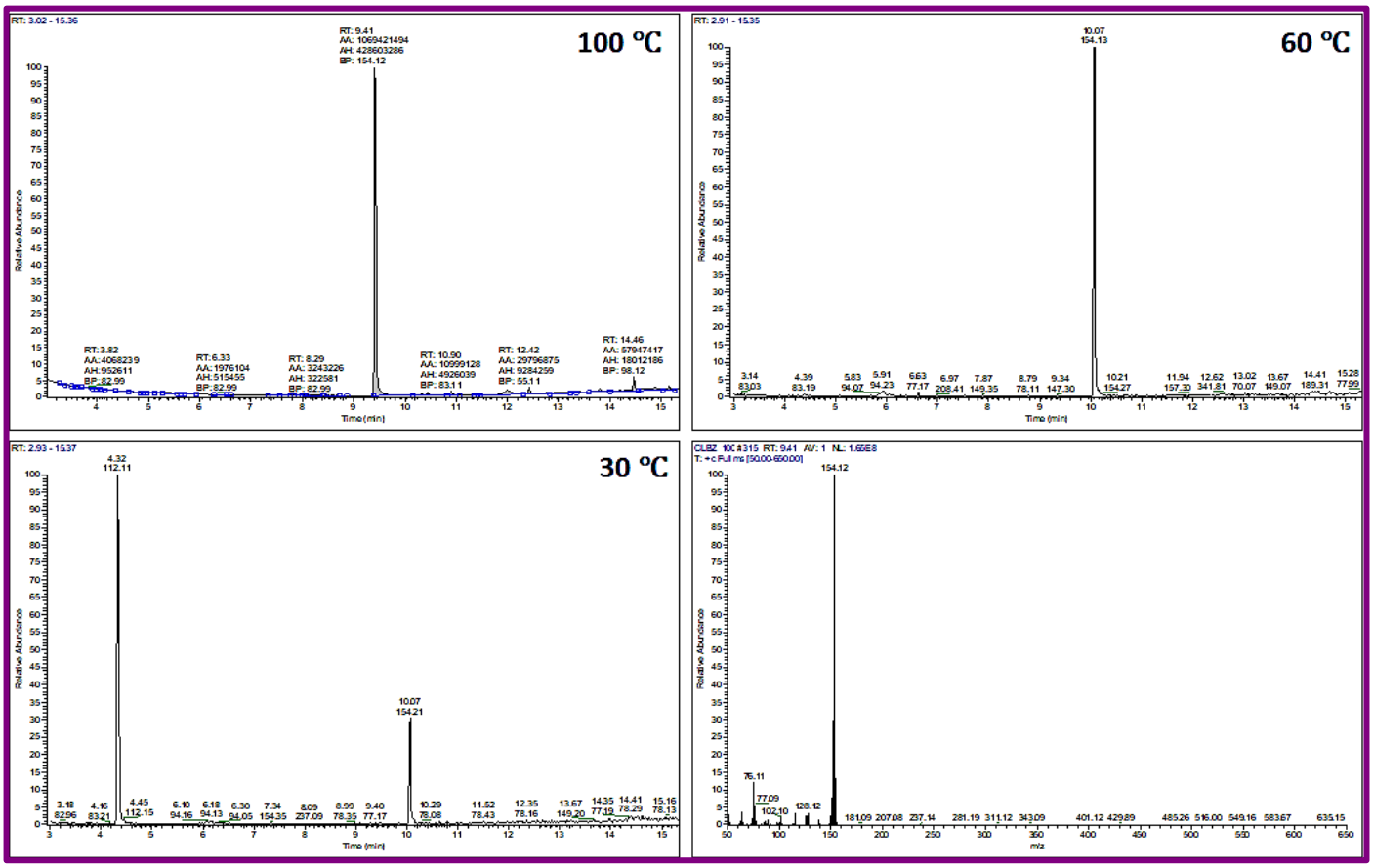

Figure 3.A49: GC-Ms spectra of crude product (Biphenyl) synthesized From Chlorobenzene at RT, 60°C and 100 °C

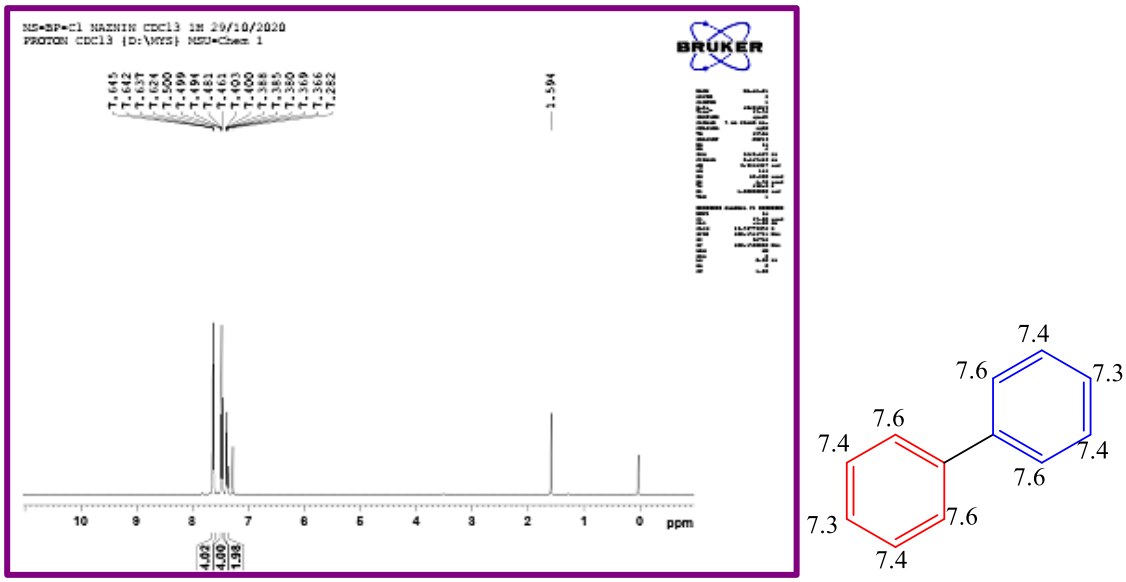

Figure 3.A50: *NMR spectra of column purified Biphenyl synthesized From Chlorobenzene*

Hot filtration test:

After 2 h the catalyst (Pd@Ni@IO-Chitosan) was separated and the reaction was then continued further for 10 h after catalyst removal. Products were isolated and analysed with GC-MS, there was no further conversion of the desired product after magnetic removal of the catalyst is detected, ascertaining the heterogeneous nature of the catalyst under study.

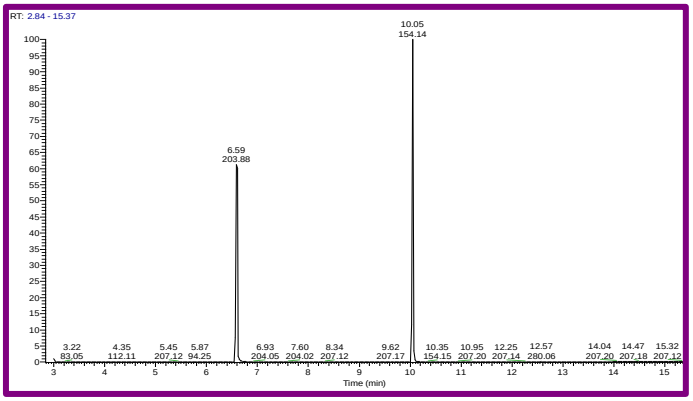

Figure 3.A51: Heterogeneity test (After 2h)

Recycling of catalyst (Pd@IO-Chitosan)

Recycling of catalyst was carried out using Iodobenzene (1.59mmol), Phenyl boronic acid (1.59 mmol), K_2CO_3 (3.18 mmol), Pd@IO-chitosan (1 mg) and H_2O (10 ml) at 90-100 °C under stirring for 6 h. Pd@IO-Chitosan maintained its activity upto 12 cycles. A 3% decrease in yield was observed during the 13th cycle. (Figure S42)

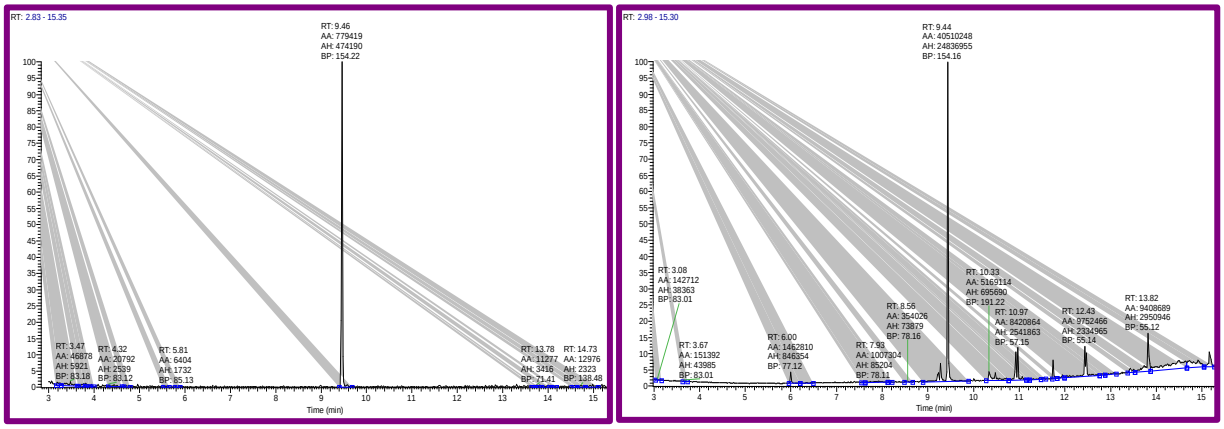

Recycle 12 Recycle 13

Figure 3.A52*: GC-MS spectra of the product for Recycled catalyst (Pd@IO-Chitosan) catalysed reaction between iodobenzene and phenyl boronic acid performed at 100 °C*

Recycling of catalyst (Pd@Ni@IO-Chitosan)

Recycling of catalyst was carried out using Iodobenzene (2 mmol), Phenyl boronic acid (2 mmol), K_2CO_3 (2 mmol), Pd@Ni@IO-chitosan (1 mg) and H_2O (10 ml) at 90-100 °C under stirring for 4 h. Pd@IO-Chitosan maintained its activity upto 17 cycles. A 2.71% decrease in yield was observed during the 13th cycle. (Figure **3.A53**)

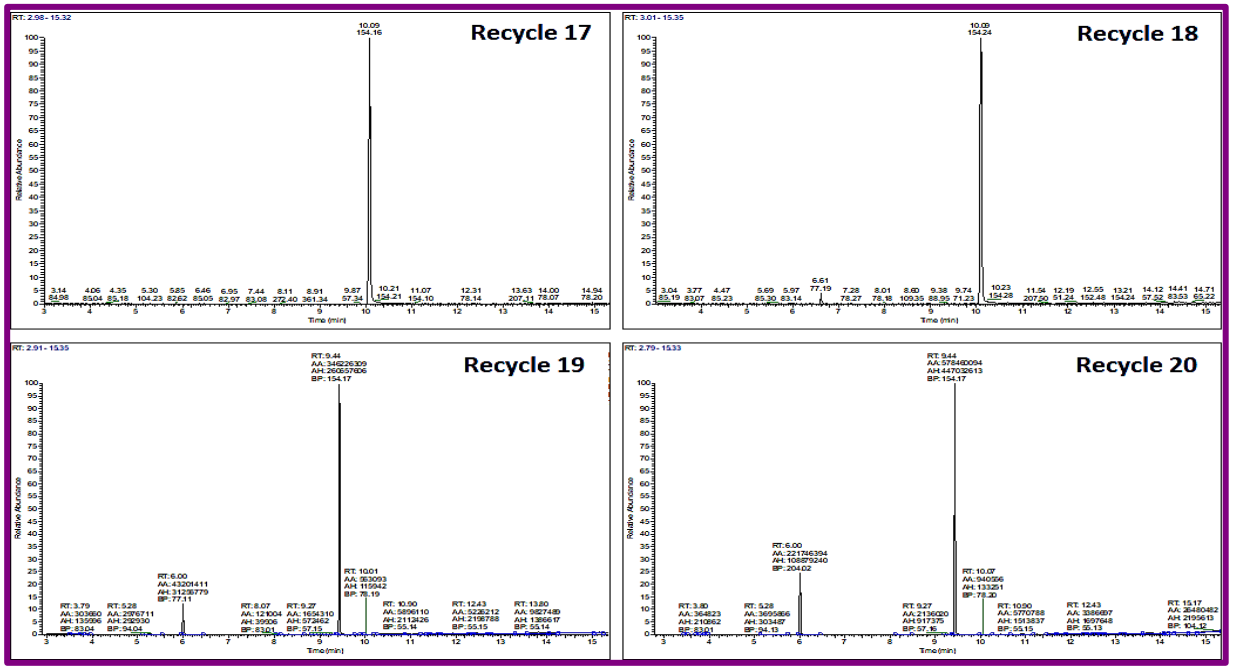

Figure 3.A53: GC-MS spectra of the product for Recycled catalyst (Pd@Ni@IO-Chitosan) catalysed reaction between iodobenzene and phenyl boronic acid performed at 100 °C

Reaction with Ni@IO-Chitosan at 100 °C

Recycling was carried out using Iodobenzene (1.59 mmol), Phenyl boronic acid (1.59 mmol), K_2CO_3 (1.59 mmol), Ni@IO-chitosan (1 mg) and H_2O (10 ml) at 90-100 °C under stirring for 12 h.

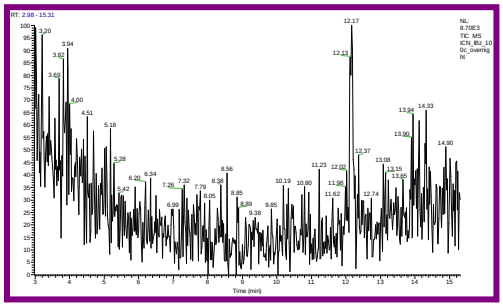

Figure 3.A54: GC-MS spectra of the product catalysed by Ni@IO-Chitosan with reaction between Iodobenzene and phenyl boronic acid performed at 100 °C.